

Review

A Review of Advances in Fabrication Methods and Assistive Technologies of Micro-Structured Surfaces

Yuting Ma, Guoqing Zhang *, Shuaikang Cao, Zexuan Huo, Junhong Han, Shuai Ma and Zejia Huang

Shenzhen Key Laboratory of High Performance Nontraditional Manufacturing, College of Mechatronics and Control Engineering, Shenzhen University, Nan-Hai Ave 3688, Shenzhen 518060, China

* Correspondence: zhanggq@szu.edu.cn; Tel.: +86-755-26536306; Fax: +86-755-26557471

Abstract: Micro-structured surfaces possess excellent properties of friction, lubrication, drag reduction, antibacterial, and self-cleaning, which have been widely applied in optical, medical, national defense, aerospace fields, etc. Therefore, it is requisite to study the fabrication methods of micro-structures to improve the accuracy and enhance the performance of micro-structures. At present, there are plenty of studies focusing on the preparation of micro-structures; therefore, systematic review of the technologies and developing trend on the fabrication of micro-structures are needed. In present review, the fabrication methods of various micro-structures are compared and summarized. Specially, the characteristics and applications of ultra-precision machining (UPM) technology in the fabrication of micro-structures are mainly discussed. Additionally, the assistive technologies applied into UPM, such as fast tool servo (FTS) technology and slow tool servo (STS) technology to fabricate micro-structures with different characteristics are summarized. Finally, the principal characteristics and applications of fly cutting technology in manufacturing special micro-structures are presented. From the review, it is found that by combining different machining methods to prepare the base layer surface first and then fabricate the sublayer surface, the advantages of different machining technologies can be greatly exerted, which is of great significance for the preparation of multi-layer and multi-scale micro-structures. Furthermore, the combination of ultra-precision fly cutting and FTS/STS possess advantages in realizing complex micro-structures with high aspect ratio and high resolution. However, residual tool marks and material recovery are still the key factors affecting the form accuracy of machined micro-structures. This review provides advances in fabrication methods and assistive technologies of micro-structured surfaces, which serves as the guidance for both fabrication and application of multi-layer and multi-scale micro-structures.

Keywords: micro-structures; ultra-precision machining; FTS/STS; fly cutting; raster milling



Citation: Ma, Y.; Zhang, G.; Cao, S.; Huo, Z.; Han, J.; Ma, S.; Huang, Z. A Review of Advances in Fabrication Methods and Assistive Technologies of Micro-Structured Surfaces.

Processes **2023**, *11*, 1337.

<https://doi.org/10.3390/pr11051337>

Academic Editor: Albert Renken

Received: 17 March 2023

Revised: 20 April 2023

Accepted: 21 April 2023

Published: 26 April 2023



Copyright: © 2023 by the authors. Licensee MDPI, Basel, Switzerland. This article is an open access article distributed under the terms and conditions of the Creative Commons Attribution (CC BY) license (<https://creativecommons.org/licenses/by/4.0/>).

1. Introduction

A micro-structured surface is small with special arranged topological structures [1,2]. The special arrangement of these microscale topological structures makes the micro-structured surface exhibit specific functions, such as superhydrophobicity, anti-fouling, drag reduction, structural color, etc., as shown in Figure 1 [3–6]. These specific functions are perfectly reflected in a range of plants and animals in nature.

In the 1980s, Barthlott et al. discovered that lotus leaf surfaces have a unique set of micro/nano structures, with thousands of microscale papillae (20–100 μm) and thousands of nanoscale wax filaments (100–500 nm) distributed on each papillae [7,8]. This unique surface result in superhydrophobicity and self-cleaning effect of the lotus leaf is known as the lotus effect. Similar to lotus leaves, rice leaves have superhydrophobicity and anisotropic wettability due to their specially arranged hierarchies [9]. These characteristics are also reflected in animals. For example, the rough nano-structures in shark skin endow it with anti-fouling and drag reduction properties [10]; the multi-scale structures on the butterfly wings can not only produce structural color but also have superhydrophobicity,

self-cleaning, sensitive chemosensory abilities, and fluorescence emission functions [3,11]; insect compound eyes have high sensitivity and anti-reflex function [12]. These special micro-structured surfaces not only endow powerful functions to natural plants and animals, but also widely apply to optics, circuit systems, information and communication, precision engineering, biomedicine, and other fields [13]. For instance, micro-structured arrays have good optical properties, higher flexibility, and uniform shape, providing greater flexibility and innovation for optical design [14–17]. Moreover, the micro-structured surface is small in size and light in weight, which is easy to realize system integration and reduce the difficulty of assembly [18]. In addition to the above functions, the micro-structured surface also has great development potential in aerospace, navigation and guidance, and other military fields.

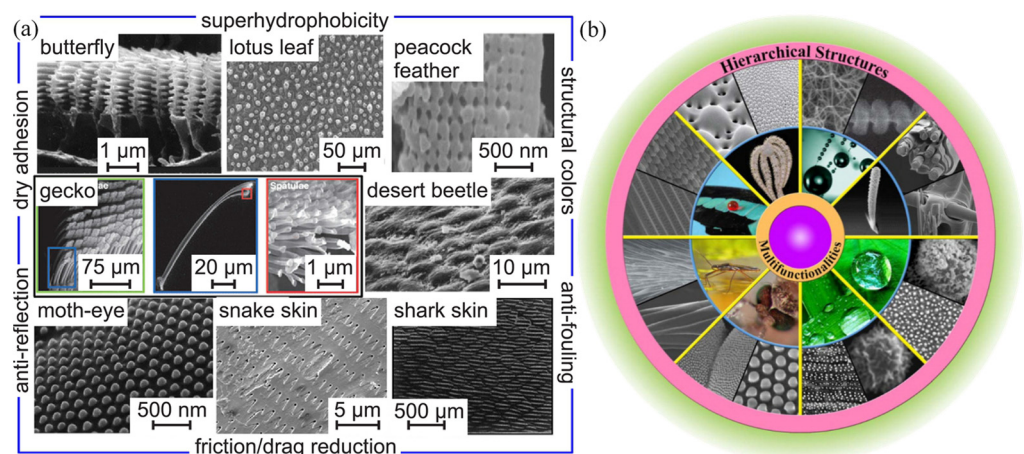


Figure 1. (a) Diversity in biological textures and their functions; and (b) hierarchical structures on the surfaces of various plants and animals. Reprinted with permission from Refs. [3,4].

However, due to the complexity of surface texture and the characteristics of high aspect ratio, the fabrication of micro-structures is very challenging. Typical machining techniques for a micro-structured surface mainly include lithography technology [19], high energy beam direct writing technology [20], special energy field machining technology [21], molding technology, LIGA technology [22], and ultra-precision machining (UPM) technology [23].

Lithography is suitable for fabricating two-dimensional (2D) and simple three-dimensional (3D) structures. For complex 3D structures, high energy beam direct writing technology and LIGA technology are more applicable, whereas the machining cost is high and it is difficult to fabricate large size micro-structures. Special energy field machining extends the machining range to difficult-to-cut materials, and the molding technology is suitable for the mass production of simple micro-structures. However, the above machining methods cannot meet all the requirements of high surface precision, complex 3D, and high aspect ratio micro-structures. UPM is an effective method to fabricate micro-structures, it has many advantages which could meet all these requirements.

UPM technology was developed in the 1960s to meet the manufacturing needs of nuclear power manufacturers, VLSI (Very Large Scale Integration), lasers, aircraft and other high-end products [24–27]. Production efficiency has been continuously improved and products have been gradually miniaturized, while higher requirements are put forward for micro-structures machining, the machining accuracy of UPM is constantly improved. The development of achievable machining accuracy is shown in Figure 2. UPM generally includes ultra-precision diamond turning, milling, scratching, ultra-precision grinding, and polishing, as shown in Figure 3. They could be employed for machining various freeform surfaces and complex micro-structures [28–34]. Ultra-precision diamond turning, milling, and scratching are usually employed with a natural single crystal diamond tool, this is called ultra-precision diamond cutting [35]. The surface roughness R_a can reach 1 nm and

the form accuracy PV can reach 0.1 μm . Grinding is mainly used for machining difficult-to-cut materials, which is hard to do with diamond cutting. Polishing is a follow-up process that achieves higher surface quality.

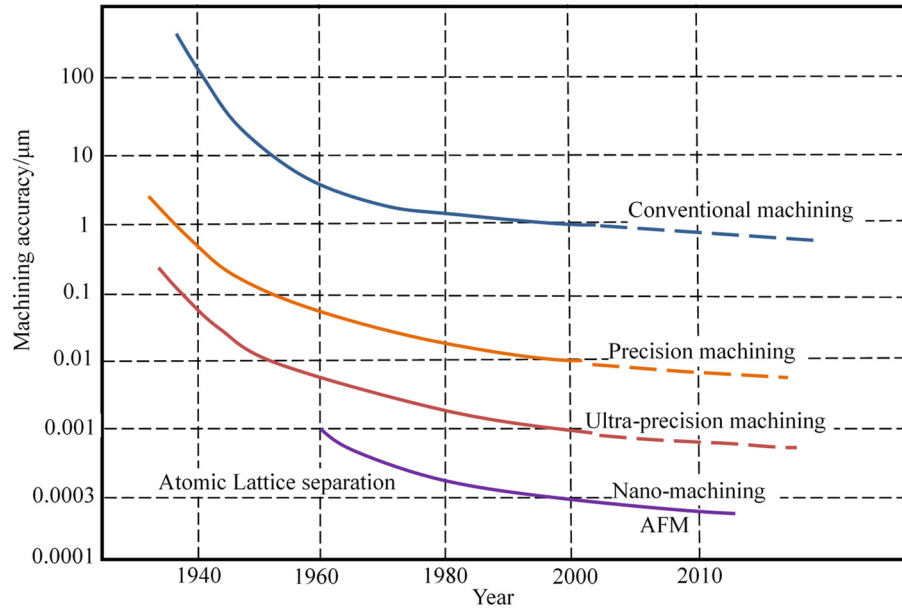


Figure 2. Achievable machining accuracy. Reprinted with permission from Ref. [36].

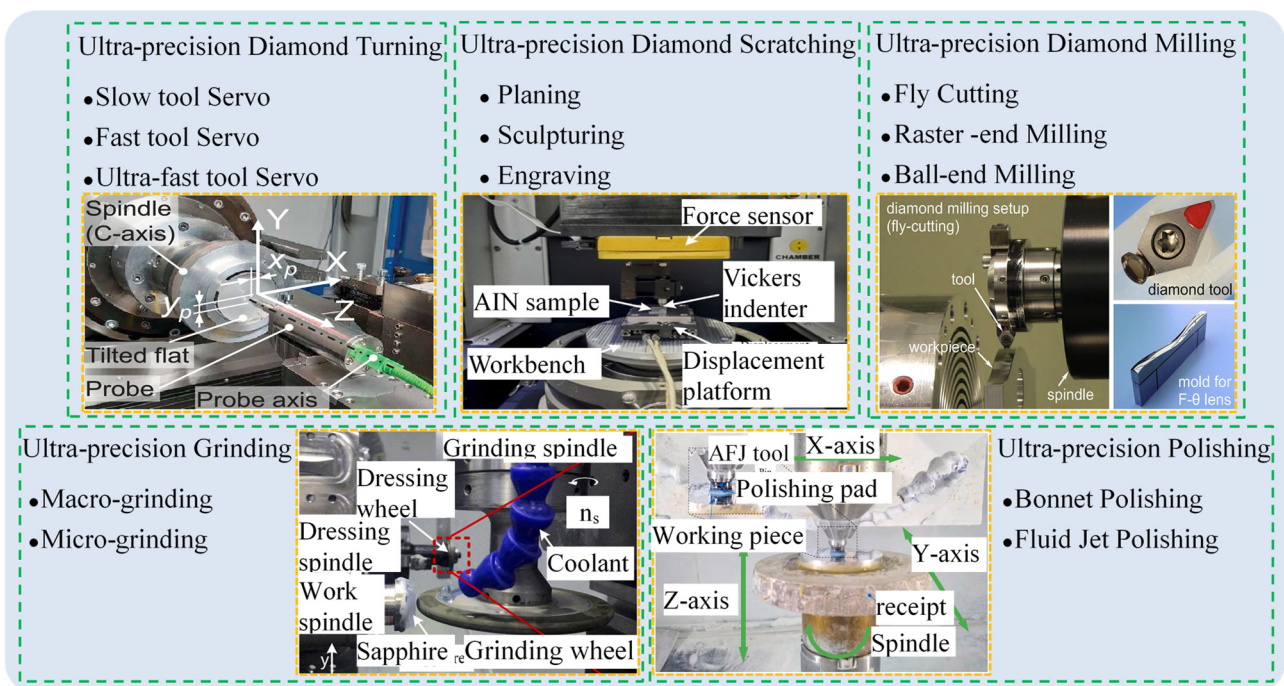


Figure 3. An overview of typical UPM methods. Reprinted with permission from Refs. [24,35,37–41].

Ultra-precision diamond turning, as a member of the UPM family, is generally employed for machining rotationally symmetric surfaces. To expand the application of turning, it is often combined with fast tool servo (FTS) technology or the slow tool servo (STS) system, where the feed depth can be dynamically adjusted and the positioning accuracy can be increased. As an assistive technology of turning, FTS system has high frequency response and high positioning accuracy. It has advantages for the surfaces with large change and complex structure machining, and the control system tracks the surface shape change in real

time to control and adjust each servo axis during machining. However, the focus of research is how to make the FTS with high frequency overcome the defect of short stroke. Similar to FTS, the STS system also expands machining performance of turning, it enlarges the Z-axis stroke, and increases the high-precision multi-axis linkage characteristic of the lathe. It is suitable for off-axis surface, array structure, and freeform surface machining. Whereas, since the STS turning generates the target surface shape according to the 3D tool path and the three-axis linkage, whether the surface can be processed depends on the generation of the tool path. On the basis of turning, ultra-precision fly cutting is developed, it is a cutting technology with constant cutting speed and more flexible cutting trajectory, which is suitable for specific micro-structures machining [42–44]. Nowadays, the micro-structures fabricated by UPM are more diversified, such as spherical/aspherical lens [45–47], multi-focal lens, Fresnel lens [48–51], polygonal mirror [52], pyramid array [53,54], micro-structure array [55], anti-reflection channel, and V-groove [56,57], etc. [58].

In this paper, different machining methods of micro-structured surfaces are compared and their characteristics are discussed. According to their typical advanced application as vital results of their micro-structures fabrication, the main research achievements of various machining strategies are reported. As an essential method of fabricating micro-structures, the characteristics and advantages of UPM are reviewed, and the application of diamond tool fabrication and improvement by focused ion beam technology are introduced. The subsequent sections review the studies and applications of FTS/STS combined with UPM to fabricate complex micro-structures, and the research of fly cutting in the fabrication of micro-structures is emphasized. This paper will provide theoretical guidance and develop new ideas for the fabrication of different micro-structures.

2. Fabrication Methods of Micro-Structured Surfaces

2.1. Lithography Technology

Lithography is based on an optical projection printing system, in which the image on the mask is reduced and projected onto a photoresist coated substrate (such as a silicon wafer) through a high numerical aperture lens system, and the image is transferred to the surface of the substrate through an etching process. The general process of lithography includes substrate pretreatment, gluing, pre-baking, exposure, development, post-baking, etching, degluing, and engraving, etc.

Lithography includes many categories, such as electron beam lithography (EBL) [59], X-ray lithography [60], ion beam lithography (IBL) [19], grayscale lithography, and extreme ultraviolet (EUV) lithography [61]. EBL uses an electron beam to trace a pattern on the resist medium. When a very narrow electron beam passes through, it changes the physical properties of the resist layer, resulting in the appearance of submicron characteristics. EBL has been most widely implemented for patterning mesoscopic structures or systems with unique advantages of high resolution in feature size, high reliability in machining, and high flexibility in pattern replication [1,62]. X-ray lithography has the ability to penetrate thick resistance and produce high aspect ratio patterns to achieve side walls with optical quality. This fabrication technique has been used to fabricate micro- and nano-structures from materials such as methyl methacrylate [63,64].

IBL mask is a transmission/scattering two-phase mask made of Si material. Ion beam exposure has higher sensitivity and higher exposure rate. Compared with electron beam, at the same acceleration voltage, ion beam exposure resolution is higher due to the shorter ion wavelength. The ions are much more massive than the electrons, therefore, there is no proximity effect in ions. Common IBL mainly includes focused ion beam (FIB) lithography and ion projection lithography (IPL). FIB lithography uses physical interactions between ions to modify the surface layer of the substrate. Depending on the weight of the ions used (typically gallium, Ga^+), the working beam current, and the acceleration voltage, FIB technology can not only perform ion implantation, but also perform imaging, and addition and subtraction processes. It is notable for its ability to process any material by surface erosion and is widely used in micro-technology and metrology. FIB has a considerable

advantage over EBL in terms of resolution when making high aspect ratio 3D structures. IPL is a mask process, it is suitable for mass production, mainly for repairing masks and writing directly to wafers [65,66].

To study the application of EBL and IBL, Palka et al. explored the applicability of As₅₀Se₅₀ thermal evaporation film in wet etching with amine solution in EBL and observed that the change of chemical resistance induced by light had the same trend as that induced by electron beam, and the chemical resistance increased significantly with the increase of irradiation dose. A diffraction grating with a period of 100 nm was prepared on As₅₀Se₅₀ film by EBL, as shown in Figure 4a [67]. Rius et al. studied the influence of electron beam and ion beam on CMOS circuit damage by local exposure of selected region and specific position around CMOS circuit. The importance of electron beam energy on exposure localization was studied, the optimal exposure conditions were determined, and the method of manufacturing monolithic nano-mechanical devices to CMOS circuit through EBL or IBL was presented, as shown in Figure 4b,c [68].

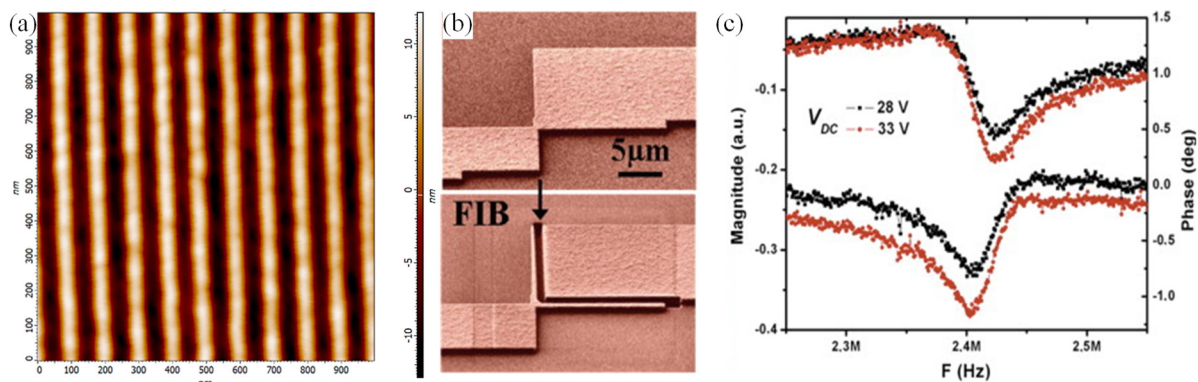


Figure 4. (a) Diffraction grating of 100 nm period prepared in As₅₀Se₅₀ thin film using EBL. (b) Nano-mechanical structures monolithically integrated into CMOS circuits have been fabricated with the combination of electron-and ion-beam lithography. (c) The compatibility of both fabrication processes is demonstrated from the electrical measurements of the nano-mechanical device in operation. Reprinted with permission from Refs. [67,68].

Micro-structures fabricated by lithography can be used in different fields. In terms of optical imaging, Bae et al. developed a new method for fabricating multi-focal micro-lens arrays with extended depth of field using multi-layer lithography and thermal reflux, providing a new approach for the development of various 3D imaging applications, such as light field cameras or 3D medical endoscopes [69]. Tong et al. used Monte Carlo simulation and EBL to study the grayscale lithography conditions systematically and copied resist as a template. The gold colored Kinoform lens B with a diameter of 200 μm and a height of 3.5 μm was successfully prepared by electroplating, as shown in Figure 5a. It has the advantages of high resolution lens and high focusing/imaging efficiency [70]. In terms of medicine, Au-Kathuria et al. fabricated polymer microneedle arrays by lithography, which provide potential applications in the delivery of low- and macro-molecular therapeutic drugs through the skin [71].

In order to solve and optimize the limitations and applications of EBL, different optimization methods have been proposed. EBL resolution below 10 nm is mainly limited by resistance contrast and proximity effect, Heusinger et al. used EBL to optimize the pseudo-stray light peak, also known as the “Rowland ghost”, and developed a method to improve the stray light performance of binary spectrograph gratings [72]. Andrea et al. used the focused helium ion beam to expose resist, which could reduce the perfect development of dense lines by 20 nm, thus compensating for the proximity effect. An optimized reactive ion etching process was used to demonstrate the pattern transfer of 10 nm line with aspect ratio of 10 in silicon, its images of scanning electron microscope (SEM) as shown in Figure 5b [73].

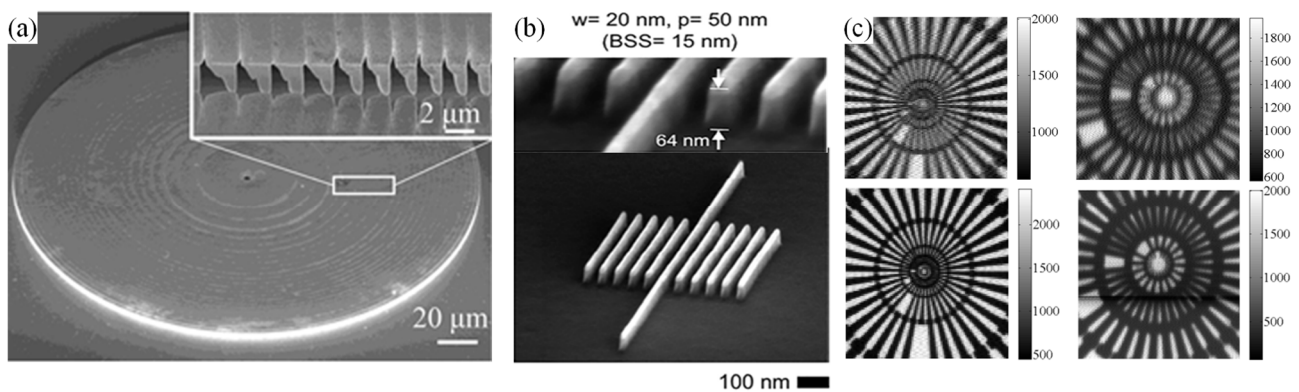


Figure 5. (a) A complete Au Kinoform lens and the insert gives the cross-sectional view of the plated zones. (b) SEM images of two examples of pattern transfer using the optimized reactive ion etching process at 80 V bias. (c) Images of 30 nm Siemens star by the 30 nm Fresnel zone plate in soft X-ray, taken with the scanning transmission X-ray microscope system. Reprinted with permission from Refs. [70,73,74].

When the width of the outermost region approaches 30 nm or less, electrodeposition of gold into EBL becomes increasingly difficult in the narrow grooves replicated in the resist. In this case, Zhu et al. studied the recent progress in the preparation of 30 nm Fresnel band sheets by EBL and controlled pulse voltage electroplating. Pulse electroplating instead of conventional direct-current has been attempted, and Siemens cluster imaging with the narrowest linewidth of 30 nm has been demonstrated in soft X-rays (706 eV) to verify system performance [74]. Figure 5c is a soft X-ray image of Siemens Star taken at 706 eV by self-made Fresnel zone plate.

Grayscale lithography displays 3D structures by modulation of ultraviolet (UV) exposure or control of UV dose through the mask to expand the lithography technology to 3D manufacturing [75]. However, it is only applicable to the manufacturing of 3D structures with small aspect ratio. For complex surface structures, it is not enough to achieve good machining accuracy [76]. The advantages of different technologies can be extended by combining different lithography and etching processes, Nachmias et al. described the use of grayscale lithography, reactive ion etching, or deep reactive ion etching to transfer patterns from grayscale resists to silicon substrates to fabricate Fresnel lenses efficiently [77].

EUV lithography uses EUV with a wavelength of 10–14 nm as a light source. EUV means that ultraviolet light is emitted from the K pole of the ultraviolet tube stimulated by electricity. It can extend lithography technology to less than 32 nm [78]. EUV is able to reflect optics, reflective masks, and vacuum environments, giving it an advantage over other lithography. EUV lithography is based on optical projection lithography, and the physical properties of 193 nm and 248 nm lithography can be directly applied to EUV. By employing an aggressive optical design with 0.45 numerical aperture and 0.32 numerical aperture, EUV can be extended to print half-pitch features of less than 22 nm. It is a reduced lithography technique, with a marking feature four times larger than the final pattern.

In addition, colloidal lithography is a very important technology for large surface area micro and nano fabrication; large area self-assembly of colloids without the need for expensive equipment can be achieved [79–82]. Liu et al. proposed an optimal demolding process to obtain high pattern transfer fidelity while avoiding distortion of soft imprinting molds and supports, and to effectively decrease the demolding force [83]. Olalla et al. proposed the use of colloidal lithography to map wavelength-sized pyramidal feature composition structures, and these top-coated structures as post-processing post-deposition solar cells to facilitate and expand their industrial applicability [84]. Centeno et al. proposed a simple, low temperature, low cost, and scalable colloidal lithography method for designing surfaces with effective light trapping and hydrophobic functions. The controllable nano/micro

structure of its surface features also produce strong anti-reflection and light scattering effects, which increase the average daily energy generation by 35.2% [85].

In summary, although the lithography technology has high resolution, it has high cost of lithography equipment. It is usually suitable for the preparation of 2D structured surfaces, not applicable for the fabrication of 3D complex micro-structures, especially curved surface structures. The development of X-ray lithography and grayscale lithography allow lithography methods to be initially applied to the preparation of 3D continuous relief micro-structured surfaces. However, it needs masks with high production cost, the complexity of 3D surface is limited, and the surface controllability is low. The characteristics of lithography technologies are summarized in Figure 6.

| Lithography | Advantages | Disadvantages | Applications |
|---------------------------------|--|--|---|
| Electron beam lithography | high resolution, flexible use without mask | high cost, slow etching speed, low output | make mask, small batch, special device production |
| X-ray lithography | fast speed, high resolution | difficult manufacturing, high cost | 3D structures and devices |
| Ion beam lithography | no mask, high resolution | limited exposure depth, difficult focusing | different processes according to ion energy |
| Grayscale lithography | 3D structures | low vertical resolution, low accuracy | 3D structures with small aspect ratio |
| Extreme ultraviolet lithography | high resolution, can be mass-produced | high cost, mask is difficult to make | 2D structures |

Figure 6. The characteristics of lithography technologies.

2.2. High Energy Beam Direct Writing Technology

High energy beam direct writing technology is a non-contact machining technology, which changes the material state and property, realizing shape control and performance control through the interaction of high energy density beam and material. High energy beam refers to the directionally transmitted high density energy beam in free space, including laser beam, electron beam, ion beam, etc. It has controllable energy, beam density, time, and space. High energy beam direct writing can produce complex structures by non-contact and selective multi-scale control or material state change. Since time and space can be manipulated, it is possible to create complex 3D structures [20]. Among them, laser direct writing technology uses laser beam with variable focusing energy and focusing position to expose anticorrosive materials and form surface relief or 3D structures on them [15,86]. The basic working principle of the laser direct writing system is to use the computer to control the high precision focused beam to scan accurately and write the designed graphics directly on the photoresist [87,88]. As an important micro-machining technology, laser direct writing technology has the advantages of high precision, strong 3D machining ability, no mask, and high production efficiency, which is conducive to the production of high precision and complex micro-optical devices and meets the development requirements of micro-optical technology. Xu et al. used focused ion beam direct writing (FIBDW) method to prepare the star structures of spokes with a width of 25 nm~16 μm , as shown in Figure 7, which is applicable to the comparison of resolution measurement methods [89]. However, the machining efficiency of this method is low, which has advantages for small size precision micro-structures machining. Mizue et al. used femtosecond laser pulses to rapidly heat and reduce glyoxylic acid metal (Cu, Ni, and Cu/Ni mixed) complexes on

glass substrates and directly write patterns of Cu, Ni, and Cu-Ni alloys without significant oxidation. This direct writing technique of pure metal and alloy allows various sensors to be printed in air [90].

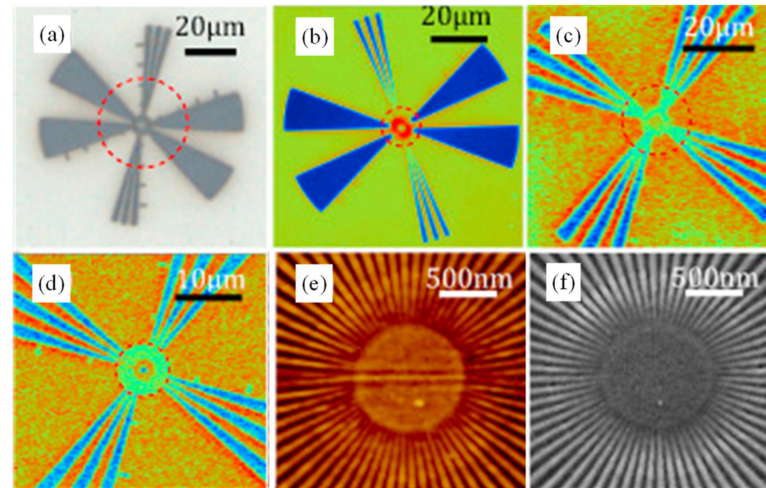


Figure 7. Star structures measured by various methods. (a,b) Star I measured by confocal laser scanning microscope with $427\times$ and phase shifting interferometry with $503\times$, respectively; (c,d) Star II measured by vertical scanning interferometry with $201\times$ and $503\times$, respectively. (e,f) Star center measured by SEM and AFM, respectively. Reprinted with permission from Ref. [89].

In summary, some high energy beam manufacturing technologies are capable of producing complex 3D structures with high resolution. For example, current electron beam manufacturing technologies have been able to produce smaller fine structures. However, high energy beam manufacturing is based on “point scanning” manufacturing technology, which has low machining efficiency and can only be used for the preparation of micro-structured surfaces with very small size.

2.3. Special Energy Field Machining Technology

Electromagnetic machining technology [21] and ultrasonic machining technology [91] can be classified as special energy field machining. Ultrasonic machining removes materials by means of ultrasonic frequency tools with small amplitude vibration in the abrasive liquid medium or dry abrasive, abrasive impact, polishing, and cavitation [92,93]. Along a certain direction of the tool or workpiece is subjected to ultrasonic vibration to carry out vibration machining, the workpiece surface materials to be processed mainly under the action of mechanical impact peeling, accompanied by polishing and super cavitation finally realize the forming process [94,95]. The workpiece is bonded to each other by ultrasonic vibration. The material removal rate is enhanced through the combination of ultrasonic vibrations and abrasive slurry actions [96,97]. It has a wide range of applications and is not limited by the electrical conductivity of materials. Special energy field machining has advantages of high strength and hardness, which can effectively solve the problem of difficult-to-cut materials [98,99]. It can obviously reduce the machining damage of cutting force, reduce tool wear, avoid surface microcrack, and improve surface machining quality and efficiency. It can machine not only hard alloy and other metal materials, but also non-metallic hard and brittle materials such as ceramics, glass, and gemstones. However, it is only suitable for the machining of simple micro-structures with low machining resolution [100]. Schematic diagram of the combined ultrasonic vibration assisted milling and minimum quantity lubrication methods is shown in Figure 8.

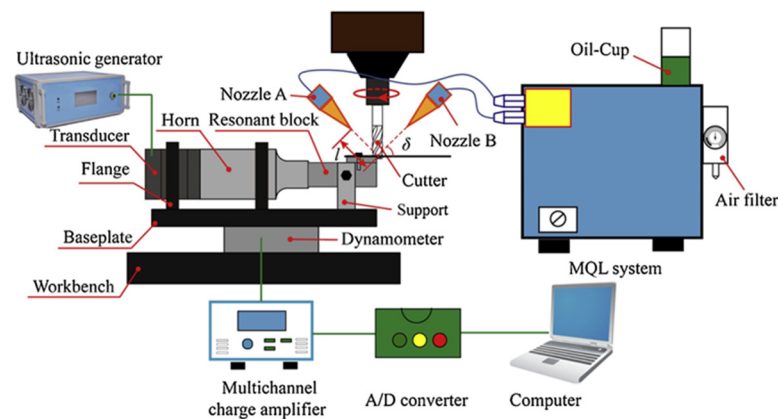


Figure 8. Schematic diagram of the combined ultrasonic vibration assisted milling and minimum quantity lubrication methods. Reprinted with permission from Ref. [101].

In conclusion, special energy field machining, including electromagnetic machining and ultrasonic machining, can be applied to ceramics, glass, and other brittle materials. However, it has low machining resolution. It can only be used for machining simple micro-structures such as micropores, but not for the fabrication of 3D complex micro-structured surfaces.

2.4. Molding Technology

Molding technology, hot pressing technology, and injection molding technology [102,103] can be unified as molding technology. Molding technology involves placing the plastic in the mold for heating to await plastic softening. Molding out of the workpiece is in line with the requirements of use under the external pressure. It is suitable for thin flat optical lenses, such as micro-lens arrays. The principle of molding equipment is simple and used for production of multiple varieties and small batches. Therefore, it has economic advantages in the manufacturing of experimental supplies and the research of optical plastic materials, and also shortens the experimental period. Hot pressing technology must go through several stages such as heating and heat preservation, hot pressing, slow cooling, and demolding. It has the advantages of high efficiency, is suitable for mass production of various optical devices, especially aspheric lens, lens array, and diffraction lens, and it is environmentally friendly and pollution-free. However, there is morphological deviation after machining. This kind of method has relatively simple equipment requirements, short machining cycle, and mass production, which is conducive to industrialization. It is widely used in the machining field of optical components with low precision requirements, such as freeform surface components for lighting. However, this method has strict requirements on technological parameters and process, and the accuracy of the product is related to the accuracy of the mold; whereas other machining methods are required to provide high-precision molds [104].

In order to optimize the method of machining high-precision products by injection molding technology, Guo et al. developed an online decision system consisting of a new reinforcement learning framework and a self-predictive artificial neural network model. The system has good convergence performance in lens production and the decision model has better robustness and effectiveness in the online production environment. Figure 9 presents the warpage results of different process conditions [105]. Warpage is one of the serious defects of thin-wall injection parts. Wang et al. used dynamic filling and filling process parameters as new design variables for the first time to optimize the warpage design. The ambiguous functional relationship between the target (maximum warpage) and the 12 process parameters was approximated by the Kriging proxy model. An efficient global optimization method (expected improvement method) is used to search for optimal solutions. Finally, a set of dynamic injection molding process parameters were given, through which the maximum warpage of plastic parts could be greatly reduced [106].

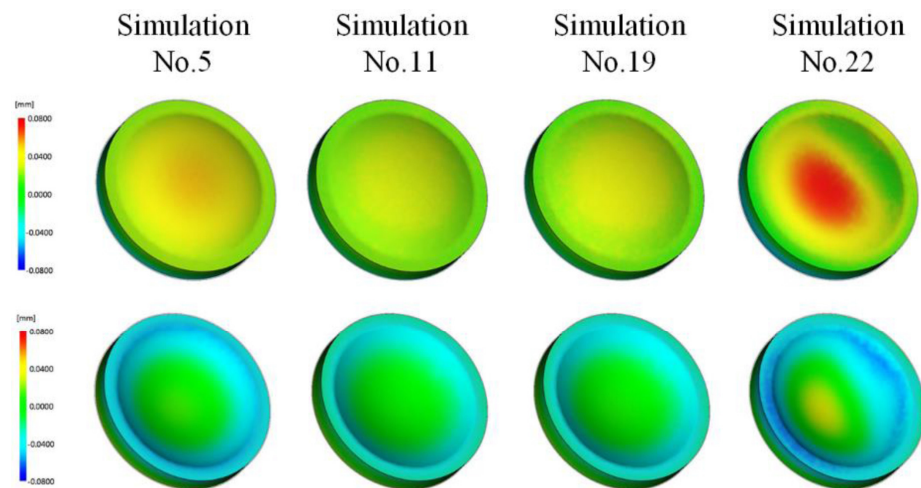


Figure 9. The warpage results of different process conditions. Reprinted with permission from Ref. [105].

2.5. LIGA Technology

LIGA technology [22,107] is a combination of lithography, molding, and injection molding technology. LIGA technology is short for German Lithographie Galvanformung and Abformug. It mainly uses X-ray deep exposure, micro-electroforming, micro-plastic forming, and other technologies to carry out micro-mechanical machining. LIGA technology can fabricate structures with large aspect ratios, up to submicron in width and hundreds of microns or even millimeters in depth, making it suitable for complex micromechanical structures [108,109]. It can be used in a wide range of materials, including metal, plastic, polymer materials, glass, ceramics, and they can also be combined. At the same time, the micro-structure obtained by LIGA technique has well-defined geometry and dimensions, straight and smooth sidewalls, and tight tolerances [110]. Polymer structures with high precision can be obtained through plastic casting after metal molds are obtained by X-ray deep exposure and micro-electroforming, which is suitable for large-scale production. It can be applied to the deep micro-structure of many research and development departments and industrial products [111]. However, LIGA technology requires expensive machining equipment, and it is difficult to fabricate micro-structures on curved substrates. Ma et al. fabricated multi-layer metal micro-structures with high precision and high quality by using ultraviolet (UV)-LIGA overlay processes, including mask manufacturing, substrate machining, and UV-LIGA overlay technology. The electroplating images of its multi-layer metal micro-structure are shown in Figure 10 [112].

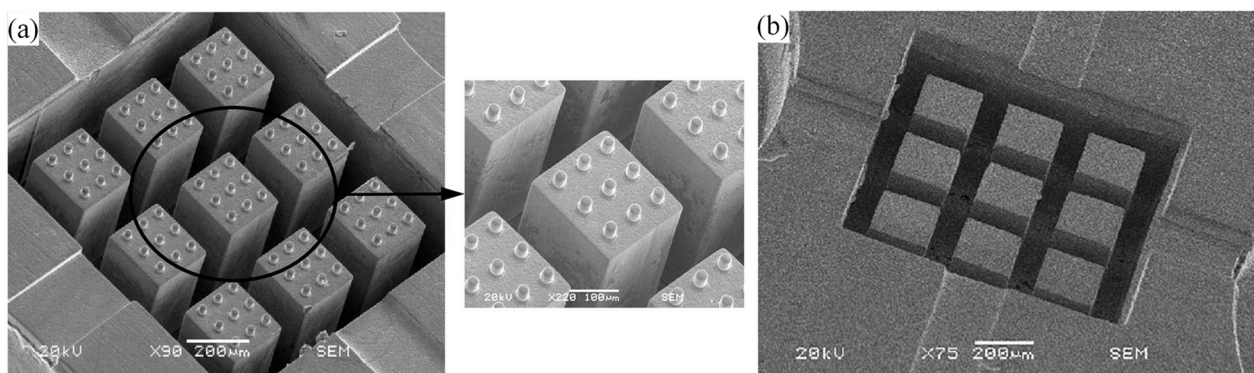


Figure 10. (a) SEM images of the multi-layer metal micro-structure was fabricated using UV-LIGA overlay technology; and (b) SEM image of the first layer micro-structures. Reprinted with permission from Ref. [112].

2.6. Ultra-Precision Machining Technology

2.6.1. Applications of Ultra-Precision Machining Technology

UPM includes ultra-precision diamond turning (turning classification as shown in Figure 11), scratching, milling, ultra-precision grinding, and polishing. The UPM technology is based on a diamond tool with a sharp cutting edge, high hardness, good wear resistance, ability to realize ultra-thin cutting thickness, and other characteristics. Diamond cutting is the most representative method of UPM.

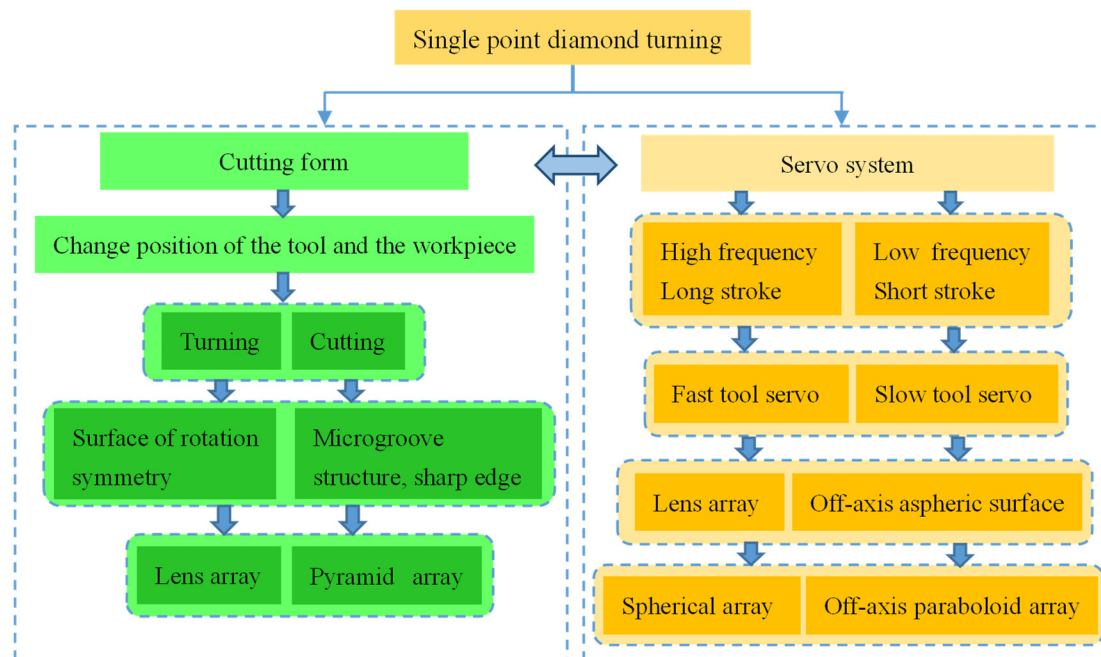


Figure 11. Classification of single point diamond turning.

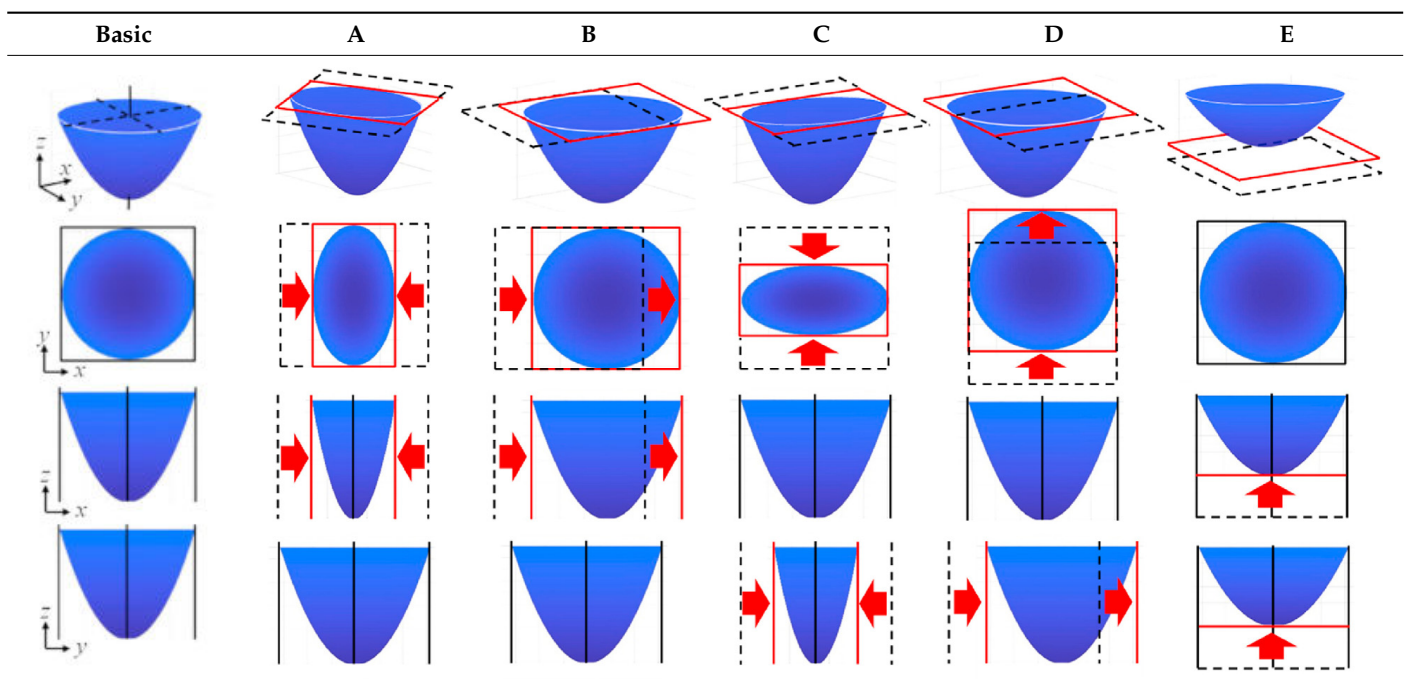
Natural diamond is regarded as an ideal tool material because of its excellent properties, such as high hardness, high thermal conductivity, low coefficient of friction, high wear resistance, and low affinity with non-iron metals [16,113]. Due to these great tool cutting edge performances, ultra-precision diamond cutting can machine various freeform surfaces and complex optical components, and generate complex optical surfaces by manipulating the cutting depth within the micrometer range. Moreover, diamond tools have inherent tool nose radius, clearance angle, rake angle, and different tool geometry, which plays a key role in mathematical calculation and experimental preparation [114]. Moreover, ultra-precision diamond cutting has an effective tool path generation strategy for complex surface structures, which has great advantages in the machining of micro-structures [114–116]. Early diamond tools were limited to machining soft and malleable non-ferrous metal materials, such as aluminum and copper [117]. At present, ultra-precision diamond cutting has been extended to silicon, steel, and other difficult-to-cut materials [23], which have special functions and meet the needs of optical, semiconductor, mold, and other industries [118–120]. However, rapid tool wear is still a problem to be solved.

Ultra-precision diamond turning technology is generally termed single point diamond turning. The relative position of the tool and the workpiece is precisely controlled by the computer numerical control system of the lathe to turn, which can directly fabricate high-precision complex surface optical components. Turning technology is mainly used for machining infrared crystal, non-ferrous metal, and part of the laser crystal and optical materials such as plastic optical element. It can machine complex surface shape or special surface form of optical element, such as high order aspheric, diffraction optical element, the diffraction hybrid optical element such as rotational symmetry complex curved surface, and

can also fabricate micro-lens array, precision die, micro-pyramid array, freeform surface, and other non-rotational symmetric surfaces [121].

The researchers developed different cutting methods based on turning. Shigeru et al. proposed a new method for single point diamond turning micro-cavity array based on fast tool servo (FTS). A computer program was developed to control the tool path, periodically arrange small quadrics on the large curved surface, and adjust the position, height, and size of each surface by using random values. Its dynamic range was preset to control spatial differences. The rotary steerable system was machined by continuous cutting method and subsection cutting method, respectively. The designed cutting method improved the edge accuracy and the form error was controlled below 10 nm level PV [122]. The basic shape of the quadric can be changed by changing the value of each coefficient of the quadric function, as shown in Table 1.

Table 1. The basic shape of a quadratic surface and typical shape changes obtained by varying the value of each coefficient of the quadratic surface function. Reprinted with permission from Ref. [122].



Ultra-precision diamond scratching is a fundamental approach to investigating surface integrity [123]. It can create the complex micro-structured surfaces such as three-focus Fresnel lens, micro cube corners, and freeform micro-lens array under the C-axis mode for re-orientating or re-positioning. In the machining, the cutting process is mainly controlled by linear slide servo motions and the C-axis is only used to orientate or position workpiece or diamond tools. Its material removal rate is also relatively low [35]. T. Moriya et al. fabricated curved V-shaped microgrooves with two flat-ends on a curved surface by using a six-axis controlled non-rotational cutting tool [124]. Y. Takeuchi et al. studied the method of designing and manufacturing micro Fresnel lenses with non-rotational diamond cutting, which can accurately and neatly produce multi-focus micro Fresnel lenses without any burrs [125]. Afterward, his team also developed a six-axis control machining CAM system using a non-rotational cutting tool. The system is used to generate microgrooves on sculpted surfaces [126].

Milling is a technology that uses workpiece fixation and tool rotation to obtain surface shape. Ultra-precision milling is generally used with a diameter of less than 50 μm milling cutter, tool materials are usually natural diamond, tungsten carbide, cubic boron nitride (CBN), etc. Machining workpiece materials are copper, aluminum, titanium, steel, and

other non-ferrous metals. It is usually used for end milling on ultra-precision five-axis machine tools, which is suitable for machining freeform surfaces, but it is difficult to install and adjust the workpiece. The surface shape is affected by the size of the milling cutter. The machined surface has a large roughness value and a long machining cycle, thus expensive multi-axis ultra-precision machine tools are needed. To improve cutting performance, Chen et al. designed a miniature end milling cutter for machining GH4169, a nickel-base superalloy with high stiffness and sharpness. One-dimensional finite element method was used to determine the optimal geometric parameters of the cutter. Polycrystalline diamond (PCD) micro end milling cutter with better cutting performance was prepared by laser-induced graphitization assisted precision grinding method [101]. Owen et al. proposed an error reduction method based on manual, using spherical artifact to establish the tool error model, and applied it to the free surface machining [127].

Grinding is the process of removing excess material from the workpiece with abrasives and tools. The machining surfaces of the workpiece processed by diamond grinding show obvious peak-valley interphase structure and the surface does not appear the situation of tool copying. The workpiece surface integrity of grinding is good and the degree of subsurface damage is low. Therefore, grinding is suitable for some specific crystal materials. However, due to the wear and dressing error of grinding wheel, the machining accuracy is affected. Yu et al. established a three-axis linkage orthotic model of diamond grinding wheel and used true diamond grinding wheel to grind the aspherical structure array of tungsten carbide. An online shaping method of ultra-thin arc-shaped diamond grinding wheel was proposed, which can achieve the expected arc radius of grinding wheel, realize efficient and accurate grinding of non-binder carbide die, and obtain the surface of tungsten carbide aspherical micro-structure array with shape accuracy of $15\ \mu\text{m}$. The micro-structure array is shown in Figure 12 [55]. Luo et al. studied the wear process of metal-bonded diamond grinding wheel in the process of sapphire single crystal surface grinding to find the mechanism of the influence of grinding wheel wear on workpiece surface quality [128].

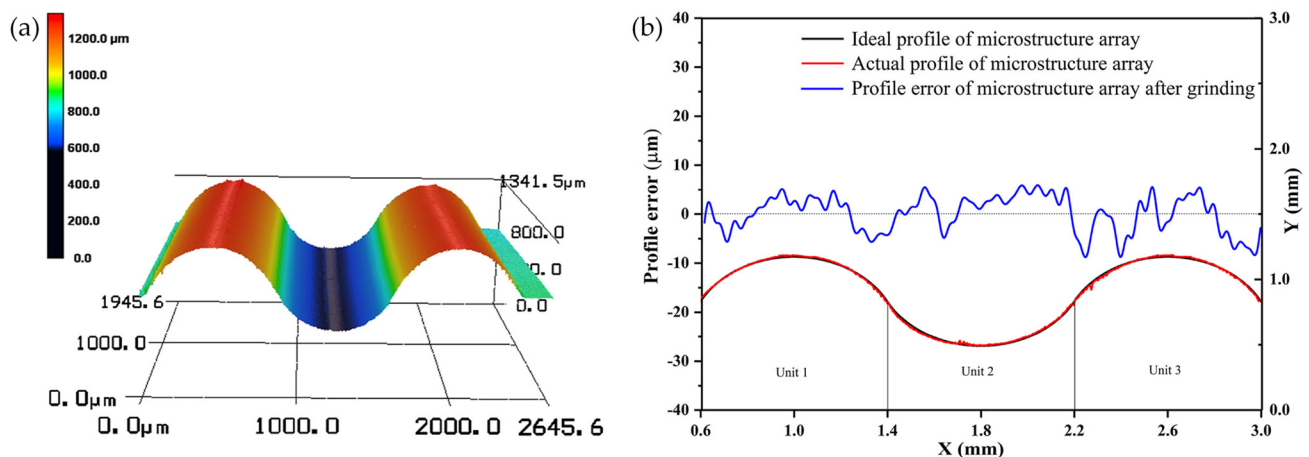


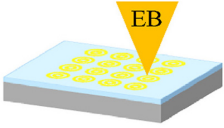
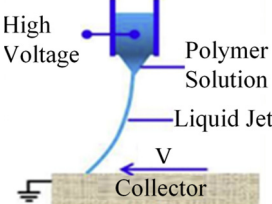
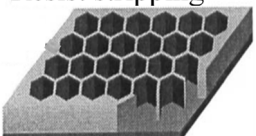
Figure 12. (a) Laser scanning microscope photos of the micro-structure array workpiece after fine machining; and (b) profile accuracy of the micro-structure array. Reprinted with permission from Ref. [55].

Polishing is usually one of the last processes of UPM, which can eliminate the surface and sub-surface damage of the machined parts and improve the surface shape. In the process of machining, it is inevitable to leave sharp points and stripes on the workpiece. These machining marks or chip residues must be removed by the polishing process [129]. Ultra-precision polishing is widely used in high-precision surface finish machining with high form accuracy and good surface roughness. Meng et al. proposed a new method for machining ultra-high precision textured surfaces from silicon carbide materials. The grooves and pits of two different sizes were compared. It is found that groove texture has a greater effect on polishing quality than pit texture at the same size [130]. Wang et al.

proposed an ultra-precision numerical control polishing method based on the principle of water dissolution, which uses small polishing tools to process large KDP surfaces [131]. Cheung et al. conducted theoretical and experimental studies on computer controlled ultra-precision polishing of the structure surface and established a model-based simulation system for structure surface generation, which was able to predict the shape error and pattern of 3D textures generated by computer controlled ultra-precision polishing [132]. Xu et al. proposed a novel computer controlled ultra-precision polishing hybrid manipulator, which is suitable for freeform surfaces polishing [129].

The characteristics of different micro-structures manufacturing methods are summarized in Table 2.

Table 2. Comparison of different fabrication methods for micro-structured surfaces. Reprinted with permission from Refs. [20,97,101,133–137].

| Method | Classification | Advantage | Disadvantage | Schematic Diagram |
|---|--|--|--|--|
| Lithography | <ul style="list-style-type: none"> • electron beam • X-ray • ion beam • grayscale • extreme ultraviolet | <ul style="list-style-type: none"> • high resolution • mass produce | <ul style="list-style-type: none"> • high cost • difficult masks |  <p>EBL (2nd lithography) on the lens array</p> |
| High energy beam direct writing | <ul style="list-style-type: none"> • laser beam • electron beam • ion beam | <ul style="list-style-type: none"> • high precision • 3D machining • no mask | <ul style="list-style-type: none"> • low efficiency • not for large size |  |
| Special energy field machining technology | <ul style="list-style-type: none"> • electromagnetic • ultrasonic | <ul style="list-style-type: none"> • wide applications • no electrical conductivity • hard materials | <ul style="list-style-type: none"> • simple structure • low resolution |  |
| Molding technology | <ul style="list-style-type: none"> • molding • hot pressing • injection | <ul style="list-style-type: none"> • simple equipment • short cycle • mass produce | <ul style="list-style-type: none"> • strict requirements • difficult mold |  <p>Resist stripping</p>  |
| LIGA technology | <ul style="list-style-type: none"> • a collection technology | <ul style="list-style-type: none"> • high aspect ratio structures • wide available materials | <ul style="list-style-type: none"> • high cost • not for curved structures |  |
| Ultra-precision machining technology | <ul style="list-style-type: none"> • turning • scratching • milling • grinding • polishing | <ul style="list-style-type: none"> • high precision • high efficiency • one-time molding • complex surface | <ul style="list-style-type: none"> • not for ferrous metal |  |

2.6.2. Studies of Diamond Tools by Focused Ion Beam Technology (FIB)

Due to the high precision of UPM, the machining quality is easily affected by various factors, such as precision machining lathes, cutting tools or grinding wheels, machining methods and parameters, machining objects, fixtures, and external environment. In ultra-precision cutting, the quality of cutting edge determines the machining quality as a tool that directly contacts the machined material. Natural single crystal diamond is generally selected as ultra-precision cutting tool material, mainly due to its own wonderful physical and chemical properties, such as high hardness, high wear resistance, good thermal conductivity, etc. FIB technology is an important method to prepare diamond tools. In recent years, the focused ion beam technology, which utilizes high-intensity focused ion beam to nano-machining materials, has become the main method for nanoscale analysis and manufacturing, combined with real-time observation by high-multiple electron microscopy such as SEM [71]. It has been widely used in diamond tool preparation, semiconductor integrated circuit modification, cutting, and fault analysis.

FIB system is a micro-cutting instrument that uses an electric lens to focus ion beam into a very small size, which can achieve material stripping, deposition, injection, cutting, and modification. At present, the ion beam of commercial systems is liquid metal ion source. The metal material is Ga because of its low melting point, low vapor pressure, and good oxidation resistance. Typical ion beam includes liquid metal ion source, lens, microscope scanning electrode, the secondary particle detector, 5–6 specimens of axial moving base, vacuum system, vibration resistance, magnetic devices, electronic control panel, and computer hardware equipment. Applying an electric field to the liquid metal ion source can make the liquid metal form a small tip, and the negative electric field is added to pull the metal or alloy at the tip, thus leading to the ion beam. The ion beam is focused through an electrostatic lens and passes through a series of automatic variable aperture (AVA) to determine its size. The desired ion species were screened by $E \times B$ mass analyzer. The ion beam is focused on the sample and scanned by an octupole deflector and an objective lens. The ion beam bombards the sample. The resulting secondary electrons and ions are collected and imaged using physical collisions to cut or grind.

There are several main functions in FIB technology. In the IC production process, if it is found that there are some errors in the etching of the micro-circuit, the original circuit can be cut by FIB, then the fixed area is sprayed with gold and connected to other circuits to achieve circuit modification, with the highest accuracy up to 5 nm. In addition, if there are micro and nano-level defects on the surface of the product, such as foreign bodies, corrosion, oxidation, and other problems, it is necessary to observe the interface between the defect and the substrate. Using FIB, the defect location section sample can be accurately positioned and cut, and the interface can be observed by SEM. For micron size samples, after surface treatment to form a film, it is necessary to observe the structure of the film and the degree of combination with the base material, using FIB cutting sample preparation, and then using SEM observation.

Different studies have been carried out to explore the characteristics of FIB technology. In order to obtain the specific tool geometry, diamond grinding wheel is an effective method for machining hard metals, with WC-Co carbide as the main material of the die. Yang et al. characterized the grinding damage of WC-Co class by FIB tomography, as shown in Figure 13a [138]. Rubanov et al. applied high pressure and high temperature annealing to graphitize the diamond implanted layer formed by a 30 keV Ga⁺ FIB. The implanted layer was studied by electron microscopy. The influence of ion implantation on diamond structure is studied by using electron microscope imaging and spectroscopy, as shown in Figure 13b,c [139]. Tong et al. established a large-scale multi-particle molecular dynamics simulation model to study the dynamic structure changes of single crystal diamond under 5 keV Ga⁺ irradiation, combined with transmission electron microscopy (TEM) experiments. Figure 13d shows the TEM section image of diamond sample irradiated by 5 keV Ga⁺ [140].

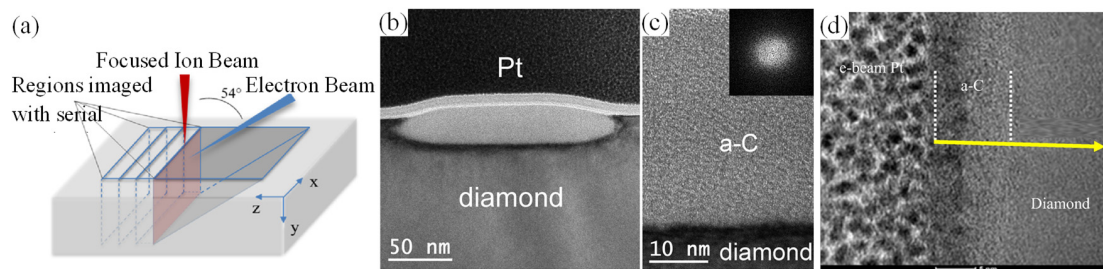


Figure 13. (a) Schematic of FIB serial sectioning process, (b) bright field image, (c) high resolution electron microscopy image with fast Fourier transformation on the inset of implanted layer with Ga fluence of 4×10^{15} ions/cm² and (d) TEM images of damage region after 5 keV Ga⁺ irradiation with fluence of 1.0×10^{18} ions/cm². Reprinted with permission from Refs. [138–140].

FIB can be used with the preparation of anisotropic wetting surfaces; Wu et al. proposed a new method for high-throughput preparation of anisotropic wetting surfaces with good transparency and developed a multi-step FIB machining method to achieve accurate and reliable machining of non-conductive materials such as single crystal diamond tools. Figure 14 shows the evolution of tool tip microfeatures in FIB multi-step milling. The tool is used to process a variety of substrates, from metals to plastics, under a variety of conditions. All machined surfaces exhibit significant anisotropy at contact angles, being hydrophobic in one direction and highly hydrophobic in the other. It is found that anisotropic wettability depends only on micro-structure design and material properties. This method can produce anisotropic wetting more quickly than other methods [141].

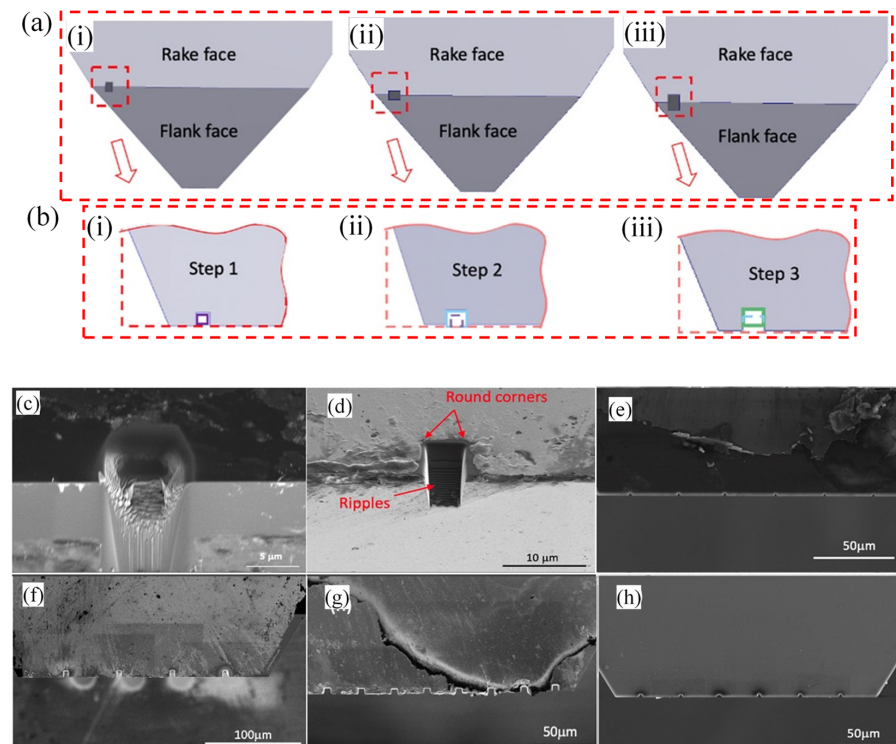


Figure 14. (a) Schematic of evolution of the micro-features on the tool tip during the multistep FIB milling process, (b) schematic of the corresponding top view of the three steps, (c) SEM image of diamond tool milled by FIB conventionally in a single step, (d) SEM images of diamond tool milling by FIB with multi-step with ripples and round corners. (e) Tool #1 with $1 \mu\text{m} \times 1 \mu\text{m}$ grooves and $30 \mu\text{m}$ spacing, (f) tool #3 with $5 \mu\text{m} \times 8 \mu\text{m}$ grooves and $50 \mu\text{m}$ spacing, (g) tool #4 with $5 \mu\text{m} \times 5 \mu\text{m}$ grooves and $20 \mu\text{m}$ spacing, (h) tool #2 with $2 \mu\text{m} \times 2 \mu\text{m}$ grooves and $30 \mu\text{m}$ spacing. Reprinted with permission from Ref. [141].

FIB can be used to study diamond tool damage. Tong et al. studied the effect of FIB on the damaged layer of single crystal diamond tool under different FIB treatment voltages by TEM measurement and molecular dynamics simulation [142]. Takenori et al. studied the sharpening of the cutting edge of a single crystal diamond tool by an argon ion beam machine tool; the etching rate could be changed by changing the irradiation angle of the beam on the processed surface [143].

FIB can also be used to prepare and improve diamond tools with different requirements. Wei et al. can produce diamond tools with edge radius of nanometer by FIB technology, which can be used for UPM. The schematic diagram of tool edge radius is shown in Figure 15. In the nano-cutting process, the ratio of the minimum chip thickness to tool edge radius is about 0.3~0.4 [144]. Wang et al. proposed a new cutting method based on force modulation method for multi-tip diamond tools to process micro-structured surfaces, its cutting schematic diagram is shown in Figure 16. A multi-tip diamond tool with periodic sinusoidal micro-structure was prepared by FIB technology [145].

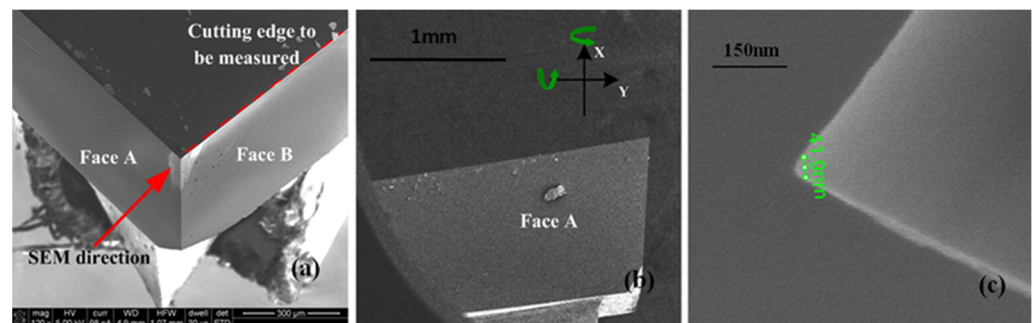


Figure 15. Field emission scanning electron microscopy measurement of the tool edge radius. (a) the cutting edge, (b) the error factors may come from the rotation of X and Y axes for the platform that fix the tool to be fabricated, (c) the measurement setup and result of a diamond tool developed by FIB with edge radius less than 20.95 nm. Reprinted with permission from Ref. [144].

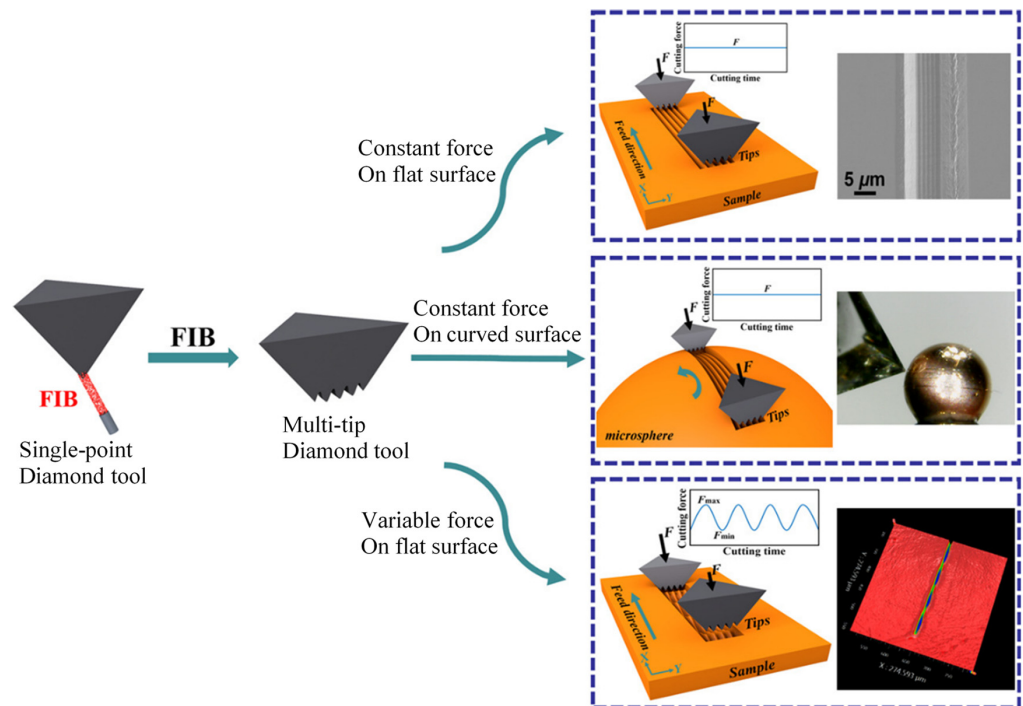


Figure 16. Schematic representation of multi-tip diamond tool cutting. Reprinted with permission from Ref. [145].

Kawasegi's research team had performed a lot of research on the preparation of diamond tools by FIB technology. Kawasegi et al. proposed a fabrication method for diamond tools with surface textures. In order to improve the machining performance of diamond tools, a texture with a depth of 43 nm and a width of 1.8 μm was prepared by FIB on the front surface of diamond tools, and heat treatment was carried out, as shown in Figure 17. Compared with femtosecond laser and direct FIB sputtering, this method has a better cutting effect on diamond tools. Due to the high resolution of FIB irradiation, FIB-induced non-diamond phase can be removed to avoid adverse effects on cutting performance [146]. Kawasegi et al. describe a technique to improve diamond tools for nanometer- and micrometer-scale machining and forming by FIB micromachining. Figure 18a,b shows NiP surface machining using FIB and processed tools [147]. Although the FIB technique is an effective means to fabricate nanometer- and micrometer-scale tool shapes, ion irradiation can lead to doping, defects, and reduce tool performance. Kawasegi et al. used 500°C heat treatment combined with aluminum deposition to remove Ga ions caused by ion irradiation in order to process FIB on a single crystal diamond tool without degrading the tool performance. The method was evaluated by machining aluminum alloy and NiP. The surface morphology of NiP is shown in Figure 18c–e [148].

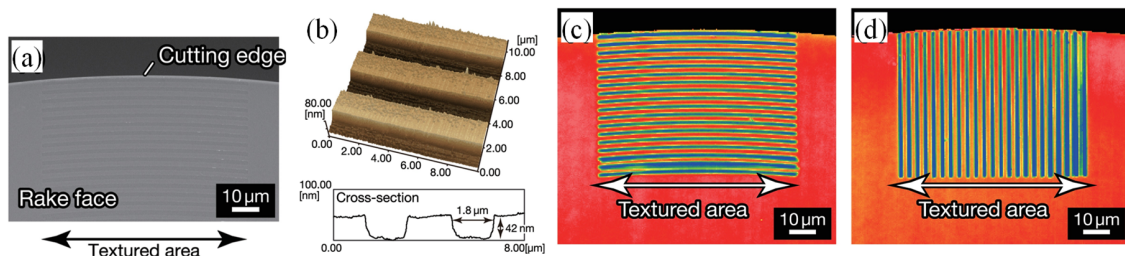


Figure 17. Textured diamond cutting tool fabricated by FIB irradiation and subsequent heat treatment. (a) SEM image of the rake face of the textured diamond cutting tool surface; (b) enlarged image of the texture measured by atomic force microscope. Surface topography of the rake faces textured in the; (c) perpendicular; and (d) parallel directions and measured with a coherence scanning interferometer. Reprinted with permission from Ref. [146].

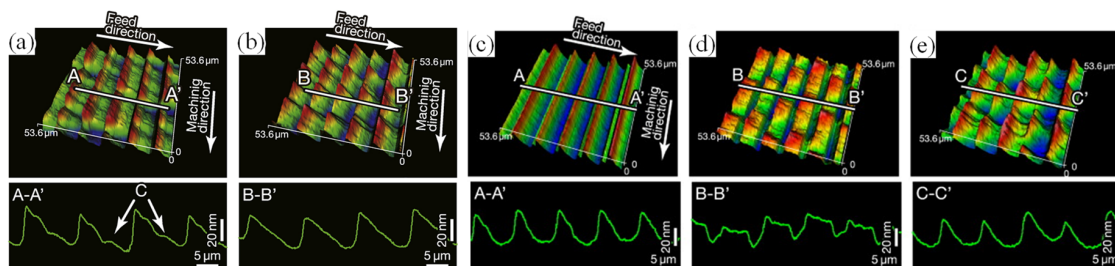


Figure 18. Cross-sectional images of the NiP surface following machining using the (a) FIB tool; (b) heat-treated tool, with a cutting distance of 19,040 m. Surface topography of the NiP surface after machining with; (c) non-FIB; (d) FIB; and (e) treated tools, measured using a white light interferometer. Reprinted with permission from Refs. [147,148].

3. Fast/Slow Tool Servo Technology

3.1. Fast Tool Servo (FTS)

With the continuous improvement of the requirements for micro-structured functional surfaces, traditional machining methods have been unable to meet the requirements of machining efficiency and accuracy. UPM technology combined with FTS has been developed and applied to the important machining methods of complex micro-structured functional surfaces [149].

FTS system is an independent closed-loop operating system, which is mainly composed of a FTS device and controller. In recent years, the guiding mechanism, actuator,

and displacement sensor are the key components of FTS devices that have attracted the most attention. Various mechanical structures and actuators, high-performance controllers and trajectory tracking control algorithms are needed to control FTS devices to obtain high precision, high bandwidth, and high motion resolution. In addition, the tool path and machining parameters of a given freeform surface need to be calculated and optimized. The 3D surface topography of micro-structures such as lens array can be represented by cylindrical coordinates. The coordinates of each point on the surface are represented by three variables, spindle rotation angles, shaft feed, and tool feed. Before machining, preset the spindle speed and feed rate, then according to the tool path to discretization of micro-structure surface form, get the points on the tool path of cylindrical coordinates. According to the spindle speed and feed speed set before, the micro-structure machining is controlled synchronously by c-axis encoder cutter servo cutting motion and C-axis rotation. The FTS module and its control system are the core of the whole machining system. By collecting the angle signal of the rotary spindle, the control system can control the precision feeding movement of the diamond tool with high frequency and short stroke in real time, so as to complete the machining of the 3D profile of the workpiece.

The FTS system has the characteristics of high stiffness, high frequency, and high positioning accuracy, which is suitable for machining complex micro-structures with large surface changes or discontinuous parts and short stroke. The feed frequency of the FTS module can reach more than 1 KHz. It has gradually developed into one of the mainstream technologies of micro-structured surface machining from the error compensation of the original ultra-precision lathe.

Researchers are constantly developing and optimizing the FTS system to improve the machining performance. Tong et al. developed a freeform surface micro-groove machining system based on a FTS machining and measuring platform. It can synchronize and control all integrated sensor systems and CNC machine tool systems to achieve closed-loop process control for freeform surface manufacturing and metering. From improving tool alignment accuracy ($<1 \mu\text{m}$), fast data synchronization and conversion, integrated machine surface measurements and surface feature functions, including lens surface micro-grooves and Alvarez lens measurements, as shown in Figure 19 [150]. Zhong et al. developed a special controller with internal data machining algorithm, and successfully integrated online surface measurement into the ultra-precision FTS system by adjusting and synchronous data flow, which greatly improved the measurement efficiency and machining accuracy [151].

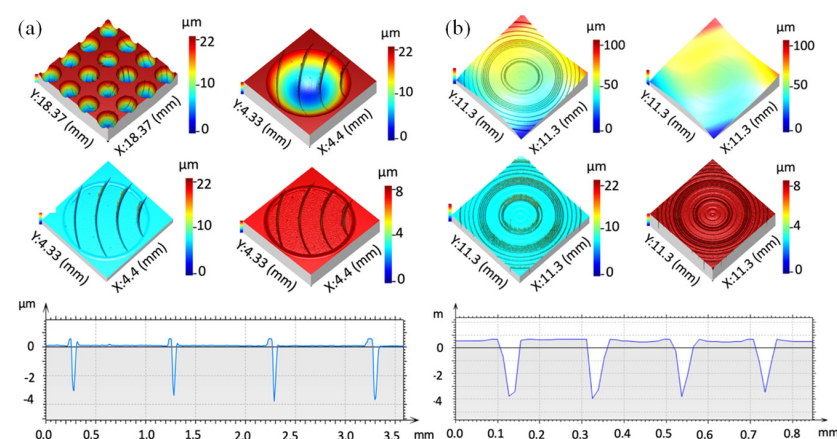


Figure 19. (a) Surface characterization of machined 4×4 lens array with micro-grooves: overview of lens array with micro-grooves, a single lens with micro-grooves, after form removal operation extracted micro-grooves after lens shape and measurement outlier removal, cross-sectional view micro-grooves. (b) Surface characterization of Alvarez lens with micro-grooves: on-machine surface measurement measured raw data, Alvarez lens shape calculated by 2nd order robust regression filter, after lens shape removal operation, extracted surface micro-grooves after optical measurement outlier removal, cross-sectional view of micro-grooves. Reprinted with permission from Ref. [150].

3.1.1. Classified by Actuators

The main difference of FTS system lies in the actuator and mechanical structure. According to the different actuators, it could be divided into piezoelectric FTS (PZT-FTS), magnetostrictive FTS (MGS-FTS), Lorentz force FTS (LRI-FTS), and Maxwell normal stress FTS (MNM-FTS) [152]. The characteristics of the FTS system driven by various drivers are concluded in Table 3.

Table 3. The characteristics of the FTS system driven by various drivers.

| Driver | Principle | Advantages | Limits | Applications |
|---------|-------------------------|---|--|---|
| PZT-FTS | Piezoelectric effect | <ul style="list-style-type: none"> compact structures maximum response frequency nanometric positioning accuracy high dynamic stiffness | <ul style="list-style-type: none"> hysteresis heating problem | widest application |
| MGS-FTS | Magnetostrictive effect | <ul style="list-style-type: none"> high output force greater stiffness simple structure | <ul style="list-style-type: none"> temperature sensitive hysteresis heating problem | micro-displacement and precise positioning |
| LRT-FTS | Lorentz force | <ul style="list-style-type: none"> large output extra-long stroke easy to control | <ul style="list-style-type: none"> low response frequency large mass of motion system heating problem | large stroke with a small bandwidth |
| MNM-FTS | Maxwell normal stress | <ul style="list-style-type: none"> ultra-high frequency high force density | <ul style="list-style-type: none"> non-linearity positioning error | ultra-high frequency response and high acceleration potential |

The piezoelectric actuator is designed by the inverse piezoelectric effect of piezoelectric materials (such as lead zirconate titanate series). They are energy transducers that convert electrical energy of voltage amplitude into mechanical energy of micro-displacement. It is a common FTS device with many advantages such as fast response speed, high acceleration, wide frequency response range—even up to several kilohertz, the closed-loop positioning accuracy can reach nanometer level and has a large output force density—high axial stiffness, simple structure, no transmission mechanism, and the open-loop system is stable and easy to control [153]. At the same time, there are some disadvantages: piezoelectric ceramic actuator requires high driving voltage, usually from several hundred volts, up to one thousand volts; its output displacement is small, and it cannot fabricate the topography with large surface drop; there are time delays and nonlinear phenomena between input voltage and output displacement; and the control algorithm is complicated. Therefore, FTS based on piezoelectric actuators is more suitable for compensating the motion errors of machine tools or machining micro-structural surfaces and small amplitude freeform surfaces.

To improve the tracking performance of traditional tool servo system, Zhao et al. developed a series two-stage FTS system driven by two piezoelectric actuators using flexible hinges for motion guidance [154]. Wang et al. developed a FTS mechanism based on piezoelectric actuator to add additional functions to the general CNC system to facilitate turning of middle-convex varying ellipse piston, which improved the requirements of cutting feed mechanism for strength, high stiffness, fast response, long stroke, and high precision [155], in order to overcome the defect of short servo stroke of PZT-FTS. Kim et al. described the optical surface of the second mirror, which is often needed in optical imaging system, in order to obtain large and high bandwidth tool motion, as shown in Figure 20.

A new long stroke fast tool servo system is proposed and installed on Z-axis of diamond lathe as an additional synchronous axis [44].

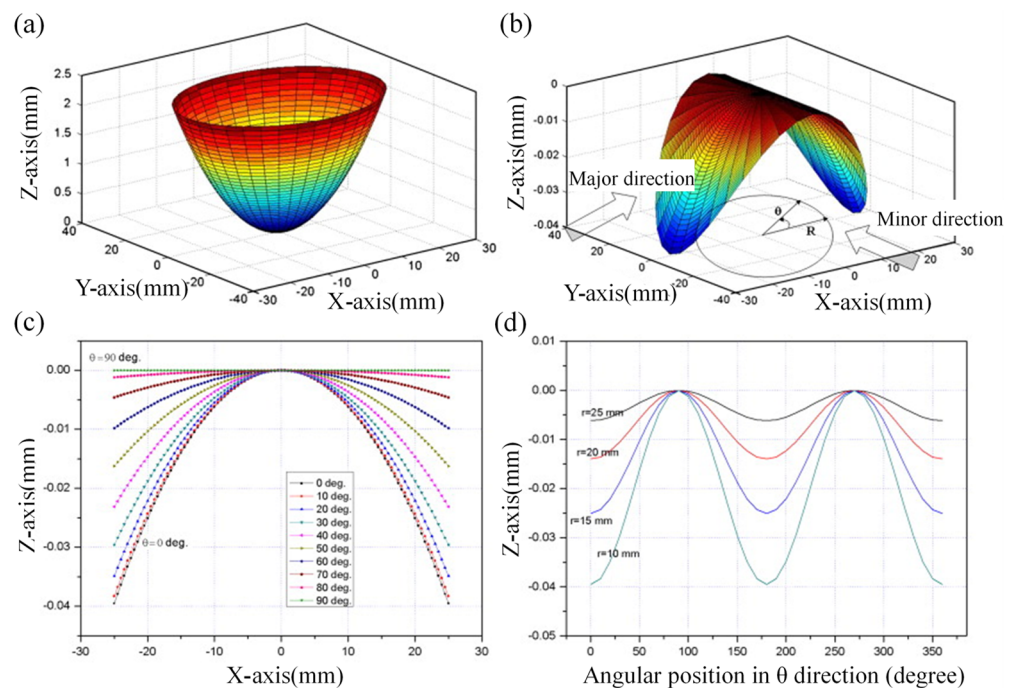


Figure 20. Freeform surface for second mirror in optical imaging system. (a) Rotationally symmetric component for the Z-axis; (b) non-rotationally symmetric components for the Long-stroke fast tool servo (LFTS); (c) the trajectories in the radial direction followed by the LFTS; and (d) the trajectories in the circumferential direction followed by the LFTS. Reprinted with permission from Ref. [44].

Magnetostrictive actuator is designed by using the properties of magnetostrictive material stretching or shortening along the direction of magnetization under the action of magnetic field [156,157]. The driving mode has the characteristics of large output force, fast frequency response, and high resolution. Compared with magnetostrictive materials, FTS driven by piezoelectric ceramics has a larger stroke, and magnetostrictive materials have inherent nonlinearity and magneto-hysteresis [158]. Hayato et al. proposed a FTS mechanism milling system based on giant magnetostrictive actuator. The system can control the axial movement of the milling cutter spindle when it is rotating in a non-contact state. FTS unit provides accurate machining movement through displacement feedback of coaxial capacitance sensor on the metering frame. The developed machining system combines the large feed movement of each straight axis of the workpiece shape with the FTS movement of the micro-geometry shape, which can efficiently process the surface with micro-geometry shape [159].

The Lorentz force driving method is suitable for long stroke FTS, which can be divided into three types, namely rotary motor, linear motor, and voice coil motor (VCM) [160]. The acceleration of linear motor and rotary motor is limited in a small range due to the limited current density and mass density of conductor material. The linear motor has a heating problem, which limits its working frequency. The rotary motor cannot directly achieve the linear requirements of FTS. It can indirectly achieve linear motion through the swing and obtain higher acceleration through the amplification of the swing radius. However, the machining accuracy and mechanism stiffness also decreased significantly.

VCM can achieve higher acceleration than linear motor. However, the accuracy of large stroke VCM is affected, with the increase of stroke brings cost increase, and it also has problems of high heat. VCM has a higher working frequency than linear motor, which is a long stroke linear FTS driving mode with a wide range of applications. The VCM adopts electric damping inside, and the flexible mechanism adopts two different viscoelastic

damping materials. It is designed by using the galvanic conductor subjected to ampere force in the permanent magnet field. The VCM used in the drive of FTS system have many advantages such as the large stroke of millimeter level, the size of output force and wire length, current intensity and magnetic field intensity is linear, easy to control, etc. VCM usually has no hysteresis in small stroke and the relationship between current and force is nearly linear. Unlike piezoelectric actuators, voice coil actuators do not provide inherent system stiffness, and controller design becomes critical for adequate stiffness during the cutting process. The motion system of voice coil motor has large inertia, high energy consumption, and high heat generation, which limit its response frequency.

Different Lorentz force actuated of FTS systems are studied. Ding et al. revealed the influence of acceleration feedback control on the performance of LRI-FTS system by establishing the theoretical model of dynamic stiffness and error propagation [161]. Rakuff et al. developed a remote, precision FTS system based on voice coil actuator. It consists of a driven bending mechanism, a custom linear current amplifier, and a laser interferometer feedback system; the tool can be accurately converted on the lathe [162]. Tao et al. proposed a FTS system driven by VCM with self-sensing function of cutting force [163]. In FTS system, flexure hinges need to withstand alternating cutting forces, and large deformation that will reduce the stiffness, resulting in machining errors. Long stroke and high stiffness are two mutual restraint units of flexible hinge, which limit the application of long stroke FTS. Qiang et al. designed a cruciform flexure hinge structure with high stiffness and selected VCM to develop a long stroke flexure hinge [164]. Tian et al. presented a new voice coil motor driven high frequency response and long stroke remote FTS system. Experiments on micro-lens array fabrication were performed by the designed FTS to demonstrate its machining capability. Figure 21 is given as a diagram of the FTS structure and the processed micro-lens array [152].

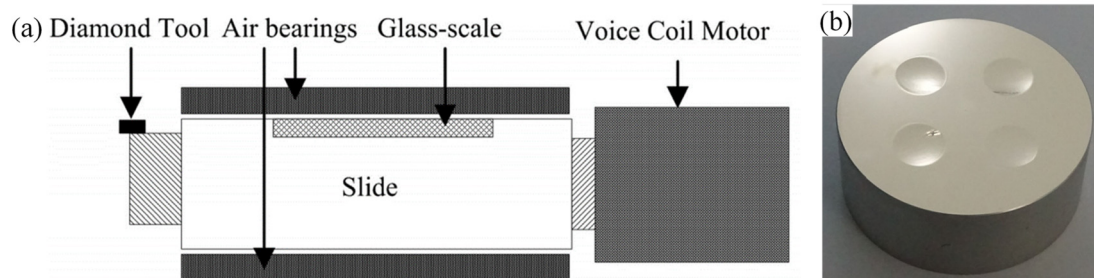


Figure 21. (a) The FTS structure diagram; and (b) the processed micro-lens array. Reprinted with permission from Ref. [165].

Maxwell normal stress actuated FTS has the characteristics of large driving force and small mass of system moving parts. The driving force of Maxwell force actuator has a linear relationship with excitation current and displacement. It has high force density, high acceleration, and low caloric value. It is a kind of FTS with the highest frequency response. Nie et al. designed and developed the FTS system driven by Maxwell Force to enable precise tool translation in a diamond turning lathe. The FTS system uses a bending-based mechanism to generate motion, a customized linear power amplifier to actuate the armature, and a capacitive sensor to gauge the precise distance. The designed FTS is capable of achieving a frequency response of 3 KHz [166].

3.1.2. Classification by Degree-of-Freedom (DOF)

Single DOF FTS is the most common type of FTS. The movement of single DOF FTS is to increase a high frequency linear motion along the spindle direction of the lathe. The projection of the diamond tip on the end face of the workpiece is an Archimedes spiral due to the joint action of the X- and Y-direction motion and the rotation of the spindle of the traditional lathe. If the Z-axis slide of the lathe moves slowly at the same time, the final workpiece shape is an axisymmetric surface. Single DOF FTS uses a high frequency

Z-direction DOF attached to the machine tool movement and carries out high frequency movement along the Z-direction in integer times of the spindle rotation angular frequency. The resulting surface will be non-axisymmetric.

Single DOF FTS are limited by stroke and frequency. In order to broaden the application scope of FTS and enhance the performance of FTS, some researchers began to look for new ways beyond the driving mode. FTS with multiple DOF began to emerge. Zhu et al. designed a piezoelectric driven 2-DOF FTS to assist diamond turning. Based on the bending deformation of Z-shaped flexure hinge beam, a new guiding bending mechanism based on Z-shaped flexure hinge beam was proposed to make the tool move in two directions with decoupled motion. A novel pseudo-random diamond turning (PRDT) method was also implemented to prepare micro-structure surfaces with scattering homogenization [167]. Liu et al. developed a piezo-actuated serial structure 2-DOF FTS system to obtain translational motions along with Z- and X-axis directions for UPM. A sinusoidal wavy surface is uniformly generated by the mechanism developed to demonstrate the effectiveness of the FTS system [168].

The cutting path types of single DOF FTS and 2-DOF FTS are limited to planar curves, which are difficult to meet 3D requirements. Therefore, the FTS mechanism with 3-DOF has high natural frequency and decoupling performance. It can construct complex 3D machining path. Han et al. designed a novel piezoelectric driven elliptic vibration assisted cutting system composed of flexible hinges. In addition, the developed elliptical vibration cutting system can not only be equipped with a variety of machine tools, but also can easily achieve arbitrary vibration in 3D space through two actuators [169]. Awatar et al. proposed a new constraint-based design of a parallel motion flexible mechanism that provides highly decoupled motion along the three translation directions (X, Y, Z) and high stiffness by rotating along the three directions [170]. Li et al. proposed a novel 3-DOF piezoelectric driven FTS with high natural frequency and decoupling characteristics, the tool path and cutting diagram are seen in Figure 22 [171].

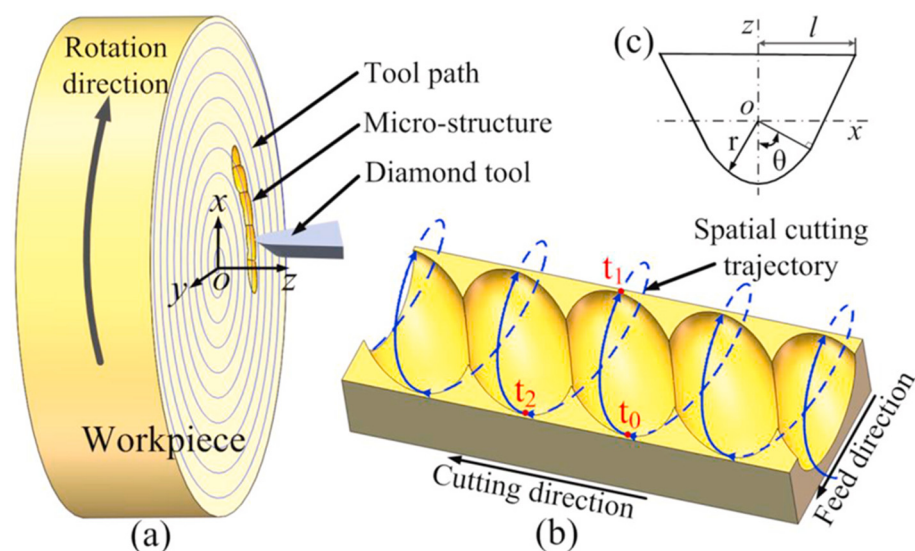


Figure 22. (a) Diagram of the designed 3-DOF FTS cutting path, (b) cutting path, and (c) tool tip shape. Reprinted with permission from Ref. [171].

3.2. Slow Tool Servo (STS)

3.2.1. Principles of STS

STS technology changes the spindle of machine tool into a C-axis with controllable position, then transforms the 3D Cartesian coordinates of complex surface workpiece into polar coordinates through the numerical control system with high performance and high programming resolution. The interpolation feed instructions are sent to all motion axes. The system coordinates and controls the relative motion of the spindle and the tool precisely,

so as to realize the diamond turning of the ultra-precision complex surface workpiece. In ultra-precision STS system, Z-axis follows X-axis and C-axis for sinusoidal reciprocating motion, which requires multi-axis precision interpolation linkage. The rotational motion of the spindle is both the main cutting motion and the feed motion. In order to ensure the normal turning motion conditions of the tool and meet the requirements of multi-axis linkage, STS has higher requirements on the dynamic characteristics of the feed axis than ordinary multi-axis linkage, especially for the Z-axis, which still needs to reciprocate with the ups and downs of the workpiece surface according to the position of C-axis even in the same radius. Therefore, high precision position servo control of spindle, high precision reciprocating motion, and high dynamic response of straight spindle are the key technical conditions necessary for ultra-precision STS system.

The Z-axis machining stroke of STS is large. Theoretically, the machining range can reach the whole z-axis stroke by using z-axis drag plate to drive the tool movement so as to process steeper and more complex surface; C, X, and Z axes are processed in linkage mode. Furthermore, the linkage of the three axes is completed by the same numerical control system, which can realize information sharing and simplify the control system structure. Moreover, the numerical control program is simplified and the tool locus calculated from the complex surface can be directly used in numerical control program.

Ultra-precision STS system is suitable for UPM industrialized production of small size optical freeform surface, and the structure of the array and off-axis surface. However, it is restricted by the structural characteristics of workpiece surface and dynamic response capability of feed shaft, some defects that exist in the actual application are summarized in Figure 23. Therefore, the selection of tool feed direction and tool contact should fully consider the workpiece surface characteristics. In order to improve the efficiency of ultra-precision production machining as much as possible, optimized machining parameters should be selected on the premise of ensuring the machining effect of the key structure.

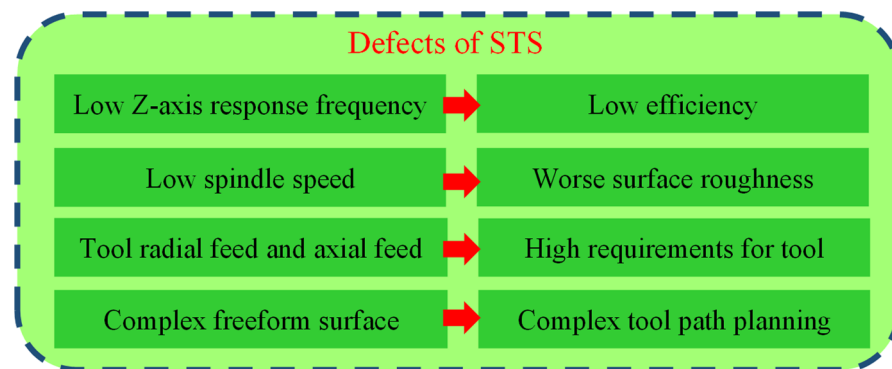


Figure 23. Some defects of STS.

3.2.2. Applications of STS

On the basis of STS technology, researchers continuously develop new methods and technologies to improve the machining performance of the system. In order to better predict the shape change trend under different tool centering errors and different cutting strategies, Yin et al. designed a method for cutting off-axis aspheric surface on an axis based on STS technology, which can achieve large stroke without additional devices [172]. In order to study the new technology of freeform surface optical high-precision manufacturing on hard and brittle materials Wang et al. proposed a new technique for optical surface generation of freeform surface based on STS of diamond grinding wheel, which improves the production efficiency and surface quality [31]. In order to accurately evaluate the contour error, Mishra et al. using STS technology to generate aspherical lens array and characterization of optical profilometer, introduced a STS machining method for machining aspherical lens array [173]. Huang et al. proposed a method of applying variable spindle speed to STS turning to reduce the turning shape error artificially [174].

In order to extend the machining capacity of existing machine tools, Kong et al. present a research method for machining wavy micro-structural patterns on precision rollers using orthogonal STS process. A tool path generator was developed for machining ripple structure patterns on roller surface. Different micro-structures, different wave patterns, and grooves were generated through modeling and simulation mode. A four-axis ultra-precision machine tool was proposed based on the initial experimental work of tool path generator. The generation of unique wave precision rollers in micro-structure mode is shown in Figure 24 [175]. Zhang et al. developed a rotating tool turning machining method based on STS for one-step machining of prisms [176].

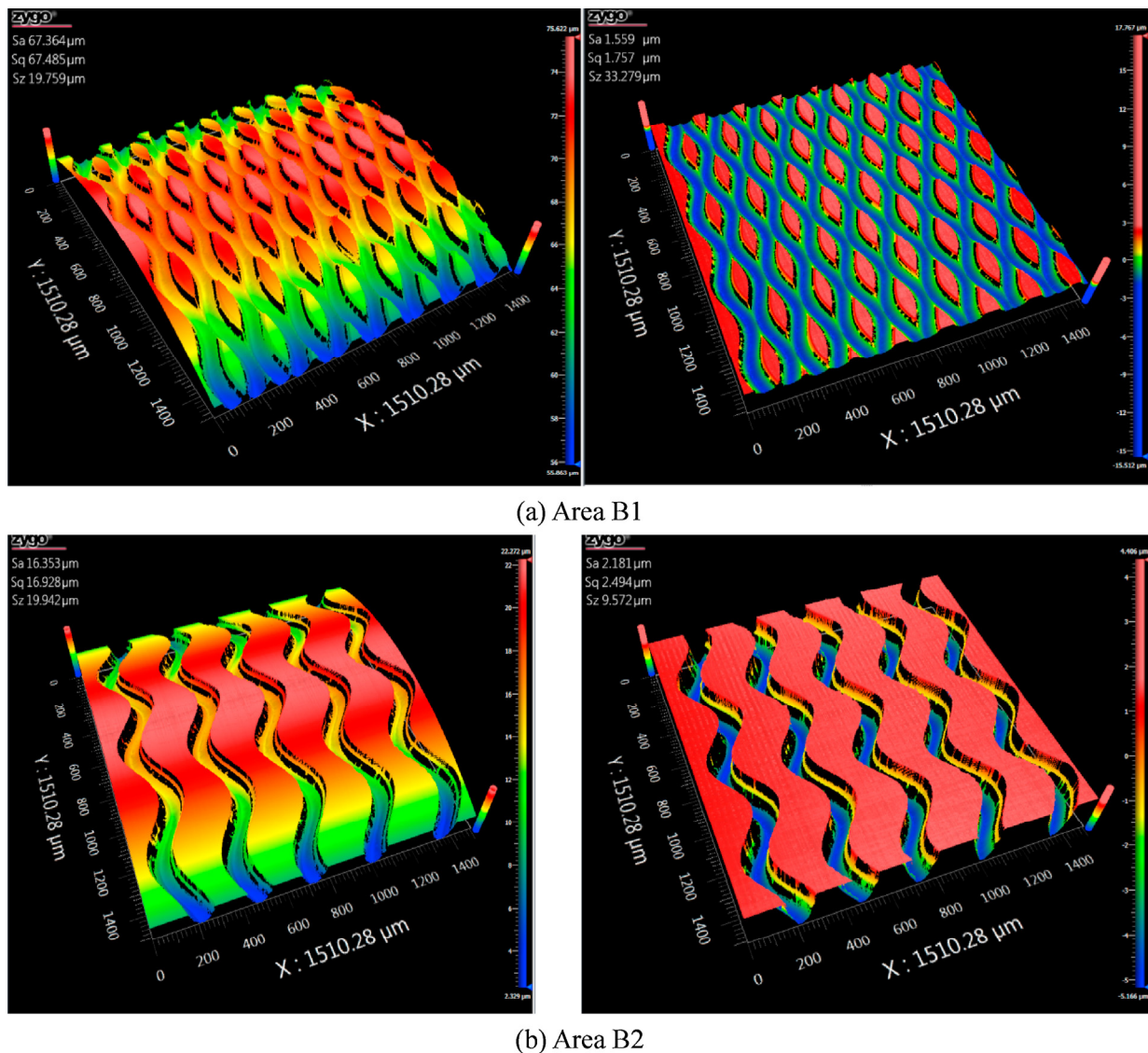


Figure 24. Three-dimensional topography on the roller surface and after cylindrical form removal (5.5X objective, 1X zoom). Reprinted with permission from Ref. [175].

Tool compensation is required to avoid overcutting, Li et al. conducted theoretical and experimental studies on surface topography generation in STS machining of freeform surfaces in order to realize nano-surface topography. A systematic tool path generation method was studied, including tool path planning, tool geometry selection, and tool radius compensation [177]. Peng et al., taking micro-lens array (MLA) as an example, analyzed the components of servo dynamics error in servo motion, including dynamic

deformation, resonant vibration and trajectory tracking error, and established a dynamic surface generation model. The surface obtained by turning is shown in the Figure 25 [178].

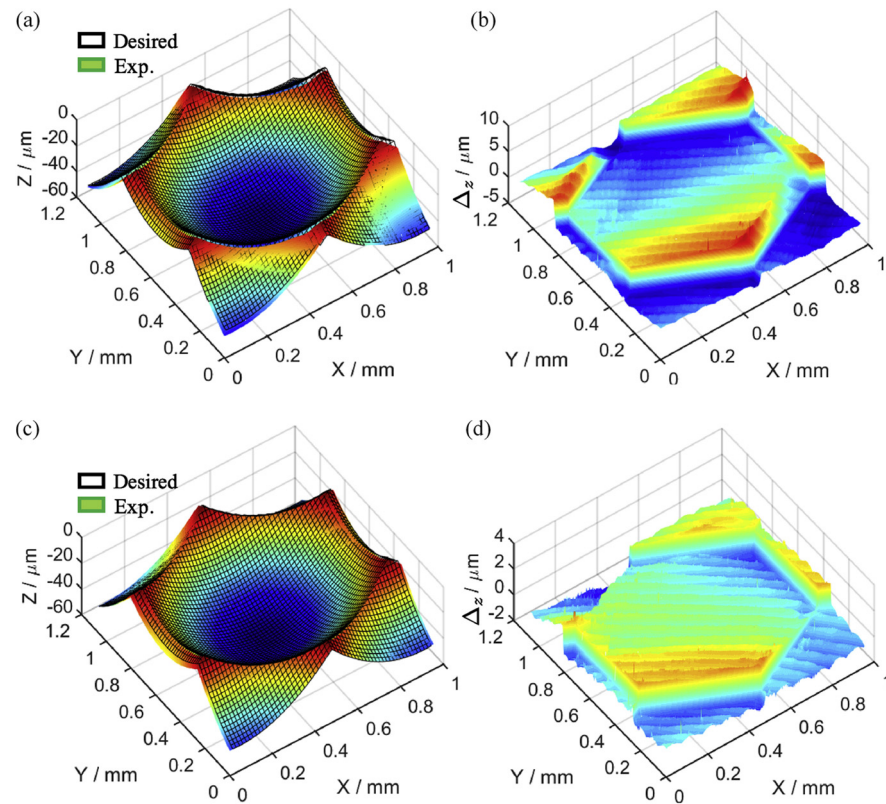


Figure 25. Characteristics of the surfaces obtained by practical turning: (a) The 3D profile; and (b) the resulting form error of the surface generated by STS turning; (c) the 3D profile; and (d) the resulting form error of the surface generated by cooperative tool servo turning. Reprinted with permission from Ref. [178].

Chen et al. established a 3D shape compensation model to solve the problem of tool path generation in the process of astigmatic contact lens asymmetric torus STS diamond turning. The ultra-high accuracy 3D profilometer with user-defined function was used to measure the shape accuracy of freeform surface [179]. Nagayama et al. proposed a deterministic machining process for low-speed servo turning manufacturing freeform surface optical components. The process comprehensively analyzed the main error factors before machining and carried out simulation and compensation based on feedforward method to accurately predict the workpiece shape error after compensation. In order to prove the effectiveness of the proposed method, a two-dimensional sinusoidal lattice cutting experiment was carried out on monocrystalline silicon (as shown in Figure 26) [180].

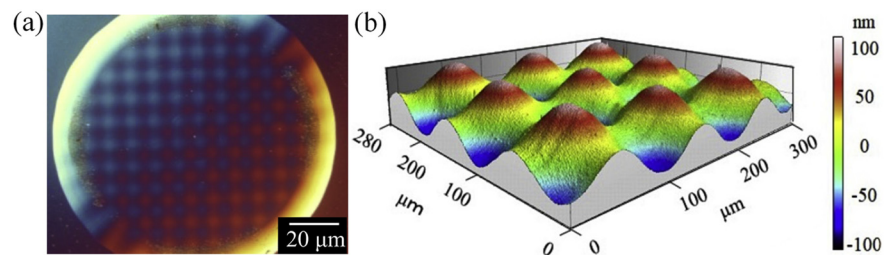


Figure 26. (a) Surface morphology of a 2D sinusoidal grid machined on a single crystal silicon workpiece; and (b) three-dimensional pictures of nanoscale sinusoidal lattices processed on single crystal silicon. Reprinted with permission from Refs. [179,180].

3.3. Comparison between FTS and STS

FTS machining and STS machining have similar machining action and machine tool structure, both need to obtain accurate spindle angle value and can realize the turning of free surface optical parts. Nevertheless, there are many differences, as can be summarized in Figure 27.

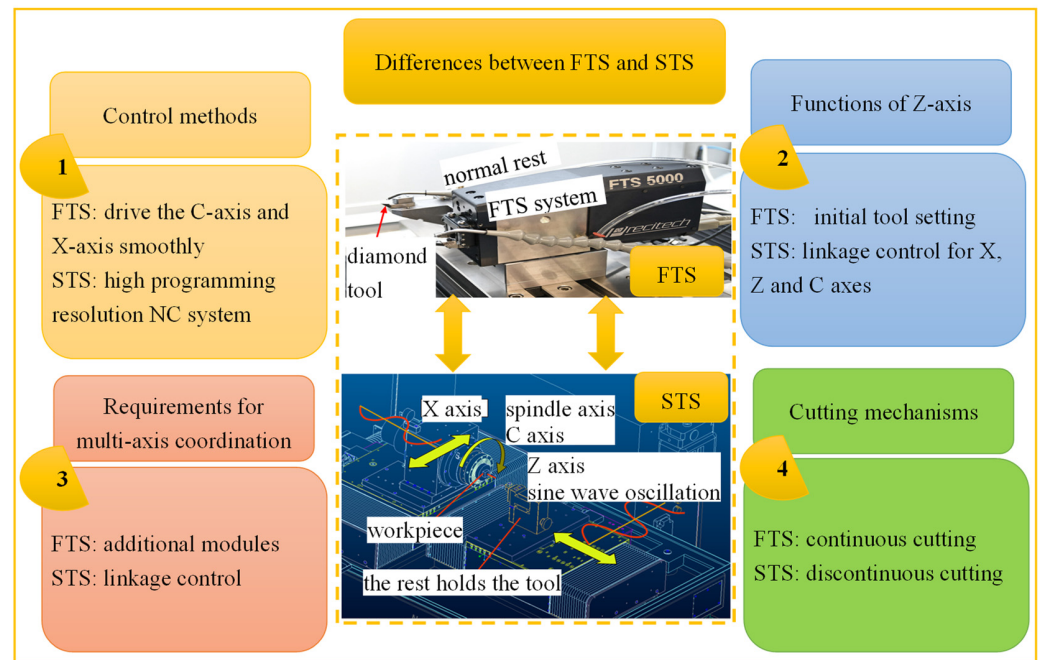


Figure 27. Differences between FTS and STS.

Having different control methods, STS requires a special high programming resolution numerical control system to carry out the three-axis interpolation algorithm including the spindle, and requires a special tool path generator and interpolation algorithm design. FTS does not necessarily need to be equipped with a special high-precision numerical control system. The task of the numerical control system is only to drive the C-axis and X-axis smoothly. Accurate position information is sensed by angle sensors and radial sensors and collected by FTS in real time [181].

Additionally, they have different functions of Z-axis. FTS module and its own control system are additional modules independent of ultra-precision machine tools. Z-direction feed is realized by FTS, and Z-axis is only used for initial tool setting. STS requires ultra-precise position servo linkage control for X, Z, and C axes, essentially three- or four-axis linkage machine tool. Therefore, the requirements on the sensors of each axis are extremely demanding, usually requiring the spindle encoder to reach hundreds of thousands of lines, and the grating ruler of X-axis and Z-axis has very high resolution, which increases the cost of the system to a certain extent.

Furthermore, they have different requirements for multi-axis coordination: The core of FTS machining is FTS servo module, and there is no linkage relationship between each axis. The sensors can meet the accuracy requirements of the final surface shape. STS needs to carry out multi-axis coordination on the surface shape of parts before machining, and then determine the tool path and tool compensation, so as to generate the optimal numerical control program.

In addition, they have different cutting mechanisms. Before FTS machining, the surface shape of parts should be accurately calculated to generate data files that can represent the surface shape of parts, and the precise cutting depends on the control performance of FTS. STS is continuous cutting, while FTS may contain discontinuous cutting at the abrupt change of profile.

Theoretically, STS can machine any complex surface shape and structures. For the small structure of surface shape mutation, it is necessary to reduce the spindle speed, and from the accuracy, efficiency and machining material consideration, the machining difficulty is greatly increased. It is not difficult to draw a conclusion that FTS and STS are completely different in control mode, complex surface shape generation, tool path planning, cutting mechanism, and process parameter selection due to the great differences in actual tool feeding mode, motion frequency response, stroke, and machining object. In a nutshell, FTS module has high motion frequency response (more than 100 Hz) and small stroke (less than 500 μm), which is more applicable for machining small structures with abrupt surface shape or discontinuous and limited stroke. STS motion has low frequency response (10 Hz) and large stroke (1–100 nm), which is applicable for machining complex surface parts with high surface roughness requirements, smooth surface, and large overall drop.

4. Ultra-Precision Fly Cutting

4.1. Fly Cutting

Ultra-precision fly cutting (UPFC) is a cutting process in which the single-crystal diamond cutter rotates simultaneously with the spindle of the lathe to cut the workpiece surface intermittently [182]. The fly cutting machining technology is a high-speed machining method with flexible trajectory and high machining efficiency. It can obtain micro-structures with nanometer surface roughness and submicron surface shape accuracy without post-polishing. In UPFC, cutting speed is constant and can deterministically generate special micro-structured surface. It is suitable for fabricating complex micro-structured surfaces, such as linear groove micro-structure, micro-groove array composed of multiple intersecting lines, pyramid matrix, F-Theta lens, repetitive prism matrix, and micro-structures applied to special reflective surface coatings, tapes and thin slices.

UPFC system installs the diamond tool on the circular fly tool disc and installs the corresponding counterweight on the fly tool disc, then install the fly tool disc on the lathe spindle, the diamond cutter rotates with the spindle at high speed. The workpiece is mounted on the workbench bracket, and the workpiece moves in a plane. UPFC is intermittent machining, and the diamond tool only contacts with the workpiece at a certain angle during each rotation, and the cutting depth changes with the rotation angle of the fly tool disc in each cutting process. For a specific micro-structure, UPFC can be divided into two machining methods from the perspective of the formation of the micro-structure morphology of the workpiece. One is the trajectory method; the shape of the processed micro-structure is formed by using the motion track of the diamond tool tip in the cutting movement. Since the workpiece surface is composed of the tool path, the tool path method can process micro-grooves of variable size without requiring accurate tool tip angle, as long as the tool does not interfere in the process of machining micro-structure. However, in this machining method, the tool trajectory is more complex, so the higher requirements for lathe, generally need multi-axis precision linkage. The other is the profile method, diamond tool geometry is consistent with the processed micro-structure. When machining, the positioning accuracy of the lathe is taken into account. The diamond tool is processed vertically in a micro-groove position, then the transverse feed is made after the ideal depth is processed. The tool is then processed vertically in the next micro-groove position until all the micro-groove matrix is processed. Compared with the trajectory method, this method has lower requirements on machine tool performance, simple tool path, easy machining, and better surface roughness. However, this machining method can only process the same sized micro-grooves, and the preparation of high requirements for cutting tools, which require precise geometric accuracy.

UPFC technology can be divided into two types according to the different tool installation direction: when the tool installation direction is parallel to the spindle axis, it is called end fly cutting [183,184]; and ultra-precision raster milling is when the tool direction is installed along the radial direction of the spindle [185,186]. Its schematic diagram is shown

in Figure 28. Some micro-structures and SEM figures of machined structures fabricated by fly cutting are shown in Figure 29 and Table 4.

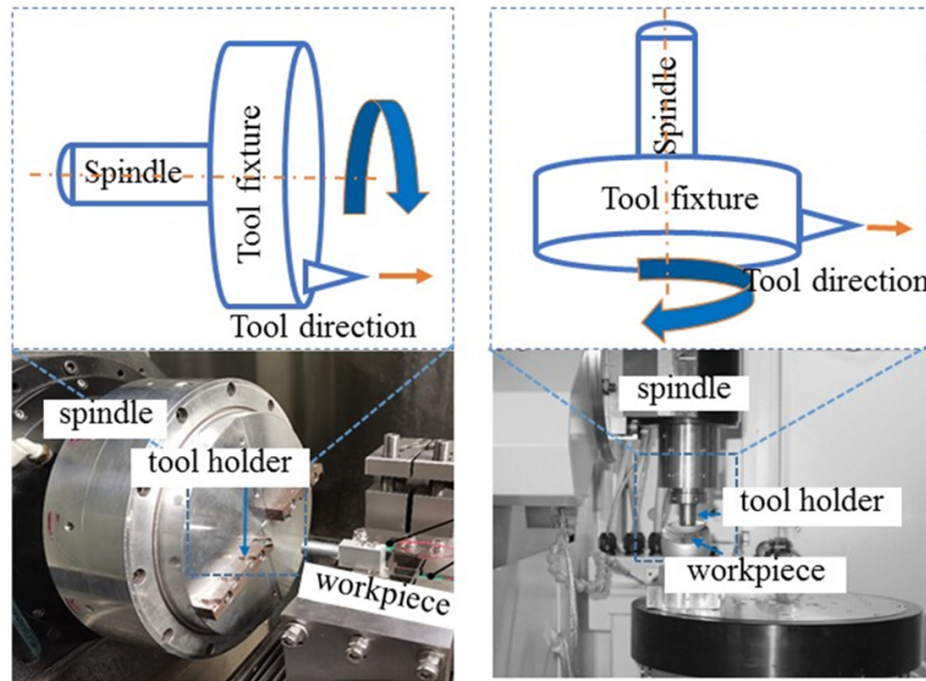


Figure 28. The two types of fly cutting. Reprinted with permission from Refs. [187,188].

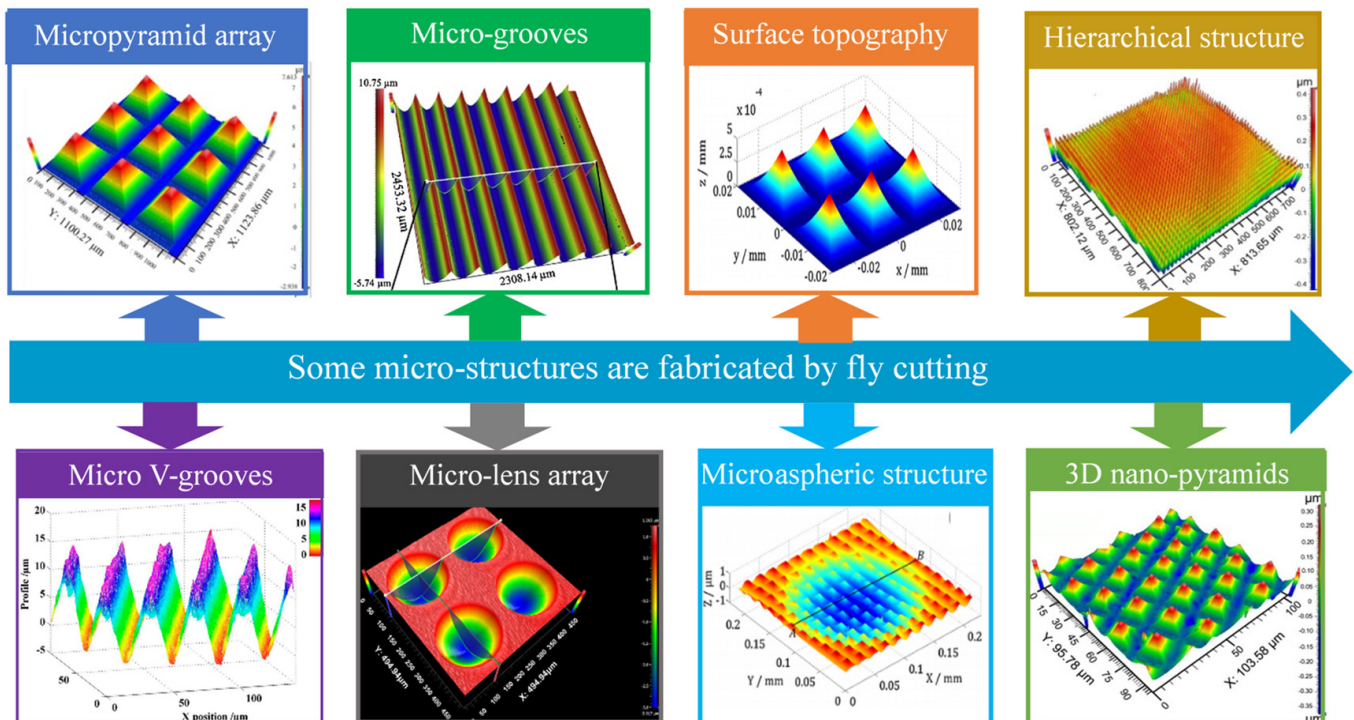
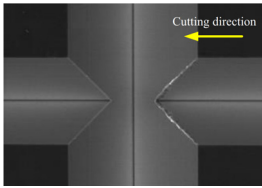
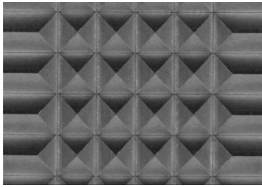
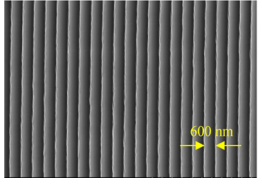
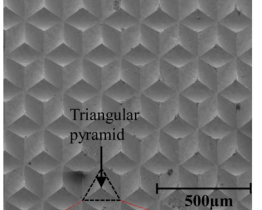
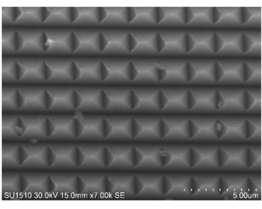


Figure 29. Some micro-structures are fabricated by fly cutting. Reprinted with permission from Refs. [119,177,184,189–191].

Table 4. SEM figures of machined structures by fly cutting [54,128,192,193].

| Micro-Structure | Diagram | Material | Parameter | Surface Quality |
|--------------------|---|--------------------------|-------------------------------------|--|
| Pyramid detail |  | Nickel phosphorus (Ni-P) | Microgroove width: 15 μm | Chipping eliminated |
| Micropyramid array |  | Nickel phosphorus (Ni-P) | Cutting depth: 10 μm | Maximum effective cutting thickness: 78.6 nm |
| Submicron grooves |  | Nickel phosphorus (Ni-P) | groove spacing: 500–800 nm | High-regularly arrayed and have a high parallelism |
| Triangular array |  | Brass | Cutting depth: 20 μm | Max deviation: 5.3 μm |
| Pyramid array |  | 6061 aluminum | Cutting depth: 0.5 μm | Max error: 0.4 μm |

4.2. End Fly Cutting

End fly cutting was originally used to fabricate large flat surfaces with a uniform surface quality. However, in recent years, fly cutting technology has been applied to UPM combined with FTS/STS to produce mixed structured surfaces such as micro-structured freeform surfaces [188]. In traditional FTS/STS, cutting is operated in a cylindrical coordinate system, where the cutting direction is always perpendicular to the polar axis of the workpiece and it is impossible to construct the intersection points of the cutting trajectory. For the end fly cutting, the diamond tool is mounted on the spindle and rotates with it, while the workpiece is sandwiched on the slide. By exchanging the position of the diamond tool and the workpiece, the operation of the end fly cutting system is transferred to the rectangular coordinate system. Due to the circumferential motion of the diamond tool, various cutting directions about the workpiece can be obtained. Translational servo motion along the Z-axis, like FTS or STS, acts on the workpiece and is responsible for determining the generation of complex micro-structures with complex shapes. Due to the unique advantages of end fly cutting in machining, it is suitable for machining complex specific micro/nano structures such as pyramid array, triangular pyramid array, and multi-layer complex micro-structures. The end fly cutting system configuration diagram is shown in Figure 30.

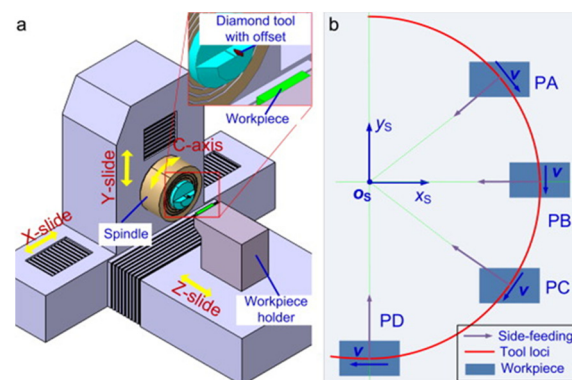


Figure 30. (a) End fly cutting system configuration diagram; (b) the induced cutting modes, where o_s - x_s - y_s denotes the coordinate system fixed on the spindle axis, and v denotes the relative cutting speed. Reprinted with permission from Refs. [177,184].

In some studies, improved methods were proposed for the preparation of large-aperture potassium dihydrogen phosphate (KDP) crystal by fly cutting. KDP is widely used in the laser path of inertial confinement fusion system. The most commonly used method to fabricate half meter KDP crystal is UPFC. When UPFC technology is used to process KDP crystal, the dynamic characteristics of the fly cutting lathe and the fluctuation of the fly cutting environment are transformed into surface errors in different spatial bands. To ensure that KDP crystal achieves the full band machining accuracy specified in the evaluation index, these machining errors should be effectively suppressed. Zhang et al. studied the anisotropic machinability of KDP crystal and the cause of typical surface errors in UPFC of materials. By analyzing the causes of machining errors in different frequency bands and measuring the brittle-ductile transition depth of the crystal, the structure, parameters and cutting environment of the fly cutting were optimized [194]. Tool tip is perpendicular to the workpiece surface due to the thermal expansion of the tool. To this end, Fu et al. established a surface cutting simulation model based on kinematic fly cutting and thermal models, then conducted UPFC tests on KDP crystals to explore the specific impact of the main cutting force on the thermal deformation of the workpiece, thus determining the relationship between the cutting parameters and the main cutting force. This model can be used to predict 3D surface topography after UPFC, and to evaluate surface corrugations, roughness, and other performance indicators [195]. In order to reveal the formation mechanism of high points on large optical surfaces during UPFC, Wang et al. established a thermodynamic model of the tool system during fly cutting. The temperature field distribution and axial displacement caused by thermal deformation of the tool system were solved and analyzed by finite element simulation [196].

To improve accuracy, researchers put forward improvement methods on fly cutting machine tools. Liang et al. proposed a mechanical structure-based design method to design and optimize UPFC machine tools. In order to study the effect of workpiece structure on machined surface roughness, an optimized spindle structure was designed to reduce workpiece roughness [197]. Lu et al. conducted dynamic modeling and simulation on the ultra-precision fly cutting machine tool to find out the relationship between structural parameters and the machined surface. The simulation surface and measurement surface of fly cutting machine tool are shown in Figure 31b,c [198]. The micro-structures fabricated by fly cutting also act as diffraction gratings, Du et al. used vibration-assisted diamond cutting process to generate structural colors on the surface of pure magnesium, and prepared periodic sawtooth micro-structures that acted as diffraction gratings to induce the generation of structural colors. The colors at different angles are shown in Figure 31e,f [199]. In order to suppress tool wear and improve cutting performance, Zhang et al. explored the tool wear by fly cutting experiments, found that increasing air pressure and the closer the nozzle position not only to improve the cutting performance, also reduced the tool wear [200].

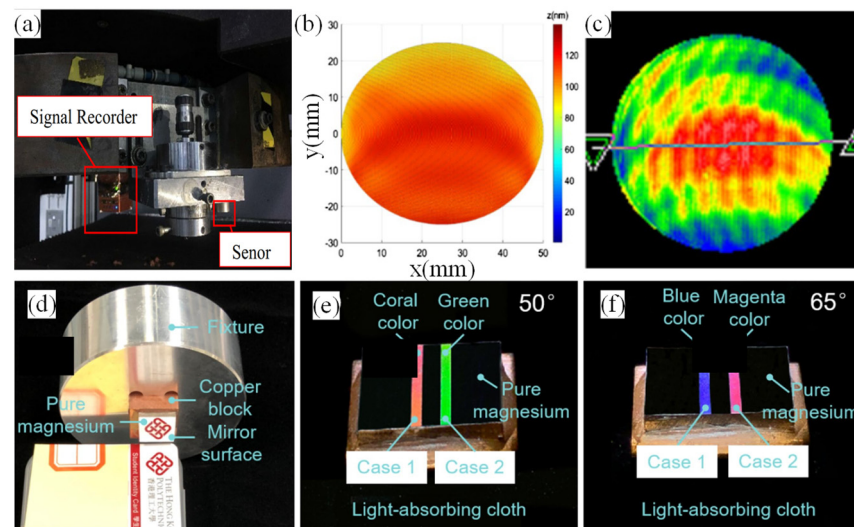


Figure 31. (a) Tool-tip acceleration test set up, ultra-precision fly-cutting machine tool; (b) simulated surface; (c) measured surface; (d) optical mirror surface; (e) coral color and green color at the viewing angle of 50° ; and (f) blue color and magenta color at the viewing angle of 65° . Reprinted with permission from Refs. [198,199].

To overcome the generation of inherent residual marks (RTM) with specific patterns during cutting, Zhu et al. developed a novel biaxial servo assisted fly cutting (BSFC) method to achieve flexible control of RTM to generate functional freeform optical elements, which is difficult to achieve in FTS/STS diamond turning. By selecting the feed speed in each cutting rotation, the height and spacing of secondary micro/nano textures can be independently generated [189]. Furthermore, to overcome the problems of inconsistencies of cutting parameters induced by cutting speed and underutilization of vibration assistance caused by cutting direction in vibration assisted turning or milling of brittle materials. Zhu et al. introduced the machining method of rotary spatial vibration (RSV) in assisted diamond cutting. The feasibility and superiority of this process for brittle materials were demonstrated by manufacturing a group of annular micro-grooves in monocrystalline silicon with gradually changing cutting depth [201].

Different cutting strategies have been proposed to achieve complex micro/nano structures with high precision at multiple levels. Combining the concept of fast/slow tool servo system, Zhu et al. proposed an end fly cutting servo system (EFCS) with four-axis motion, which can be used for deterministic generation of layered micro/nano structures that are difficult to achieve by other methods. A nano-structured micro-aspheric array and nano-structured F-Theta freeform surface were successfully prepared, as shown in Figure 32a–c [177]. To et al. continuously develops the performance of EFCS and proposes a new machining method to generate hierarchical structure microstructure. By combining different cutting directions in the EFCS system, a variety of nano-polygons can be generated as secondary structures. Nano-pyramids for advanced optical applications are experimentally generated on the F-Theta freeform surface and high-precision micro-aspherical array. The fabricated nano-pyramid ellipsoidal aspherical array is shown in Figure 32d–f [184]. Zhu and co-researchers went further, they proposed a new mechanical micro/nano machining process that combines the rotary space vibration (RSV) of a diamond tool with the servo movement of the workpiece and applied it to the generation of multi-layer micro/nano structures. By combining non-resonant triaxial vibration with servo motion, a variety of micro/nano structures with complex shapes and flexible and adjustable feature sizes can be generated, as shown in Figure 32g–i [202]. In addition, Zhu et al. extended the application of FTS/STS diamond turning technology in end fly cutting because it could not achieve good large-scale machining of micro-lens array (MLA). Higher spindle speeds can also

achieve higher cutting efficiency, and this method achieves uniform mass MLA in a large area, as shown in Figure 33 [190].

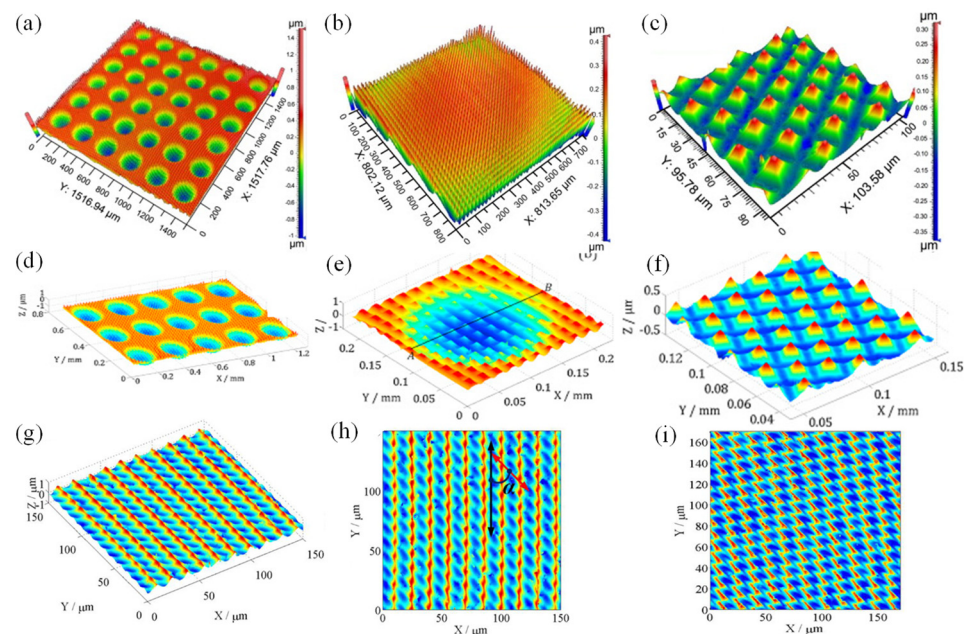


Figure 32. Surface characterizations of the micro-aspheric array with nano-pyramids: (a) large area structures; and (b) the extracted 3D nano-pyramids; (c) surface characterizations of the F-theta freeform surface with nano-pyramids, the 3D hierarchical structure. Characterizations of (d) the micro-aspheric array with nano-pyramids; (e) a single micro-aspheric structure with nano-pyramids; (f) the enlarged view of the secondary nano-pyramids. Characteristics of nano-structures fabricated by rotary vibration assistance with a single frequency: (g) the 3D, and (h,i) projected 2D nano-dimple array generated. Reprinted with permission from Refs. [177,184,202].

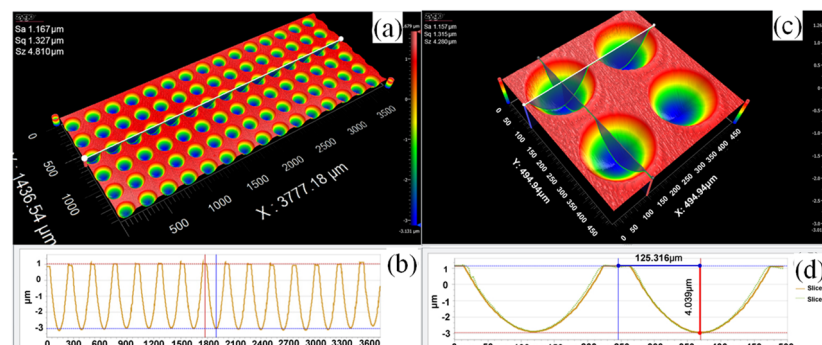


Figure 33. Characteristics of the machined micro-lens array: (a) the 3D structure of a large area; (b) the 2D profile of the cross-section; (c) an extracted square area; and (d) the corresponding profiles along the cross-hair directions of the micro-lens array. Reprinted with permission from Ref. [190].

To improve the shape accuracy, Huang et al. studied the influence of machine tool error on the shape accuracy of cone in fly cutting. The relationship between the minimum single cutting depth and the maximum tool displacement error is analyzed to avoid the size error of micro-cone [54]. Jiang et al. extended the application of fly cutting and proposed a new offset fly-cutting-servo system (OFCS) combining the concepts of fly cutting and STS, which can process straight slot microstructural arrays on commercial machine tools containing only X, Z, and C axes, such as pyramid array and triangular pyramid array. On the basis of this model, groove array, pyramid array, and triangular pyramid array are machined respectively, as shown in Figure 34 [128].

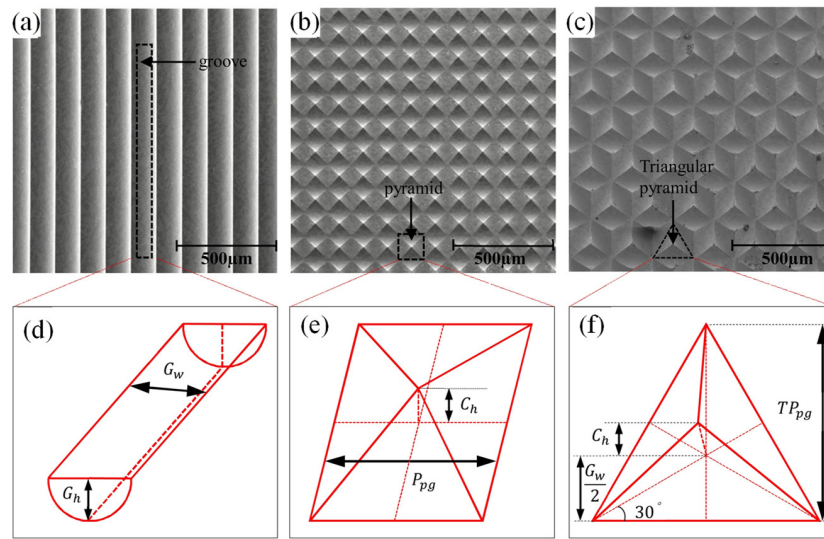


Figure 34. SEM figures of machined structure arrays: (a) micro groove array; (b) micro pyramid array; (c) micro triangular pyramid array; and (d–f) their geometric descriptions. Reprinted with permission from Ref. [128].

Single-crystal silicon is a brittle material widely used in infrared optics and optoelectronics industry. However, due to its extremely low fracture toughness, it is difficult to obtain ultra-smooth deep micro-structure on single-crystal silicon based on cutting, diamond milling and grinding. Sun et al. proposed a new UPFC ductile machining model to efficiently process deep micro-structure on silicon. The 3D topography of the optical micro-grating composed of 15 μm deep curved micro-grooves prepared by UPFC on monocrystal silicon is shown in Figure 35a,b [119]. Furthermore, Sun et al. proposed a novel UPFC ductile machining model of silicon. By preparing two kinds of freeform surfaces on silicon, namely micro-grooves and F-Theta lenses; experiments were carried out to verify the superiority of UPFC in realizing deep ductile cutting regions. Figure 35c–e shows the surface characteristics of the F-Theta lens and its surface profile in the diagonal direction measured by the 3D optical surface profilometer. The surface roughness is up to nanometer level and the shape error is up to micron level without brittle fracture. Moreover, the model can be used to process freeform surfaces of other brittle materials under large cutting depth [120].

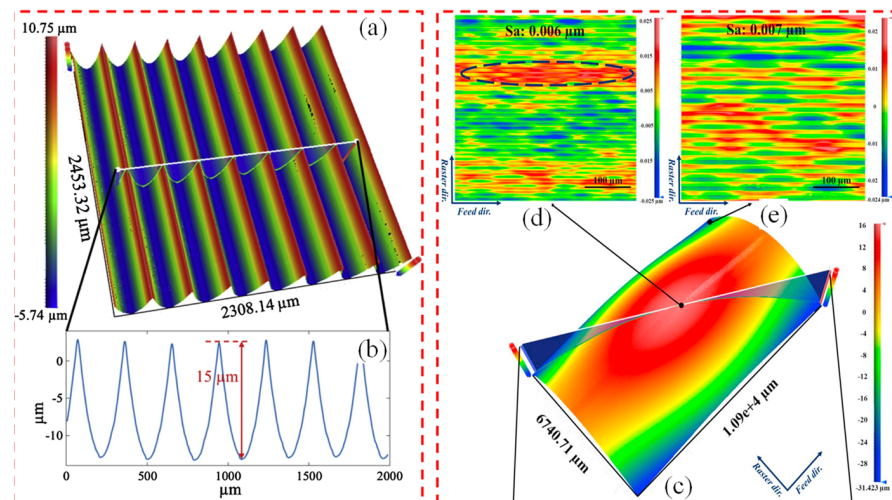


Figure 35. 15 μm deep micro-raster composed by arc-shaped micro-grooves in $\langle 100 \rangle$ direction: (a) 3D surface topography; (b) cross-sectional profile. Surface morphology of the F-theta lens surface machined by UPFC, (c) 3D morphology and (d) center area and (e) marginal area. Reprinted with permission from Refs. [119,120].

4.3. Raster Milling

In fly cutting, Ultra-precision Raster Milling (UPRM) is when the tool direction is perpendicular to the spindle. UPRM can be performed using horizontal and vertical cutting strategies and their geometry is shown in Figure 36. The diamond tool is fixed on the spindle and rotates with the spindle. The cutting process consists of two kinds of motion: feed motion and grating motion, determining the appropriate cutting strategy such as transverse cutting or longitudinal cutting. Horizontal cutting is performed by cutting the tool in a horizontal direction. After cutting a section, the diamond tool moves along the milling to process the entire workpiece surface. In vertical cutting, the cutter feeds vertically and moves horizontally. The surface roughness profile of the machined surface in both cutting methods is formed by the repeated cutting of the tool tip at intervals of the tool feed rate, by the tool moving a specified distance under ideal cutting conditions. The feed direction is perpendicular to the milling direction, and the two directions in horizontal cutting are opposite to those in vertical cutting [203].

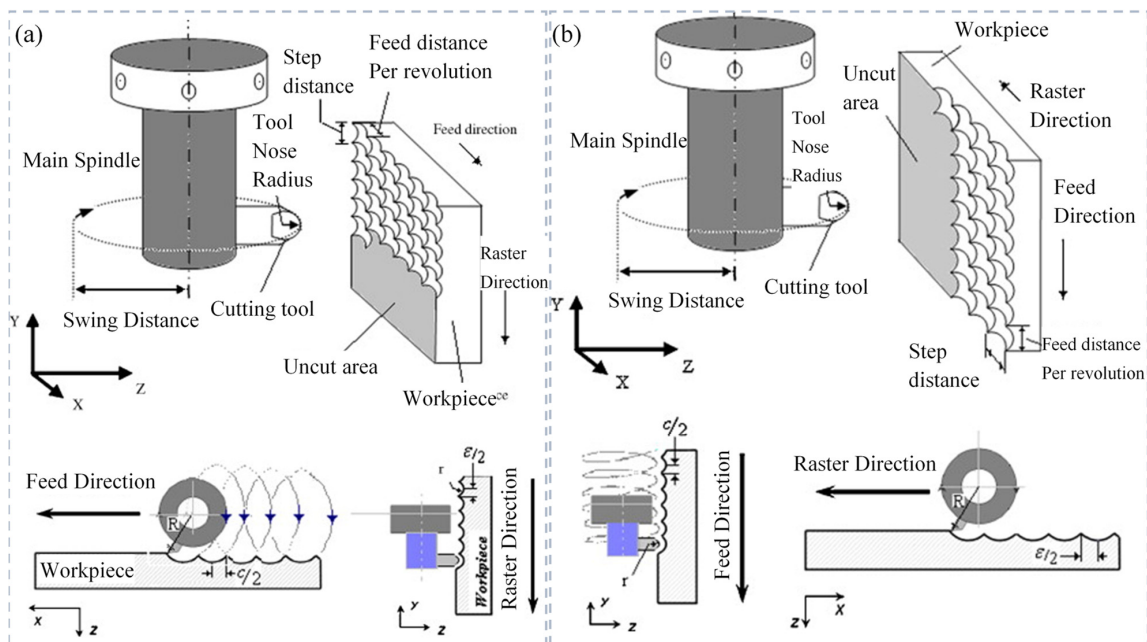


Figure 36. Cutting geometry for ultra-precision raster milling using: (a) horizontal cutting strategy; and (b) vertical cutting strategy. Reprinted with permission from Ref. [203].

To avoid a lot of trial-and-error experiments, the researchers proposed different simulation models to verify the cutting experiment. Cheung et al. established a simulation model to optimize the prediction mechanism of optical freeform surface generation during UPRM. It is not only possible to predict shape accuracy and simulate surface generation, but also to identify the optimal machining area to minimize shape error prior to actual production [185]. Cheng et al. conducted theoretical and experimental analysis on the generation of nano-surface in UPRM and established a theoretical model for surface roughness prediction [187].

Due to different cutting mechanisms, compared with ultra-precision diamond turning and conventional milling, the process factors that affect surface quality in UPRM are more complex. The process factors and cutting strategies have a certain influence on the surface quality. The influence of technological factors can be minimized or even eliminated by selecting reasonable cutting conditions and cutting strategies. Cheng et al. studied the process factors affecting the surface quality of UPRM and found that step spacing is one of the key factors affecting the surface quality of UPRM. The influence of process factors can be minimized through reasonable operation settings and control of dynamic characteristics of machine tools [52].

There are some studies on optimizing the precision of UPRM. Cheng et al. proposed an optimization system for surface roughness analysis UPRM. According to the minimum surface roughness criterion, the system studies the optimal cutting conditions of different cutting strategies within the preset process parameters [204]. Kong et al. studied the factors affecting the surface generation in UPRM. Compensation strategy was designed to improve surface generation and improve surface quality of UPRM [203]. The cutting force in milling process can be better studied by establishing motion model. Kong et al. has established a theoretical dynamic model for UPRM of optical freeform surfaces. The modification of machining parameters provides guidance for the control of cutting force excitation [205].

The special vibration of spindle has great influence on the surface formation of work-piece. Zhang et al. conducted relevant research on spindle vibration. Based on the 5-DOF dynamic model of the hydrostatic bearing spindle, a special model under the excitation of the batch cutting force was established, and the corresponding mathematical solution was derived. The surface topography is shown in Figure 37a,b [206]. In addition, Zhang et al. studied the surface generation problem under the excitation of spindle vibration in UPRM, proposed the nonlinear equation of spindle vibration in detail, and studied its special influence on the surface generation. The surface topography of spindle under horizontal cutting conditions is shown in Figure 37c,d [186].

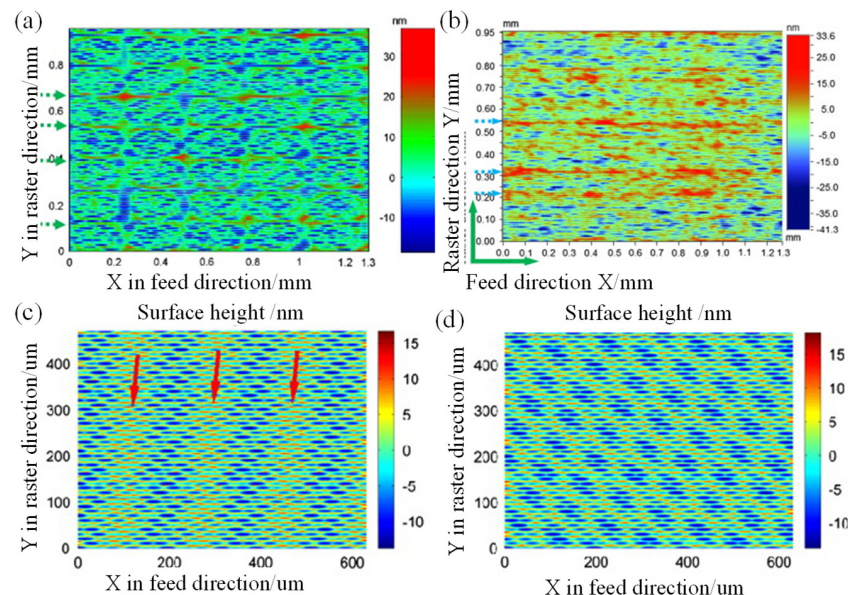


Figure 37. Surface generation under the cutting conditions: (a) simulated topography; (b) measured topography, simulated surface topographies with; (c) the uniform phase shift; and (d) the phase shift of 0.5. Reprinted with permission from Refs. [186,206].

To meet the requirements of precise forming control, the corresponding machining and measurement methods are proposed. Zhu et al. proposed a new method of fly cutting micro-structured surface measurement based on the principle of scanning tunneling microscope. Figure 38a,b shows the surface morphology of unremoved machined tissue. It is suitable for the fly cutting process with frequent micro-V-shaped grooves, and significantly improves the surface form of rectangular pyramid array [191]. Cai et al. proposed a diamond fly cutting method based on tool path generation, which includes tool radius compensation and surface morphology simulation. The surface topography under different feed speeds and spindle speeds was simulated [207].

UPRM can also be applied to other aspects of optics. Submicron structure surface can produce view-angle dependent rainbow, which is widely used in multi-color printing, micro-display projection, invisibility cloak technology, and so on. He et al. designed several two-stage structures, including first-order microscopic geometric features corresponding to pattern shapes and second-order submicron grooves corresponding to diffraction gratings,

which directly induced a variety of glow patterns according to their shape laws. The second-order submicron grooves at different feed rates are shown in Figure 39a–d [193]. The fabrication of micro-structures on brittle materials by grating milling is also the focus of research in recent years. Dong et al. analyzed a transverse planning method for machining NI-P die with micro-pyramid array. High-quality micron-scale micro-pyramid array was prepared on the phosphor nickel coating, as shown in Figure 39e,f [192]. To optimize the processing morphology of UPRM on brittle materials, Peng et al. introduced a simple model to analyze the mechanical properties around diamond tip. It is found that the stress state in the chip formation zone can be changed and the stress intensity factor at the crack tip can be reduced, which is beneficial to the plastic deformation of brittle materials [208]. Aramid fiber reinforced plastics (AFRP) is a typical hard cutting material due to burrs and cracks during machining. Bao et al. established a cutting mechanics model of AFRP to predict the influence of the angle between the feed direction and the fiber direction on tensile and shear behavior during cutting [209]. The cutting chip, microwave, and burr produced in the machining process will greatly affect the machining accuracy. To reduce machining errors and obtain good surface roughness, researchers studied the error generation mechanism. Zhang et al. studied the influence of cutting chips and tool movement during cutting. By increasing spindle speed and decreasing feed speed, the probability of surface roughness patterns occurrence can be minimized [182]. Zhang et al. found that the microwaves on the UPRM surface were caused by the sliding of the material [210].

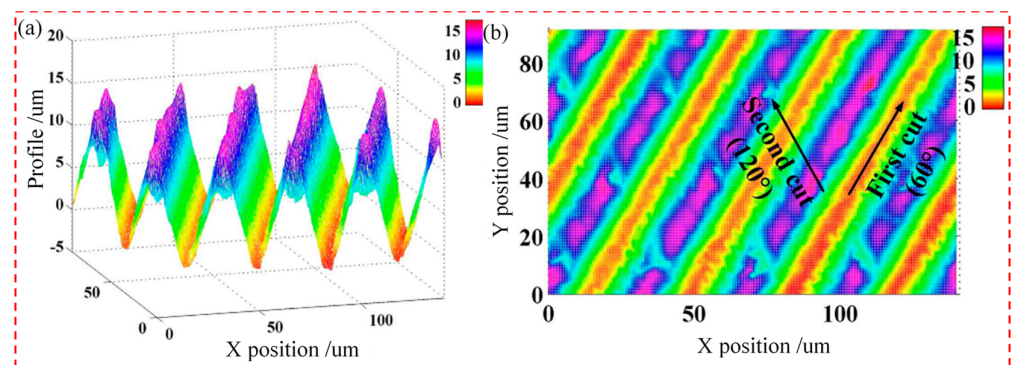


Figure 38. (a) Top view of on-machine measured surface of crossed micro-V-grooves; (b) top view of the measured surface. Reprinted with permission from Ref. [191].

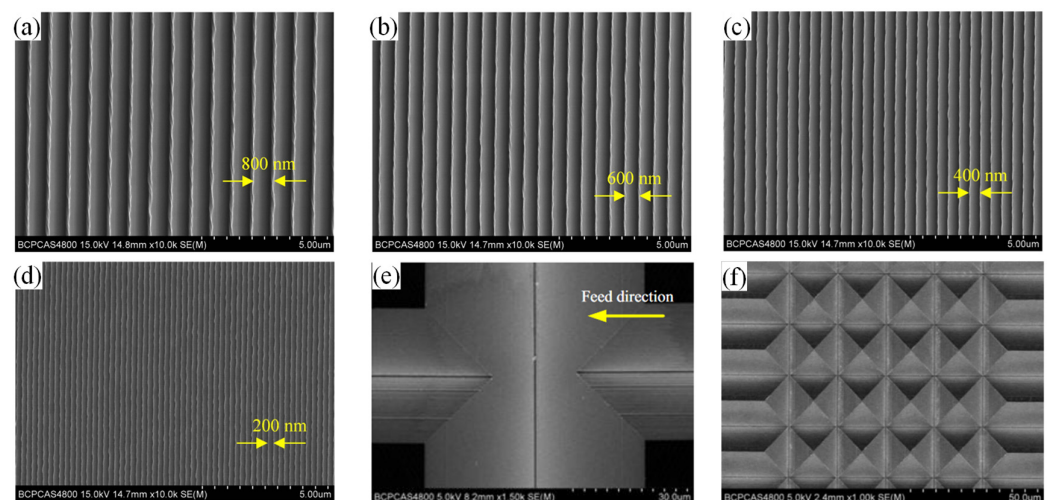


Figure 39. Second-order submicron grooves with different spacing: (a) 800 nm; (b) 600 nm; (c) 400 nm; (d) 200 nm; (e) High-quality exit and the entry part of the micro-pyramid; and (f) micro-pyramid array machined by fly cutting. Reprinted with permission from Refs. [192,193].

5. Summary and Outlook

5.1. Summary

Micro-structured surfaces not only show excellent performance in natural plants and animals, but also are widely used in many fields such as optical engineering, biomedicine etc. In this review, the advanced fabrication methods and assistive technologies for fabrication of micro-structures are reviewed. According to their specific applications, the main research achievements of various machining strategies are reported. From the review, typical machining technologies for micro-structured surface are mainly classified into lithography technology, high energy beam direct writing technology, special energy field machining technology, molding technology, LIGA technology, and UPM technology. However, these methods cannot meet all the requirements alone in the fabrication of high accuracy, complex 3D, and high aspect ratio micro-structure surface.

Among these methods, UPM exhibits unique advantages in obtaining micro-structures with certain geometry. As the key assistive technologies, FTS/STS system is combined with UPM to extend the machining technology to freeform surfaces and complex micro/nano structured surfaces. FTS system has high frequency response, which is applicable for machining the micro-structures with complex surface shape and small drop.

The different actuators in FTS device provide the possibility of machining a diversity of micro-structures. The piezoelectric actuated FTS system is suitable for machining small amplitude micro-structures such as micro-lens arrays with high frequency; magnetostrictive FTS system is usually used in micro-displacement and precise positioning; voice coil actuated FTS system is applicable for machining micro-structures with high aspect ratio; Maxwell actuated FTS system can achieve ultra-high frequency response and has great potential for micro-structures machining. FTS system can also be designed into different DOF according to machining requirements of complex structures. The versatility of FTS brings more possibilities for micro-structured surfaces machining. Different from FTS, STS system has low frequency response but large stroke for the feed shaft, which is applicable for machining micro-structures with high surface roughness, smooth surface shape and large overall drop. The different advantages of FTS/STS system broaden the machining performance of micro-structures.

Based on ultra-precision diamond turning, UPFC is a developed cutting technology. Under the turning mode, the cutting speed varies with the feed radius, which may lead to a uniformly surface quality. Compared with turning, though UPFC is discontinuous cutting with low cutting efficiency, its cutting speed is constant and it can generate special micro-structured surfaces deterministically. In UPFC, EFCS is applicable for machining freeform surfaces and periodic micro-structures, like pyramid array, triangular pyramid array, lens array, etc. And UPRM is applicable for machining V-grooves and large freeform surfaces. In the future, UPFC combined with FTS/STS system has great application potential in the preparation of special micro-structured surfaces.

5.2. Outlook

With the increasing demands of large size, high form accuracy and surface finish of micro-structures, UPM technology has developed rapidly. High precision, intelligence, automation, high efficiency, information, flexibility, and integration become the future development trend of UPM, as shown in Table 5 for details. Besides, the progress of micromachining trends in machining micro-structures is shown in Figure 40.

Specially, combining different machining methods together is of great significance for the fabrication of multi-layer and multi-scale micro-structures. For example, the compound eye structure can be obtained by fabricating planar substrate micro-lens using laser direct writing technology and fabricating sublayer surface using lithography and replication transfer technology. Higher flexibility and accuracy can be achieved by combination of various machining technologies, which is conducive to the realization of complex micro-structures with different characteristic sizes. It also can produce more diverse micro-structured surfaces and provide more possibilities for optical structures. In addition, UPM

as a key method for machining micro-structures, combining with FTS/STS technology and FIB technology, will be fully exploited to their advantage. However, residual tool marks and material recovery are still the key factors affecting the micro-structured surface morphology, and more solutions are needed in the future.

Table 5. UPM future trends.

| Trend | Content | Research |
|--------------|--|---|
| Precision | Improving the workpiece size, shape, position accuracy, surface roughness. | Aerospace, satellite, mobile phone, optical parts [17]. |
| Intelligence | Replacing part of human mental work, independent analysis, reasoning, judgment, decision-making. | The dynamic adjustment model realizes the self-adjustment of the system's situational perception [211]. Intelligent monitoring [212,213]. |
| Automation | Replacing part of human physical labor and realizing simple operation. | Quasi-online compensation method improves automatic adjustment of lathe accuracy [214–216]. Adjusting virtual model and controlling the process online [217]. |
| Efficiency | Improving production efficiency and save time. | Efficient production [218]. |
| Information | The collection, combination, input and machining of manufacturing information. | Real-time monitoring and data acquisition of digital twin in grinding machine system [219]. |
| Flexibility | Computer numerical control machine tool-based manufacturing equipment to carry out large quantities, many varieties of production. | Dynamic clamping and positioning method of flexible machining system based on digital twin technology [220]. |
| Integration | Multiple independently operating single modules are integrated into a coordinated and functional system. | Feedback-forward combined adaptive regulator of tool rest platform for active vibration control [221]. |

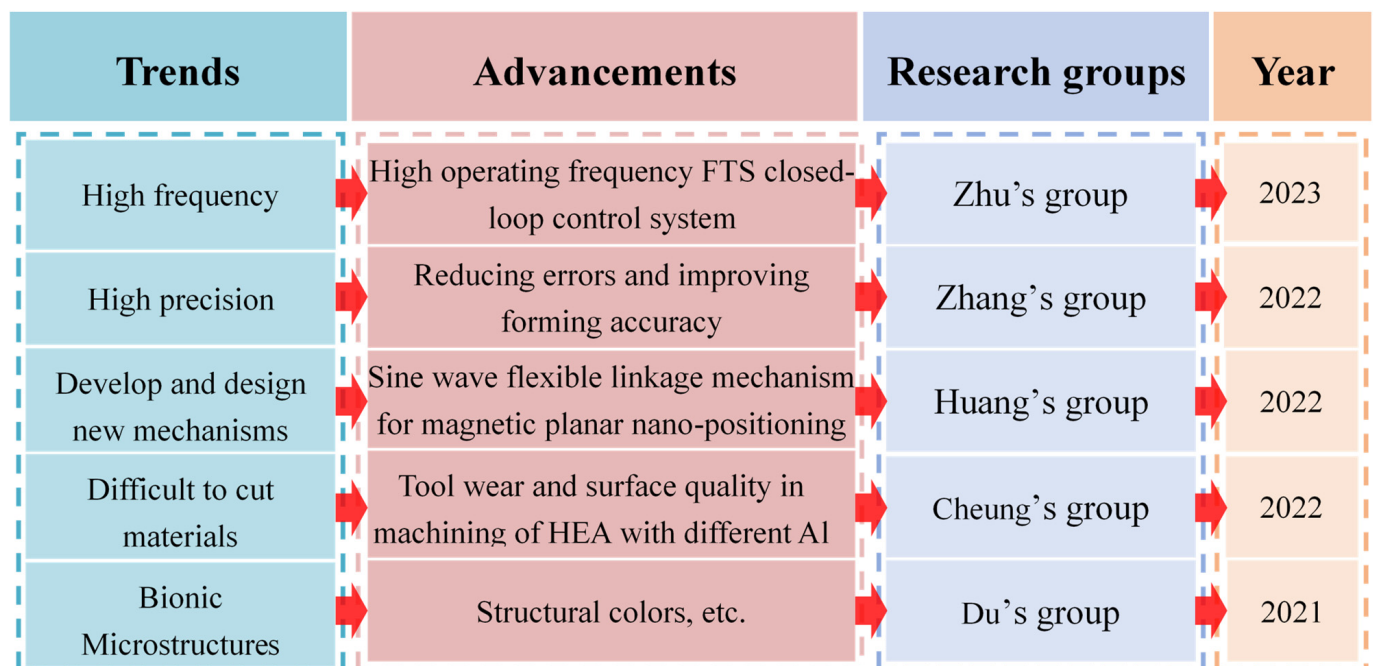


Figure 40. The progress of micromachining trends in machining micro-structures [199,222–225].

Author Contributions: Conceptualization, G.Z. and Y.M.; methodology, S.C.; validation, J.H., S.M. and Z.H. (Zexuan Huo); resources, G.Z.; data curation, Y.M.; writing—original draft preparation, Y.M.; writing—review and editing, J.H., S.M. and Z.H. (Zeja Huang); visualization, Y.M.; supervision, Y.M.; funding acquisition, G.Z. All authors have read and agreed to the published version of the manuscript.

Funding: The research proposed in this paper was supported by the National Natural Science Foundation of China (Grant No. 52275454, U2013603, 51827901) and the Shenzhen Natural Science Foundation (Grant No. JCYJ20220531103614032, 20200826160002001, JCYJ20220818102409021).

Data Availability Statement: Not applicable.

Conflicts of Interest: The authors declare no conflict of interest.

References

1. Tan, N.Y.J.; Zhang, X.; Neo, D.W.K.; Huang, R.; Liu, K.; Senthil Kumar, A. A review of recent advances in fabrication of optical Fresnel lenses. *J. Manuf. Process.* **2021**, *71*, 113–133. [[CrossRef](#)]
2. Kong, L.B.; Cheung, C.F. Modeling and characterization of surface generation in fast tool servo machining of microlens arrays. *Comput. Ind. Eng.* **2012**, *63*, 957–970. [[CrossRef](#)]
3. Liu, K.; Jiang, L. Bio-inspired design of multiscale structures for function integration. *Nano Today* **2011**, *6*, 155–175. [[CrossRef](#)]
4. Brinksmeier, E.; Karpuschewski, B.; Yan, J.; Schönemann, L. Manufacturing of multiscale structured surfaces. *CIRP Ann.* **2020**, *69*, 717–739. [[CrossRef](#)]
5. Fu, Y.F.; Yuan, C.Q.; Bai, X.Q. Marine drag reduction of shark skin inspired riblet surfaces. *Biosurf. Biotribol.* **2017**, *3*, 11–24. [[CrossRef](#)]
6. Wei, H.M.; Gong, H.B.; Chen, L.; Zi, M.; Cao, B.Q. Photovoltaic Efficiency Enhancement of Cu₂O Solar Cells Achieved by Controlling Homojunction Orientation and Surface Microstructure. *J. Phys. Chem. C* **2012**, *116*, 10510–10515. [[CrossRef](#)]
7. Zhong, M.; Huang, T. Laser hybrid fabrication of tunable micro- and nano-scale surface structures and their functionalization. In *Laser Surface Engineering*; Lawrence, J., Waugh, D.G., Eds.; Woodhead Publishing: Cambridge, UK, 2015; pp. 213–235, ISBN 978-1-78242-074-3.
8. Neinhuis, C.; Barthlott, W. Characterization and Distribution of Water-repellent, Self-cleaning Plant Surfaces. *Ann. Bot.* **1997**, *79*, 667–677. [[CrossRef](#)]
9. Zhao, W.; Wang, L.; Xue, Q. Fabrication of Low and High Adhesion Hydrophobic Au Surfaces with Micro/Nano-Biomimetic Structures. *J. Phys. Chem. C* **2010**, *114*, 11509–11514. [[CrossRef](#)]
10. Natarajan, E.; Inácio Freitas, L.; Rui Chang, G.; Abdulaziz Majeed Al-Talib, A.; Hassan, C.S.; Ramesh, S. The hydrodynamic behaviour of biologically inspired bristled shark skin vortex generator in submarine. *Mater. Today Proc.* **2021**, *46*, 3945–3950. [[CrossRef](#)]
11. Han, Z.; Fu, J.; Wang, Z.; Wang, Y.; Li, B.; Mu, Z.; Zhang, J.; Niu, S. Long-term durability of superhydrophobic properties of butterfly wing scales after continuous contact with water. *Colloids Surf. A* **2017**, *518*, 139–144. [[CrossRef](#)]
12. Gao, X.; Yan, X.; Yao, X.; Xu, L.; Zhang, K.; Zhang, J.; Yang, B.; Jiang, L. The Dry-Style Antifogging Properties of Mosquito Compound Eyes and Artificial Analogues Prepared by Soft Lithography. *Adv. Mater.* **2007**, *19*, 2213–2217. [[CrossRef](#)]
13. Malshe, A.P.; Bapat, S.; Rajurkar, K.P.; Haitjema, H. Bio-inspired textures for functional applications. *CIRP Ann.* **2018**, *67*, 627–650. [[CrossRef](#)]
14. Jung, H.; Jeong, K.-H. Monolithic polymer microlens arrays with high numerical aperture and high packing density. *ACS Appl. Mater. Interfaces* **2015**, *7*, 2160–2165. [[CrossRef](#)] [[PubMed](#)]
15. Zhou, W.; Li, R.; Li, M.; Tao, P.; Wang, X.; Dai, S.; Song, B.; Zhang, W.; Lin, C.; Shen, X.; et al. Fabrication of microlens array on chalcogenide glass by wet etching-assisted femtosecond laser direct writing. *Ceram. Int.* **2022**, *48*, 18983–18988. [[CrossRef](#)]
16. Zong, W.J.; Li, D.; Sun, T.; Cheng, K. Contact accuracy and orientations affecting the lapped tool sharpness of diamond cutting tools by mechanical lapping. *Diam. Relat. Mater.* **2006**, *15*, 1424–1433. [[CrossRef](#)]
17. Fang, F.Z.; Zhang, X.D.; Weckenmann, A.; Zhang, G.X.; Evans, C. Manufacturing and measurement of freeform optics. *CIRP Ann.* **2013**, *62*, 823–846. [[CrossRef](#)]
18. Luo, G.; Wu, D.; Zhou, Y.; Hu, Y.; Yao, Z. Laser printing of large-scale metal micro/nanoparticle array: Deposition behavior and microstructure. *Int. J. Mach. Tools Manuf.* **2022**, *173*, 103845. [[CrossRef](#)]
19. Lee, L.P.; Berger, S.A.; Liepmann, D.; Pruitt, L. High aspect ratio polymer microstructures and cantilevers for bioMEMS using low energy ion beam and photolithography. *Sens. Actuators A* **1998**, *71*, 144–149. [[CrossRef](#)]
20. Zhang, Z.; He, H.; Fu, W.; Ji, D.; Ramakrishna, S. Electro-Hydrodynamic Direct-Writing Technology toward Patterned Ultra-Thin Fibers: Advances, Materials and Applications. *Nano Today* **2020**, *35*, 100942. [[CrossRef](#)]
21. Biesuz, M.; Saunders, T.; Ke, D.; Reece, M.J.; Hu, C.; Grasso, S. A review of electromagnetic processing of materials (EPM): Heating, sintering, joining and forming. *J. Mater. Sci. Technol.* **2021**, *69*, 239–272. [[CrossRef](#)]
22. Stephens, L.S.; Siripuram, R.; Hayden, M.; McCartt, B. Deterministic Micro Asperities on Bearings and Seals Using a Modified LIGA Process. *J. Eng. Gas Turbines Power* **2004**, *126*, 147–154. [[CrossRef](#)]
23. Wang, Y.; Zhao, Q.; Shang, Y.; Lv, P.; Guo, B.; Zhao, L. Ultra-precision machining of Fresnel microstructure on die steel using single crystal diamond tool. *J. Mater. Process. Technol.* **2011**, *211*, 2152–2159. [[CrossRef](#)]
24. Wu, L.; Leng, J.; Ju, B. Digital twins-based smart design and control of ultra-precision machining: A Review. *Symmetry* **2021**, *13*, 1717. [[CrossRef](#)]
25. Joshi, S.S. Ultra-precision Machining. In *Encyclopedia of Nanotechnology*; Bhushan, B., Ed.; Springer: Dordrecht, The Netherlands, 2016; p. 4253, ISBN 978-94-017-9780-1.
26. Taniguchi, N. Current Status in, and Future Trends of, Ultraprecision Machining and Ultrafine Materials Processing. *CIRP Ann.* **1983**, *32*, 573–582. [[CrossRef](#)]
27. Byrne, G.; Dornfeld, D.; Denkena, B. Advancing Cutting Technology. *CIRP Ann.* **2003**, *52*, 483–507. [[CrossRef](#)]

28. Wang, Z.; Luo, X.; Sun, J.; Seib, P.; Phuagkhaopong, S.; Chang, W.; Gao, J.; Mir, A.; Cox, A. Investigation of chip formation mechanism in ultra-precision diamond turning of silk fibroin film. *J. Manuf. Process.* **2022**, *74*, 14–27. [[CrossRef](#)]
29. Foy, K.; Wei, Z.; Matsumura, T.; Huang, Y. Effect of tilt angle on cutting regime transition in glass micromilling. *Int. J. Mach. Tools Manuf.* **2009**, *49*, 315–324. [[CrossRef](#)]
30. Geng, R.; Yang, X.; Xie, Q.; Zhang, W.; Kang, J.; Liang, Y.; Li, R. Ultra-precision diamond turning of ZnSe ceramics: Surface integrity and ductile regime machining mechanism. *Infrared Phys. Technol.* **2021**, *115*, 103706. [[CrossRef](#)]
31. Wang, S.; Zhang, Q.; Zhao, Q.; Guo, B. Surface generation and materials removal mechanism in ultra-precision grinding of biconical optics based on slow tool servo with diamond grinding wheels. *J. Manuf. Process.* **2021**, *72*, 1–14. [[CrossRef](#)]
32. Zheng, Z.; Huang, K.; Lin, C.; Zhang, J.; Wang, K.; Sun, P.; Xu, J. An analytical force and energy model for ductile-brittle transition in ultra-precision grinding of brittle materials. *Int. J. Mech. Sci.* **2022**, *220*, 107107. [[CrossRef](#)]
33. Guo, J.; Goh, M.H.; Wang, P.; Huang, R.; Lee, X.; Wang, B.; Nai, S.M.L.; Wei, J. Investigation on surface integrity of electron beam melted Ti-6Al-4 V by precision grinding and electropolishing. *Chin. J. Aeronaut.* **2021**, *34*, 28–38. [[CrossRef](#)]
34. Arnold, T.; Pietag, F. Ion beam figuring machine for ultra-precision silicon spheres correction. *Precis. Eng.* **2015**, *41*, 119–125. [[CrossRef](#)]
35. Zhang, S.; Zhou, Y.; Zhang, H.; Xiong, Z.; To, S. Advances in ultra-precision machining of micro-structured functional surfaces and their typical applications. *Int. J. Mach. Tools Manuf.* **2019**, *142*, 16–41. [[CrossRef](#)]
36. Zhang, S.J.; To, S.; Wang, S.J.; Zhu, Z.W. A review of surface roughness generation in ultra-precision machining. *Int. J. Mach. Tools Manuf.* **2015**, *91*, 76–95. [[CrossRef](#)]
37. Buhmann, M.; Roth, R.; Liebrich, T.; Frick, K.; Carelli, E.; Marxer, M. New positioning procedure for optical probes integrated on ultra-precision diamond turning machines. *CIRP Ann.* **2020**, *69*, 473–476. [[CrossRef](#)]
38. Schönemann, L.; Riemer, O. Thermo-mechanical tool setting mechanism for ultra-precision milling with multiple cutting edges. *Precis. Eng.* **2019**, *55*, 171–178. [[CrossRef](#)]
39. Huang, X.-F.; Tang, P.; Yang, S.; Feng, J.-Y.; Wan, Z.-P. Investigation of AlN ceramic anisotropic deformation behavior during scratching. *J. Eur. Ceram. Soc.* **2022**, *42*, 2678–2690. [[CrossRef](#)]
40. Wang, S.; Zhao, Q.; Yang, X. Surface and subsurface microscopic characteristics in sapphire ultra-precision grinding. *Tribol. Int.* **2022**, *174*, 107710. [[CrossRef](#)]
41. Zhang, H.; Zhang, X.; Li, Z.; Wang, P.; Guo, Z. Removing single-point diamond turning marks using form-preserving active fluid jet polishing. *Precis. Eng.* **2022**, *76*, 237–254. [[CrossRef](#)]
42. Zhang, S.J.; To, S.; Zhang, G.Q.; Zhu, Z.W. A review of machine-tool vibration and its influence upon surface generation in ultra-precision machining. *Int. J. Mach. Tools Manuf.* **2015**, *91*, 34–42. [[CrossRef](#)]
43. Hong, D.; Zeng, W.; Yang, N.; Tang, B.; Liu, Q.-J. The micro-wear mechanism of diamond during diamond tool fly-cutting KDP (KH₂PO₄) from first principle calculations. *J. Mol. Model.* **2020**, *26*, 284. [[CrossRef](#)] [[PubMed](#)]
44. Kim, H.-S.; Lee, K.-I.; Lee, K.-M.; Bang, Y.-B. Fabrication of free-form surfaces using a long-stroke fast tool servo and corrective figuring with on-machine measurement. *Int. J. Mach. Tools Manuf.* **2009**, *49*, 991–997. [[CrossRef](#)]
45. Nakamura, M.; Mano, I.; Taniguchi, J. Fabrication of micro-lens array with antireflection structure. *Microelectron. Eng.* **2019**, *211*, 29–36. [[CrossRef](#)]
46. Zhang, X.; Chen, Z.; Chen, J.; Wang, Z.; Zhu, L. Fabrication of a microlens array featuring a high aspect ratio with a swinging diamond tool. *J. Manuf. Process.* **2022**, *75*, 485–496. [[CrossRef](#)]
47. Tang, L.; Zhou, T.; Zhou, J.; Liang, Z.; Wang, X. Research on single point diamond turning of chalcogenide glass aspheric lens. *Procedia CIRP* **2018**, *71*, 293–298. [[CrossRef](#)]
48. Meng, S.; Yin, Z.; Guo, Y.; Yao, J.; Chai, N. Ultra-precision machining of polygonal Fresnel lens on roller mold. *Int. J. Adv. Manuf. Technol.* **2020**, *108*, 2445–2452. [[CrossRef](#)]
49. Gao, X.; Li, Y.; Kong, Q.C.; Tan, Q.F.; Li, C.J. Uniform concentrating design and mold machining of Fresnel lens for photovoltaic systems. *Int. J. Adv. Manuf. Technol.* **2018**, *96*, 451–460. [[CrossRef](#)]
50. Huang, R.; Zhang, X.Q.; Rahman, M.; Kumar, A.S.; Liu, K. Ultra-precision machining of radial Fresnel lens on roller moulds. *Cirp Ann.-Manuf. Technol.* **2015**, *64*, 121–124. [[CrossRef](#)]
51. Meng, S.T.; Yin, Z.Q.; Xia, S.B.; Yao, J.H.; Zhang, J.W. Diamond micro-scraping for the fabrication of polygonal Fresnel lens structure array on roller molds. *Int. J. Adv. Manuf. Technol.* **2021**, *116*, 1951–1959. [[CrossRef](#)]
52. Cheng, M.N.; Cheung, C.F.; Lee, W.B.; To, S. A Study of Factors Affecting Surface Quality in Ultra-Precision Raster Milling. *Key Eng. Mater.* **2007**, *339*, 400–406. [[CrossRef](#)]
53. Xu, R.; Deng, Z.; Yue, Y.; Wang, S.; Li, X.; Ma, Z.; Jiang, Y.; Wang, L.; Du, C.; Jia, H.; et al. Fabrication of large-scale uniform submicron inverted pyramid pit arrays on silicon substrates by laser interference lithography. *Vacuum* **2019**, *165*, 1–6. [[CrossRef](#)]
54. Huang, Y.; Li, S.; Zhang, J.; Yang, C.; Liu, W. Research on shape error of microstructure array fabricated by fly cutting. *Optik* **2021**, *241*, 167031. [[CrossRef](#)]
55. Yu, S.; Yao, P.; Huang, C.; Chu, D.; Zhu, H.; Zou, B.; Liu, H. On-machine precision truing of ultrathin arc-shaped diamond wheels for grinding aspherical microstructure arrays. *Precis. Eng.* **2022**, *73*, 40–50. [[CrossRef](#)]
56. Wang, S.J.; To, S.; Chen, X.; Wang, H.; Xia, H.J. A study of the fabrication of v-groove structure in ultra-precision milling. *Int. J. Comput. Integr. Manuf.* **2014**, *27*, 986–996. [[CrossRef](#)]

57. Wacogne, B.; Sadani, Z.; Gharbi, T. Compensation structures for V-grooves connected to square apertures in KOH-etched (100) silicon: Theory, simulation and experimentation. *Sens. Actuators A-Phys.* **2004**, *112*, 328–339. [[CrossRef](#)]
58. Zhang, S.J.; To, S.; Zhang, G.Q. Diamond tool wear in ultra-precision machining. *Int. J. Adv. Manuf. Technol.* **2017**, *88*, 613–641. [[CrossRef](#)]
59. Mudgal, T.; Dwivedi, P.; Kulkarni, M. *Nano/Micro Structure Fabrication Using Combination of Self Organization, Electron Beam and Photolithography*; Centre For Nano-Sciences, Indian Institute of Technology (IIT): Kanpur, India, 2018.
60. Park, J.M.; Park, S.; Shin, D.S.; Kim, J.; Cho, H.; Yang, W.S.; Son, S.; Park, S.J. Microfabrication of Ni-Fe Mold Insert via Hard X-ray Lithography and Electroforming Process. *Metals* **2020**, *10*, 486. [[CrossRef](#)]
61. Finders, J.; de Winter, L.; Last, T. Mitigation of mask three-dimensional induced phase effects by absorber optimization in ArF i and extreme ultraviolet lithography. *J. Micro/Nanolithogr. MEMS MOEMS* **2016**, *15*, 021408. [[CrossRef](#)]
62. Chen, Y. Nanofabrication by electron beam lithography and its applications: A review. *Microelectron. Eng.* **2015**, *135*, 57–72. [[CrossRef](#)]
63. Andreev, M.; Marmiroli, B.; Schennach, R.; Amenitsch, H. Patterning a cellulose based dual-tone photoresist via deep X-ray lithography. *Microelectron. Eng.* **2022**, *256*, 111720. [[CrossRef](#)]
64. Marmiroli, B.; Amenitsch, H. X-ray lithography and small-angle X-ray scattering: A combination of techniques merging biology and materials science. *Eur. Biophys. J.* **2012**, *41*, 851–861. [[CrossRef](#)] [[PubMed](#)]
65. Watt, F.; Bettioli, A.A.; Van Kan, J.A.; Teo, E.J.; Breese, M.B.H. Ion beam lithography and nanofabrication: A review. *Int. J. Nanosci.* **2005**, *4*, 269–286. [[CrossRef](#)]
66. Reyntjens, S.; Puers, R. A review of focused ion beam applications in microsystem technology. *J. Micromech. Microeng.* **2001**, *11*, 287–300. [[CrossRef](#)]
67. Palka, K.; Kurka, M.; Slang, S.; Vlcek, M. Utilization of As₅₀Se₅₀ thin films in electron beam lithography. *Mater. Chem. Phys.* **2021**, *259*, 124052. [[CrossRef](#)]
68. Rius, G.; Llobet, J.; Arcamone, J.; Borrissé, X.; Pérez-Murano, F. Electron- and ion-beam lithography for the fabrication of nanomechanical devices integrated on CMOS circuits. *Microelectron. Eng.* **2009**, *86*, 1046–1049. [[CrossRef](#)]
69. Kathuria, H.; Kochhar, J.S.; Fong MH, M.; Hashimoto, M.; Iliescu, C.; Yu, H.; Kang, L. Microneedle Array Fabrication by Photolithography. *JoVE* **2015**, e52914. [[CrossRef](#)]
70. Tong, X.; Xu, C.; Zhu, J.; Mao, C.; Zhen, X.; Huang, W.; Chen, Y. A study of greyscale electron beam lithography for a 3D round shape Kinoform lens for hard X-ray optics. *Microelectron. Eng.* **2020**, *234*, 111435. [[CrossRef](#)]
71. Langford, R.M.; Nellen, P.M.; Gierak, J.; Fu, Y. Focused Ion Beam Micro- and Nanoengineering. *MRS Bull.* **2007**, *32*, 417–423. [[CrossRef](#)]
72. Heusinger, M.; Banasch, M.; Zeitner, U.D. Rowland ghost suppression in high efficiency spectrometer gratings fabricated by e-beam lithography. *Opt. Express* **2017**, *25*, 6182–6191. [[CrossRef](#)]
73. Cattoni, A.; Mailly, D.; Dalstein, O.; Faustini, M.; Seniutinas, G.; Rösner, B.; David, C. Sub-10nm electron and helium ion beam lithography using a recently developed alumina resist. *Microelectron. Eng.* **2018**, *193*, 18–22. [[CrossRef](#)]
74. Zhu, J.; Chen, Y.; Xie, S.; Zhang, L.; Wang, C.; Tai, R. Nanofabrication of 30 nm Au zone plates by e-beam lithography and pulse voltage electroplating for soft x-ray imaging. *Microelectron. Eng.* **2020**, *225*, 111254. [[CrossRef](#)]
75. Chung, J.; Hsu, W. Enhancement on forming complex three dimensional microstructures by a double-side multiple partial exposure method. *J. Vac. Sci. Technol. B* **2007**, *25*, 1671–1678. [[CrossRef](#)]
76. Totsu, K.; Fujishiro, K.; Tanaka, S.; Esashi, M. Fabrication of three-dimensional microstructure using maskless gray-scale lithography. *Sens. Actuators A* **2006**, *130*, 387–392. [[CrossRef](#)]
77. Nachmias, T.; Ohayon, A.; Meltzer, S.; Kabla, M.; Louzon, E.; Levy, U. Shallow Fresnel lens fabrication using grayscale lithography made by high energy beam sensitive mask (HEBS) technology and reactive ion etching. *SPIE* **2009**, *7205*, 68–79. [[CrossRef](#)]
78. Kuo, H.-F. Effect of Source Pupil Shape on Process Windows in EUV Lithography. *IEEE Trans. Nanotechnol.* **2014**, *13*, 136–142. [[CrossRef](#)]
79. Chen, H.L.; Chuang, S.Y.; Lin, C.H.; Lin, Y.H. Using colloidal lithography to fabricate and optimize sub-wavelength pyramidal and honeycomb structures in solar cells. *Opt. Express* **2007**, *15*, 14793–14803. [[CrossRef](#)]
80. Kosiorek, A.; Kandulski, W.; Glaczynska, H.; Giersig, M. Fabrication of Nanoscale Rings, Dots, and Rods by Combining Shadow Nanosphere Lithography and Annealed Polystyrene Nanosphere Masks. *Small* **2005**, *1*, 439–444. [[CrossRef](#)]
81. Vossen, D.L.J.; Fific, D.; Penninkhof, J.; van Dillen, T.; Polman, A.; van Blaaderen, A. Combined Optical Tweezers/Ion Beam Technique to Tune Colloidal Masks for Nanolithography. *Nano Lett.* **2005**, *5*, 1175–1179. [[CrossRef](#)]
82. Lee, J.-S.; Yu, J.-H.; Hwang, K.-H.; Nam, S.-H.; Boo, J.-H.; Yun, S.H. Patterning ITO by template-assisted colloidal-lithography for enhancing power conversion efficiency in organic photovoltaic. *J. Nanosci. Nanotechnol.* **2016**, *16*, 5024–5028. [[CrossRef](#)]
83. Hongzhong, L.; Yucheng, D.; Weitao, J.; Qin, L.; Lei, Y.; Yongsheng, S.; Bingheng, L. Novel imprint lithography process used in fabrication of micro/nanostructures in organic photovoltaic devices. *J. Micro/Nanolithography MEMS MOEMS* **2009**, *8*, 021170. [[CrossRef](#)]
84. Sanchez-Sobrado, O.; Mendes, M.J.; Haque, S.; Mateus, T.; Aguas, H.; Fortunato, E.; Martins, R. Lightwave trapping in thin film solar cells with improved photonic-structured front contacts. *J. Mater. Chem. C* **2019**, *7*, 6456–6464. [[CrossRef](#)]
85. Centeno, P.; Alexandre, M.F.; Chapa, M.; Pinto, J.V.; Deuermeier, J.; Mateus, T.; Fortunato, E.; Martins, R.; Águas, H.; Mendes, M.J. Self-Cleaned Photonic-Enhanced Solar Cells with Nanostructured Parylene-C. *Adv. Mater. Interfaces* **2020**, *7*, 2000264. [[CrossRef](#)]

86. Chen, J.; Liu, Z.; Su, F.; Wu, S.; Liang, C.; Liu, J. Surface modification of carbon fiber cloth by femtosecond laser direct writing technology. *Mater. Lett.* **2022**, *323*, 132483. [[CrossRef](#)]
87. Zhao, J.; Zhao, Y.; Peng, Y.; Lv, R.-q.; Zhao, Q. Review of femtosecond laser direct writing fiber-optic structures based on refractive index modification and their applications. *Opt. Laser Technol.* **2022**, *146*, 107473. [[CrossRef](#)]
88. Zhou, W.; Li, R.; Qi, Q.; Yang, Y.; Wang, X.; Dai, S.; Song, B.; Xu, T.; Zhang, P. Fabrication of Fresnel zone plate in chalcogenide glass and fiber end with femtosecond laser direct writing. *Infrared Phys. Technol.* **2022**, *120*, 104004. [[CrossRef](#)]
89. Xu, Z.; Fang, F.; Gao, H.; Zhu, Y.; Wu, W.; Weckenmann, A. Nano fabrication of star structure for precision metrology developed by focused ion beam direct writing. *CIRP Ann.* **2012**, *61*, 511–514. [[CrossRef](#)]
90. Mizoshiri, M.; Hayashi, T.; Narushima, J.; Ohishi, T. Femtosecond laser direct writing of Cu–Ni alloy patterns in ambient atmosphere using glyoxylic acid Cu/Ni mixed complexes. *Opt. Laser Technol.* **2021**, *144*, 107418. [[CrossRef](#)]
91. Egashira, K.; Kumagai, R.; Okina, R.; Yamaguchi, K.; Ota, M. Drilling of microholes down to 10µm in diameter using ultrasonic grinding. *Precis. Eng.* **2014**, *38*, 605–610. [[CrossRef](#)]
92. Banerjee, B.; Mondal, K.; Adhikary, S.; Nath Paul, S.; Pramanik, S.; Chatterjee, S. Optimization of process parameters in ultrasonic machining using integrated AHP-TOPSIS method. *Mater. Today Proc.* **2022**, *62*, 2857–2864. [[CrossRef](#)]
93. Airao, J.; Nirala, C.K. Machinability of Ti-6Al-4V and Nimonic-90 in ultrasonic-assisted turning under sustainable cutting fluid. *Mater. Today Proc.* **2022**, *62*, 7396–7400. [[CrossRef](#)]
94. Chen, F.; Bie, W.; Wang, X.; Zhao, B. Longitudinal-torsional coupled rotary ultrasonic machining of ZrO₂ ceramics: An experimental study. *Ceram. Int.* **2022**, *48*, 28154–28162. [[CrossRef](#)]
95. Chen, Y.; Hu, Z.; Yu, Y.; Lai, Z.; Zhu, J.; Xu, X.; Peng, Q. Processing and machining mechanism of ultrasonic vibration-assisted grinding on sapphire. *Mater. Sci. Semicond. Process.* **2022**, *142*, 106470. [[CrossRef](#)]
96. Sapkota, G.; Das, S.; Sharma, A.; Kumar Ghadai, R. Comparison of various multi-criteria decision methods for the selection of quality hole produced by ultrasonic machining process. *Mater. Today Proc.* **2022**, *58*, 702–708. [[CrossRef](#)]
97. Sabareesan, S.; Vasudevan, D.; Sridhar, S.; Kannan, R.; Sankar, V. Response analysis of ultrasonic machining process under different materials—Review. *Mater. Today Proc.* **2021**, *45*, 2340–2342. [[CrossRef](#)]
98. Juri, A.Z.; Nakanishi, Y.; Yin, L. Microstructural influence on damage-induced zirconia surface asperities produced by conventional and ultrasonic vibration-assisted diamond machining. *Ceram. Int.* **2021**, *47*, 25744–25754. [[CrossRef](#)]
99. Gao, H.; Ma, B.; Zhu, Y.; Yang, H. Enhancement of machinability and surface quality of Ti-6Al-4V by longitudinal ultrasonic vibration-assisted milling under dry conditions. *Measurement* **2022**, *187*, 110324. [[CrossRef](#)]
100. Xu, S.; Shimada, K.; Mizutani, M.; Kuriyagawa, T. Fabrication of hybrid micro/nano-textured surfaces using rotary ultrasonic machining with one-point diamond tool. *Int. J. Mach. Tools Manuf.* **2014**, *86*, 12–17. [[CrossRef](#)]
101. Ni, C.; Zhu, L. Investigation on machining characteristics of TC4 alloy by simultaneous application of ultrasonic vibration assisted milling (UVAM) and economical-environmental MQL technology. *J. Mater. Process. Technol.* **2020**, *278*, 116518. [[CrossRef](#)]
102. Liu, S.-J.; Chen, Y.-S. The manufacturing of thermoplastic composite parts by water-assisted injection-molding technology. *Compos. Pt. A-Appl. Sci. Manuf.* **2004**, *35*, 171–180. [[CrossRef](#)]
103. Michaeli, W.; Spennemann, A. A new injection molding technology for micro parts. *J. Polym. Eng.* **2001**, *21*, 87–98. [[CrossRef](#)]
104. Tsai, S.-W.; Chen, P.-Y.; Lee, Y.-C. Fabrication of a seamless roller mold with wavy microstructures using mask-less curved surface beam pen lithography. *J. Micromech. Microeng.* **2014**, *24*, 045022. [[CrossRef](#)]
105. Guo, F.; Zhou, X.; Liu, J.; Zhang, Y.; Li, D.; Zhou, H. A reinforcement learning decision model for online process parameters optimization from offline data in injection molding. *Appl. Soft Comput.* **2019**, *85*, 105828. [[CrossRef](#)]
106. Wang, X.; Gu, J.; Shen, C.; Wang, X. Warpige optimization with dynamic injection molding technology and sequential optimization method. *Int. J. Adv. Manuf. Technol.* **2015**, *78*, 177–187. [[CrossRef](#)]
107. Willke, T.; Gearhart, S. LIGA micromachined planar transmission lines and filters. *IEEE Trans. Microw. Theory Tech.* **1997**, *45*, 1681–1688. [[CrossRef](#)]
108. Us Sarwar, M.S.; Dahmardeh, M.; Nojeh, A.; Takahata, K. Batch-mode micropatterning of carbon nanotube forests using UV-LIGA assisted micro-electro-discharge machining. *J. Mater. Process. Technol.* **2014**, *214*, 2537–2544. [[CrossRef](#)]
109. Huang, M.-S.; Li, C.-J.; Yu, J.-C.; Huang, Y.-M.; Hsieh, L.-C. Robust parameter design of micro-injection molded gears using a LIGA-like fabricated mold insert. *J. Mater. Process. Technol.* **2009**, *209*, 5690–5701. [[CrossRef](#)]
110. Luo, S.Y.; Yu, T.H.; Liu, C.Y.; Chen, M.H. Grinding characteristics of micro-abrasive pellet tools fabricated by a LIGA-like process. *Int. J. Mach. Tools Manuf.* **2009**, *49*, 212–219. [[CrossRef](#)]
111. Malek, C.K.; Saile, V. Applications of LIGA technology to precision manufacturing of high-aspect-ratio micro-components and -systems: A review. *Microelectron. J.* **2004**, *35*, 131–143. [[CrossRef](#)]
112. Ma, Y.; Liu, W.; Liu, C. Research on the process of fabricating a multi-layer metal micro-structure based on UV-LIGA overlay technology. *Nanotechnol. Precis. Eng.* **2019**, *2*, 83–88. [[CrossRef](#)]
113. Zong, W.J.; Li, Z.Q.; Sun, T.; Cheng, K.; Li, D.; Dong, S. The basic issues in design and fabrication of diamond-cutting tools for ultra-precision and nanometric machining. *Int. J. Mach. Tools Manuf.* **2010**, *50*, 411–419. [[CrossRef](#)]
114. Yuan, Z.J.; Yao, Y.X.; Zhou, M.; Bal, Q.S. Lapping of Single Crystal Diamond Tools. *CIRP Ann.* **2003**, *52*, 285–288. [[CrossRef](#)]
115. Fujii, S.; Hayama, Y.; Imamura, K.; Kumazaki, H.; Kakinuma, Y.; Tanabe, T. All-precision-machining fabrication of ultrahigh-Q crystalline optical microresonators. *Optica* **2020**, *7*, 694–701. [[CrossRef](#)]

116. Vu, V.T.; Ui Hasan, S.A.; Youn, H.; Park, Y.; Lee, H. Imaging performance of an ultra-precision machining-based Fresnel lens in ophthalmic devices. *Opt. Express* **2021**, *29*, 32068–32080. [[CrossRef](#)] [[PubMed](#)]
117. Abou-El-Hossein, K.; Olufayo, O.; Mkokko, Z. Diamond tool wear during ultra-high precision machining of rapidly solidified aluminium RSA 905. *Wear* **2013**, *302*, 1105–1112. [[CrossRef](#)]
118. Peng, J.-W.; Zhang, F.-L.; Huang, Y.-J.; Liu, J.-M.; Li, K.-J.; Zhou, Y.-M.; Long, Y.; Wang, C.-Y.; Wu, S.-H.; Tang, H.-Q. Comparative study on NiAl and FeAl intermetallic-bonded diamond tools and grinding performance for Si₃N₄ ceramic. *Ceram. Int.* **2021**, *47*, 32736–32746. [[CrossRef](#)]
119. Sun, Z.; To, S.; Yu, K.M. Feasibility investigation on ductile machining of single-crystal silicon for deep micro-structures by ultra-precision fly cutting. *J. Manuf. Process.* **2019**, *45*, 176–187. [[CrossRef](#)]
120. Sun, Z.; To, S.; Zhang, S. A novel ductile machining model of single-crystal silicon for freeform surfaces with large azimuthal height variation by ultra-precision fly cutting. *Int. J. Mach. Tools Manuf.* **2018**, *135*, 1–11. [[CrossRef](#)]
121. Yuetian, H. Research on Single Point Diamond Turning Technology for Complex Surface. Ph.D. Thesis, University of Chinese Academy of Sciences, Beijing, China, 2019.
122. Tanikawa, S.; Yan, J. Fabrication of micro-structured surface with controllable randomness by using FTS-based diamond turning. *Precis. Eng.* **2022**, *73*, 363–376. [[CrossRef](#)]
123. Zhang, Z.; Wang, B.; Kang, R.; Zhang, B.; Guo, D. Changes in surface layer of silicon wafers from diamond scratching. *CIRP Ann.* **2015**, *64*, 349–352. [[CrossRef](#)]
124. Moriya, T.; Nakamoto, K.; Ishida, T.; Takeuchi, Y. Creation of V-shaped microgrooves with flat-ends by 6-axis control ultraprecision machining. *CIRP Ann.* **2010**, *59*, 61–66. [[CrossRef](#)]
125. Takeuchi, Y.; Maeda, S.; Kawai, T.; Sawada, K. Manufacture of Multiple-focus Micro Fresnel Lenses by Means of Nonrotational Diamond Grooving. *CIRP Ann.* **2002**, *51*, 343–346. [[CrossRef](#)]
126. Takeuchi, Y.; Yoneyama, Y.; Ishida, T.; Kawai, T. 6-Axis control ultraprecision microgrooving on sculptured surfaces with non-rotational cutting tool. *CIRP Ann.* **2009**, *58*, 53–56. [[CrossRef](#)]
127. Owen, J.D.; Shultz, J.A.; Suleski, T.J.; Davies, M.A. Error correction methodology for ultra-precision three-axis milling of freeform optics. *CIRP Ann.* **2017**, *66*, 97–100. [[CrossRef](#)]
128. Jiang, J.; Luo, T.; Zhang, G.; Dai, Y. Novel tool offset fly cutting straight-groove-type micro structure arrays. *J. Mater. Process. Technol.* **2021**, *288*, 116900. [[CrossRef](#)]
129. Xu, P.; Cheung, C.-F.; Li, B.; Ho, L.-T.; Zhang, J.-F. Kinematics analysis of a hybrid manipulator for computer controlled ultra-precision freeform polishing. *Rob. Comput. Integr. Manuf.* **2017**, *44*, 44–56. [[CrossRef](#)]
130. Meng, X.; Wu, W.; Liao, B.; Dai, H. Atomic simulation of textured silicon carbide surface ultra-precision polishing. *Ceram. Int.* **2022**, *48*, 17034–17045. [[CrossRef](#)]
131. Wang, X.; Gao, H.; Yuan, J. Experimental investigation and analytical modelling of the tool influence function of the ultra-precision numerical control polishing method based on the water dissolution principle for KDP crystals. *Precis. Eng.* **2020**, *65*, 185–196. [[CrossRef](#)]
132. Cheung, C.F.; Kong, L.B.; Ho, L.T.; To, S. Modelling and simulation of structure surface generation using computer controlled ultra-precision polishing. *Precis. Eng.* **2011**, *35*, 574–590. [[CrossRef](#)]
133. Maillard, D.; Benes, Z.; Piacentini, N.; Villanueva, L.G. Electron-beam lithography on M108Y and M35G chemically amplified DUV photoresists. *Micro Nano Eng.* **2021**, *13*, 100095. [[CrossRef](#)]
134. Senzaki, S.; Okabe, T.; Taniguchi, J. Fabrication of bifocal lenses using resin that can be processed by electron beam lithography after ultraviolet-nanoimprint lithography. *Microelectron. Eng.* **2022**, *258*, 111776. [[CrossRef](#)]
135. Janer, M.; López, T.; Plantà, X.; Riera, D. Ultrasonic nodal point, a new configuration for ultrasonic moulding technology. *Ultrasonics* **2021**, *114*, 106418. [[CrossRef](#)]
136. Song-Jo, C.; Herbert, H.; Juergen, M.; Franz Josef, P.; Joachim, S.; Ulrike, W. LIGA technology today and its industrial applications. *Proc.SPIE* **2000**, *4194*, 44–55. [[CrossRef](#)]
137. Ehrfeld, W.; Lehr, H. Synchrotron radiation and the LIGA technique. *Synchrotron Radiat. News* **1994**, *7*, 9–13. [[CrossRef](#)]
138. Yang, J.; Roa, J.J.; Odén, M.; Johansson-Jõesaar, M.P.; Llanes, L. 3D FIB/FESEM tomography of grinding-induced damage in WC-Co cemented carbides. *Procedia CIRP* **2020**, *87*, 385–390. [[CrossRef](#)]
139. Rubanov, S.; Suvorova, A.; Popov, V.P.; Kalinin, A.A.; Pal'yanov, Y.N. Fabrication of graphitic layers in diamond using FIB implantation and high pressure high temperature annealing. *Diam. Relat. Mater.* **2016**, *63*, 143–147. [[CrossRef](#)]
140. Tong, Z.; Xu, Z.; Wu, W.; Luo, X. Molecular dynamic simulation of low-energy FIB irradiation induced damage in diamond. *Nucl. Instrum. Methods Phys. Res. Sect. B* **2015**, *358*, 38–44. [[CrossRef](#)]
141. Wu, R.; Tauhiduzzaman, M.; Ravi Selvaganapathy, P. Anisotropic wetting surfaces machined by diamond tool with tips microstructured by focused ion beam. *Mater. Des.* **2021**, *210*, 110014. [[CrossRef](#)]
142. Tong, Z.; Luo, X. Investigation of focused ion beam induced damage in single crystal diamond tools. *Appl. Surf. Sci.* **2015**, *347*, 727–735. [[CrossRef](#)]
143. Ono, T. Sharpening of the diamond tool edge by the Ar ion beam machine tool. *Procedia Manuf.* **2021**, *53*, 246–250. [[CrossRef](#)]
144. Wu, W.; Xu, Z.; Fang, F.; Liu, B.; Xiao, Y.; Chen, J.; Wang, X.; Liu, H. Decrease of FIB-induced lateral damage for diamond tool used in nano cutting. *Nucl. Instrum. Methods Phys. Res. Sect. B* **2014**, *330*, 91–98. [[CrossRef](#)]

145. Wang, Y.; Fan, P.; Luo, X.; Geng, Y.; Goel, S.; Wu, W.; Li, G.; Yan, Y. Fabrication of three-dimensional sin-shaped ripples using a multi-tip diamond tool based on the force modulation approach. *J. Manuf. Process.* **2021**, *72*, 262–273. [[CrossRef](#)]
146. Kawasegi, N.; Ozaki, K.; Morita, N.; Nishimura, K.; Yamaguchi, M. Development and machining performance of a textured diamond cutting tool fabricated with a focused ion beam and heat treatment. *Precis. Eng.* **2017**, *47*, 311–320. [[CrossRef](#)]
147. Kawasegi, N.; Ozaki, K.; Morita, N.; Nishimura, K.; Sasaoka, H. Single-crystal diamond tools formed using a focused ion beam: Tool life enhancement via heat treatment. *Diam. Relat. Mater.* **2014**, *49*, 14–18. [[CrossRef](#)]
148. Kawasegi, N.; Niwata, T.; Morita, N.; Nishimura, K.; Sasaoka, H. Improving machining performance of single-crystal diamond tools irradiated by a focused ion beam. *Precis. Eng.* **2014**, *38*, 174–182. [[CrossRef](#)]
149. Gong, Z.; Huo, D.; Niu, Z.; Chen, W.; Shyha, I. Investigation of control algorithm for long-stroke fast tool servo system. *Precis. Eng.* **2022**, *75*, 12–23. [[CrossRef](#)]
150. Tong, Z.; Zhong, W.; To, S.; Zeng, W. Fast-tool-servo micro-grooving freeform surfaces with embedded metrology. *CIRP Ann.* **2020**, *69*, 505–508. [[CrossRef](#)]
151. Zhong, W.; Tong, Z.; Jiang, X. Integration of On-machine Surface Measurement into Fast Tool Servo Machining. *Procedia CIRP* **2021**, *101*, 238–241. [[CrossRef](#)]
152. Gong, Z.; Huo, D.; Niu, Z.; Chen, W.; Cheng, K. A novel long-stroke fast tool servo system with counterbalance and its application to the ultra-precision machining of microstructured surfaces. *Mech. Syst. Sig. Process.* **2022**, *173*, 109063. [[CrossRef](#)]
153. Chang, K.-M.; Cheng, J.-L.; Liu, Y.-T. Machining control of non-axisymmetric aspheric surface based on piezoelectric fast tool servo system. *Precis. Eng.* **2022**, *76*, 160–172. [[CrossRef](#)]
154. Zhao, D.; Zhu, Z.; Huang, P.; Guo, P.; Zhu, L.; Zhu, Z. Development of a piezoelectrically actuated dual-stage fast tool servo. *Mech. Syst. Sig. Process.* **2020**, *144*, 106873. [[CrossRef](#)]
155. Wang, H.; Yang, S. Design and control of a fast tool servo used in noncircular piston turning process. *Mech. Syst. Sig. Process.* **2013**, *36*, 87–94. [[CrossRef](#)]
156. Karunanidhi, S.; Singaperumal, M. Design, analysis and simulation of magnetostrictive actuator and its application to high dynamic servo valve. *Sens. Actuators A* **2010**, *157*, 185–197. [[CrossRef](#)]
157. Xiaobo, T.; Baras, J.S. Modeling and control of a magnetostrictive actuator. In Proceedings of the 41st IEEE Conference on Decision and Control, Las Vegas, NV, USA, 10–13 December 2002; Volume 1, pp. 866–872. [[CrossRef](#)]
158. Park, G.; Bement, M.T.; Hartman, D.A.; Smith, R.E.; Farrar, C.R. The use of active materials for machining processes: A review. *Int. J. Mach. Tools Manuf.* **2007**, *47*, 2189–2206. [[CrossRef](#)]
159. Yoshioka, H.; Kojima, K.; Toyota, D. Micro patterning on curved surface with a fast tool servo system for micro milling process. *CIRP Ann.* **2020**, *69*, 325–328. [[CrossRef](#)]
160. Chen, Y.-L.; Tao, Y.; Hu, P.; Wu, L.; Ju, B.-F. Self-sensing of cutting forces in diamond cutting by utilizing a voice coil motor-driven fast tool servo. *Precis. Eng.* **2021**, *71*, 178–186. [[CrossRef](#)]
161. Ding, F.; Luo, X.; Cai, Y.; Chang, W. Acceleration feedback control for enhancing dynamic stiffness of fast tool servo system considering the sensor imperfections. *Mech. Syst. Sig. Process.* **2020**, *141*, 106429. [[CrossRef](#)]
162. Rakuff, S.; Cuttino, J.F. Design and testing of a long-range, precision fast tool servo system for diamond turning. *Precis. Eng.* **2009**, *33*, 18–25. [[CrossRef](#)]
163. Tao, Y.; Chen, Y.-L.; Hu, P.; Ju, B.-F.; Du, H. Development of a voice coil motor based fast tool servo with a function of self-sensing of cutting forces. *Precis. Eng.* **2020**, *65*, 130–137. [[CrossRef](#)]
164. Liu, Q.; Zhou, X.; Liu, Z.; Lin, C.; Ma, L. Long-stroke fast tool servo and a tool setting method for freeform optics fabrication. *Opt. Eng.* **2014**, *53*, 092005. [[CrossRef](#)]
165. Tian, F.; Yin, Z.; Li, S. A novel long range fast tool servo for diamond turning. *Int. J. Adv. Manuf. Technol.* **2016**, *86*, 1227–1234. [[CrossRef](#)]
166. Nie, Y.H.; Fang, F.Z.; Zhang, X.D. System design of Maxwell force driving fast tool servos based on model analysis. *Int. J. Adv. Manuf. Technol.* **2014**, *72*, 25–32. [[CrossRef](#)]
167. Zhu, Z.; Zhou, X.; Liu, Z.; Wang, R.; Zhu, L. Development of a piezoelectrically actuated two-degree-of-freedom fast tool servo with decoupled motions for micro-/nanomachining. *Precis. Eng.* **2014**, *38*, 809–820. [[CrossRef](#)]
168. Liu, Y.; Zheng, Y.; Gu, Y.; Lin, J.; Lu, M.; Xu, Z.; Fu, B. Development of Piezo-Actuated Two-Degree-of-Freedom Fast Tool Servo System. *Micromachines* **2019**, *10*, 337. [[CrossRef](#)] [[PubMed](#)]
169. Han, J.; Lin, J.; Li, Z.; Lu, M.; Zhang, J. Design and Computational Optimization of Elliptical Vibration-Assisted Cutting System With a Novel Flexure Structure. *IEEE Trans. Ind. Electron.* **2019**, *66*, 1151–1161. [[CrossRef](#)]
170. Awtar, S.; Ustick, J.; Sen, S. An XYZ Parallel-Kinematic Flexure Mechanism With Geometrically Decoupled Degrees of Freedom. *J. Mech. Rob.* **2012**, *5*, 015001. [[CrossRef](#)]
171. Li, H.; Tang, H.; Li, J.; Chen, X. Design, fabrication, and testing of a 3-DOF piezo fast tool servo for microstructure machining. *Precis. Eng.* **2021**, *72*, 756–768. [[CrossRef](#)]
172. Yin, Z.Q.; Dai, Y.F.; Li, S.Y.; Guan, C.L.; Tie, G.P. Fabrication of off-axis aspheric surfaces using a slow tool servo. *Int. J. Mach. Tools Manuf.* **2011**, *51*, 404–410. [[CrossRef](#)]
173. Mishra, V.; Kumar, N.; Sharma, R.; Garg, H.; Karara, V. Development of Aspheric Lenslet Array by Slow Tool Servo Machining. *Mater. Today Proc.* **2020**, *24*, 1602–1607. [[CrossRef](#)]

174. Huang, W.; Yu, D.; Chen, D.; Zhang, M.; Liu, J.; Yao, J. Investigation of variable spindle speed in slow tool servo-based turning of noncircular optical components. *Proc. SPIE* **2016**, *9683*, 17–25. [[CrossRef](#)]
175. Kong, L.B.; Cheung, C.F.; Lee, W.B. A theoretical and experimental investigation of orthogonal slow tool servo machining of wavy microstructured patterns on precision rollers. *Precis. Eng.* **2016**, *43*, 315–327. [[CrossRef](#)]
176. Zhang, X.; Gao, H.; Guo, Y.; Zhang, G. Machining of optical freeform prisms by rotating tools turning. *CIRP Ann.* **2012**, *61*, 519–522. [[CrossRef](#)]
177. Li, D.; Qiao, Z.; Walton, K.; Liu, Y.; Xue, J.; Wang, B.; Jiang, X. Theoretical and Experimental Investigation of Surface Topography Generation in Slow Tool Servo Ultra-Precision Machining of Freeform Surfaces. *Materials* **2018**, *11*, 2566. [[CrossRef](#)] [[PubMed](#)]
178. Huang, P.; Wu, X.; To, S.; Zhu, L.; Zhu, Z. Deterioration of form accuracy induced by servo dynamics errors and real-time compensation for slow tool servo diamond turning of complex-shaped optics. *Int. J. Mach. Tools Manuf.* **2020**, *154*, 103556. [[CrossRef](#)]
179. Chen, C.C.; Cheng, Y.C.; Hsu, W.Y.; Chou, H.Y.; Wang, P.J.; Tsai, D.P. Slow tool servo diamond turning of optical freeform surface for astigmatic contact lens. *Proc. SPIE Opt. Manuf. Test. IX* **2011**, *8126*, 358–366. [[CrossRef](#)]
180. Nagayama, K.; Yan, J. Deterministic error compensation for slow tool servo-driven diamond turning of freeform surface with nanometric form accuracy. *J. Manuf. Process.* **2021**, *64*, 45–57. [[CrossRef](#)]
181. Yu, S.; Wang, Y.; Yao, P.; Wang, H.J.; Liu, Z.L.; Jin, X.Y.; Liu, C.H.; Bao, X.Y.; Chu, D.K.; Qu, S.S.; et al. A novel machining approach of freeform multi-mirror mold via normal swing cutting. *J. Manuf. Process.* **2023**, *94*, 316–327. [[CrossRef](#)]
182. Zhang, G.; Ran, J.; To, S.; Wu, X.; Huang, P.; Kuz'min, M.P. Size effect on surface generation of multiphase alloys in ultra-precision fly cutting. *J. Manuf. Process.* **2020**, *60*, 23–36. [[CrossRef](#)]
183. Zhu, Z.; To, S.; Zhang, S. Theoretical and experimental investigation on the novel end-fly-cutting-servo diamond machining of hierarchical micro-nanostructures. *Int. J. Mach. Tools Manuf.* **2015**, *94*, 15–25. [[CrossRef](#)]
184. To, S.; Zhu, Z.; Zeng, W. Novel end-fly-cutting-servo system for deterministic generation of hierarchical micro-nanostructures. *CIRP Ann.* **2015**, *64*, 133–136. [[CrossRef](#)]
185. Cheung, C.F.; Kong, L.B.; Lee, W.B.; To, S. Modelling and simulation of freeform surface generation in ultra-precision raster milling. *Proc. Inst. Mech. Eng. Part B J. Eng. Manuf.* **2006**, *220*, 1787–1801. [[CrossRef](#)]
186. Zhang, S.J.; To, S. A theoretical and experimental study of surface generation under spindle vibration in ultra-precision raster milling. *Int. J. Mach. Tools Manuf.* **2013**, *75*, 36–45. [[CrossRef](#)]
187. Cheng, M.N.; Cheung, C.F.; Lee, W.B.; To, S.; Kong, L.B. Theoretical and experimental analysis of nano-surface generation in ultra-precision raster milling. *Int. J. Mach. Tools Manuf.* **2008**, *48*, 1090–1102. [[CrossRef](#)]
188. Zhang, S.J.; To, S.; Zhu, Z.W.; Zhang, G.Q. A review of fly cutting applied to surface generation in ultra-precision machining. *Int. J. Mach. Tools Manuf.* **2016**, *103*, 13–27. [[CrossRef](#)]
189. Zhu, Z.; To, S.; Zhang, S. Active control of residual tool marks for freeform optics functionalization by novel biaxial servo assisted fly cutting. *Optica* **2015**, *54*, 7656–7662. [[CrossRef](#)]
190. Zhu, Z.; To, S.; Zhang, S. Large-scale fabrication of micro-lens array by novel end-fly-cutting-servo diamond machining. *Opt. Express* **2015**, *23*, 20593–20604. [[CrossRef](#)]
191. Zhu, W.-L.; Yang, S.; Ju, B.-F.; Jiang, J.; Sun, A. Scanning tunneling microscopy-based on-machine measurement for diamond fly cutting of micro-structured surfaces. *Precis. Eng.* **2016**, *43*, 308–314. [[CrossRef](#)]
192. Dong, X.; Zhou, T.; Pang, S.; Liang, Z.; Yu, Q.; Ruan, B.; Wang, X. Comparison of fly cutting and transverse planing for micropyramid array machining on nickel phosphorus plating. *Int. J. Adv. Manuf. Technol.* **2019**, *102*, 2481–2489. [[CrossRef](#)]
193. He, Y.; Zhou, T.; Dong, X.; Liu, P.; Zhao, W.; Wang, X.; Hu, Y.; Yan, J. Generation of high-saturation two-level iridescent structures by vibration-assisted fly cutting. *Mater. Des.* **2020**, *193*, 108839. [[CrossRef](#)]
194. Zhang, F.H.; Wang, S.F.; An, C.H.; Wang, J.; Xu, Q. Full-band error control and crack-free surface fabrication techniques for ultra-precision fly cutting of large-aperture KDP crystals. *Front. Mech. Eng.* **2017**, *12*, 193–202. [[CrossRef](#)]
195. Fu, P.; Xue, J.; Zhou, L.; Wang, Y.; Lan, Z.; Zhan, L.; Zhang, F. Influence of the heat deformation of ultra-precision fly cutting tools on KDP crystal surface microstructure. *Int. J. Adv. Manuf. Technol.* **2019**, *103*, 1009–1018. [[CrossRef](#)]
196. Wang, M.; Zhang, Y.; Guo, S.; An, C.; Zhang, F. Understanding the high-point formation mechanism on large optical surface during ultra precision fly cutting process. *Int. J. Adv. Manuf. Technol.* **2018**, *95*, 2521–2528. [[CrossRef](#)]
197. Liang, Y.; Chen, W.; Sun, Y.; Luo, X.; Lu, L.; Liu, H. A mechanical structure-based design method and its implementation on a fly-cutting machine tool design. *Int. J. Adv. Manuf. Technol.* **2014**, *70*, 1915–1921. [[CrossRef](#)]
198. Lu, H.; Ding, Y.; Chang, Y.; Chen, G.; Rui, X. Dynamics Modelling and Simulating of Ultra-precision Fly-Cutting Machine Tool. *Int. J. Precis. Eng. Manuf.* **2020**, *21*, 189–202. [[CrossRef](#)]
199. Du, H.; Yin, T.; Yip, W.S.; Zhu, Z.; To, S. Generation of structural colors on pure magnesium surface using the vibration-assisted diamond cutting. *Mater. Lett.* **2021**, *299*, 130041. [[CrossRef](#)]
200. Zhang, X.; Huang, R.; Wang, Y.; Liu, K.; Deng, H.; Neo, D.W.K. Suppression of diamond tool wear with sub-millisecond oxidation in ultrasonic vibration cutting of steel. *J. Mater. Process. Technol.* **2022**, *299*, 117320. [[CrossRef](#)]
201. Zhu, Z.; To, S.; Xiao, G.; Ehmann, K.F.; Zhang, G. Rotary spatial vibration-assisted diamond cutting of brittle materials. *Precis. Eng.* **2016**, *44*, 211–219. [[CrossRef](#)]
202. Zhu, Z.; To, S.; Ehmann, K.F.; Xiao, G.; Zhu, W. A novel diamond micro-/nano-machining process for the generation of hierarchical micro-/nano-structures. *J. Micromech. Microeng.* **2016**, *26*, 035009. [[CrossRef](#)]

203. Kong, L.B.; Cheung, C.F.; To, S.; Lee, W.B. An investigation into surface generation in ultra-precision raster milling. *J. Mater. Process. Technol.* **2009**, *209*, 4178–4185. [[CrossRef](#)]
204. Cheng, M.N.; Cheung, C.F.; Lee, W.B.; To, S. Optimization of Surface Finish in Ultra-precision Raster Milling (Ultra-precision machining). In Proceedings of the International Conference on Leading Edge Manufacturing in 21st Century: LEM21 2005.3, Nagoya, Japan, 19–22 October 2005; The Japan Society of Mechanical Engineers: Tokyo, Japan, 2005; pp. 1019–1024. [[CrossRef](#)]
205. Kong, L.B.; Cheung, C.F.; To, S.; Lee, W.B. Development of a Dynamic Model for Ultra-Precision Raster Milling. *Key Eng. Mater.* **2008**, *364–366*, 58–63. [[CrossRef](#)]
206. Zhang, S.J.; To, S. The effects of spindle vibration on surface generation in ultra-precision raster milling. *Int. J. Mach. Tools Manuf.* **2013**, *71*, 52–56. [[CrossRef](#)]
207. Cai, H.; Shi, G. Ultra-Precision Machining for Micro Structural Functional Surfaces. In Proceedings of the 2018 3rd International Conference on Mechanical, Control and Computer Engineering (ICMCCE), Huhhot, China, 14–16 September 2018; pp. 277–280. [[CrossRef](#)]
208. Peng, Y.; Jiang, T.; Ehmann, K.F. Research on single-point diamond fly-grooving of brittle materials. *Int. J. Adv. Manuf. Technol.* **2014**, *75*, 1577–1586. [[CrossRef](#)]
209. Bao, Y.-J.; Hao, W.; Wang, Y.-Q.; Gao, H.; Liu, X.-S. Formation mechanism of burr defect in aramid fiber composites based on fly-cutting test. *Int. J. Adv. Manuf. Technol.* **2019**, *104*, 1531–1540. [[CrossRef](#)]
210. Zhang, G.; To, S.; Zhang, S.; Zhu, Z. Case study of surface micro-waves in ultra-precision raster fly cutting. *Precis. Eng.* **2016**, *46*, 393–398. [[CrossRef](#)]
211. Zhao, R.; Yan, D.; Liu, Q.; Leng, J.; Wan, J.; Chen, X.; Zhang, X. Digital Twin-Driven Cyber-Physical System for Autonomously Controlling of Micro Punching System. *IEEE Access* **2019**, *7*, 9459–9469. [[CrossRef](#)]
212. Selvaraj, V.; Xu, Z.; Min, S. Intelligent Operation Monitoring of an Ultra-Precision CNC Machine Tool Using Energy Data. *Int. J. Precis Eng Manuf.-Green Technol.* **2022**, *10*, 59–69. [[CrossRef](#)]
213. Cai, W.; Zhang, W.; Hu, X.; Liu, Y. A hybrid information model based on long short-term memory network for tool condition monitoring. *J. Intell. Manuf.* **2020**, *31*, 1497–1510. [[CrossRef](#)]
214. Li, D.; Wang, B.; Tong, Z.; Blunt, L.; Jiang, X. On-machine surface measurement and applications for ultra-precision machining: A state-of-the-art review. *Int. J. Adv. Manuf. Technol.* **2019**, *104*, 831–847. [[CrossRef](#)]
215. Jeong, S.-H.; Park, J.-A. System identification and admittance model-based nanodynamic control of ultra-precision cutting process. *KSME Int. J.* **1997**, *11*, 620–628. [[CrossRef](#)]
216. Tao, H.; Chen, R.; Xuan, J.; Xia, Q.; Yang, Z.; Zhang, X.; He, S.; Shi, T. A new approach to identify geometric errors directly from the surface topography of workpiece in ultra-precision machining. *Int. J. Adv. Manuf. Technol.* **2020**, *106*, 5159–5173. [[CrossRef](#)]
217. Altintas, Y.; Aslan, D. Integration of virtual and on-line machining process control and monitoring. *CIRP Ann.* **2017**, *66*, 349–352. [[CrossRef](#)]
218. Lin, C.-J.; Lin, C.-H.; Wang, S.-H. Using Fuzzy Control for Feedrate Scheduling of Computer Numerical Control Machine Tools. *Appl. Sci.* **2021**, *11*, 4701. [[CrossRef](#)]
219. Qi, B.; Park, H.S. Data-driven digital twin model for predicting grinding force. *IOP Conf. Ser. Mater. Sci. Eng.* **2020**, *916*, 012092. [[CrossRef](#)]
220. Liu, J.; Du, X.; Zhou, H.; Liu, X.; ei Li, L.; Feng, F. A digital twin-based approach for dynamic clamping and positioning of the flexible tooling system. *Procedia CIRP* **2019**, *80*, 746–749. [[CrossRef](#)]
221. Aggogeri, F.; Merlo, A.; Pellegrini, N. Active vibration control development in ultra-precision machining. *J. Vib. Control* **2020**, *27*, 107754632093347. [[CrossRef](#)]
222. Zhao, D.; Du, H.; Wang, H.; Zhu, Z. Development of a novel fast tool servo using topology optimization. *Int. J. Mech. Sci.* **2023**, *250*, 108283. [[CrossRef](#)]
223. Guo, P.; Li, Z.; Xiong, Z.; Zhang, S. A theoretical and experimental investigation into tool setting induced form error in diamond turning of micro-lens array. *Int. J. Adv. Manuf. Technol.* **2023**, *124*, 2515–2525. [[CrossRef](#)]
224. Niu, Y.; Chen, X.; Chen, L.; Zhu, Z.; Huang, P. Development of a Sinusoidal Corrugated Dual-Axial Flexure Mechanism for Planar Nanopositioning. *Actuators* **2022**, *11*, 276. [[CrossRef](#)]
225. Liang, X.; Zhang, C.; Wang, C.; Li, K.; Loh, Y.M.; Cheung, C.F. Tool wear mechanisms and surface quality assessment during micro-milling of high entropy alloy FeCoNiCrAlx. *Tribol. Int.* **2023**, *178*, 108053. [[CrossRef](#)]

Disclaimer/Publisher’s Note: The statements, opinions and data contained in all publications are solely those of the individual author(s) and contributor(s) and not of MDPI and/or the editor(s). MDPI and/or the editor(s) disclaim responsibility for any injury to people or property resulting from any ideas, methods, instructions or products referred to in the content.